Diplomarbeit

MEMS E-Field Sensor with Stabilized Optical Readout

ausgeführt zum Zwecke der Erlangung des akademischen Grades eines DI, eingereicht am

Institut für Sensor- und Aktuatorsysteme
Technische Universität Wien

vorgelegt von:
Hajrudin Besic
Matriculation number: 01226946

betreut von:
Ao. Univ. Prof. Dr. Franz Keplinger
Dr. Andreas Kainz

Wien, am July 20, 2020

Die approbierte gedruckte Originalversion dieser Diplomarbeit ist an der TU Wien Bibliothek verfügbar.
The approved original version of this thesis is available in print at TU Wien Bibliothek.

Die approbierte gedruckte Originalversion dieser Diplomarbeit ist an der TU Wien Bibliothek verfügbar.
The approved original version of this thesis is available in print at TU Wien Bibliothek.

Eidesstattliche Erklärung

Ich erkläre an Eides statt, dass ich die vorliegende Masterarbeit selbstständig und ohne fremde Hilfe verfasst, andere als die angegebenen Quellen und Hilfsmittel nicht benutzt bzw. die wörtlich oder sinngemäß entnommenen Stellen als solche kenntlich gemacht habe.

Wien, July 20, 2020

Unterschrift (Author)

Die approbierte gedruckte Originalversion dieser Diplomarbeit ist an der TU Wien Bibliothek verfügbar.
The approved original version of this thesis is available in print at TU Wien Bibliothek.
TU WIEN Bibliothek Your knowledge hub

Die approbierte gedruckte Originalversion dieser Diplomarbeit ist an der TU Wien Bibliothek verfügbar.
The approved original version of this thesis is available in print at TU Wien Bibliothek.

Wenn wir wüssten, was wir tun, würden wir es nicht Forschung nennen.
- Albert Einstein

Die approbierte gedruckte Originalversion dieser Diplomarbeit ist an der TU Wien Bibliothek verfügbar.
The approved original version of this thesis is available in print at TU Wien Bibliothek.

Die approbierte gedruckte Originalversion dieser Diplomarbeit ist an der TU Wien Bibliothek verfügbar.
The approved original version of this thesis is available in print at TU Wien Bibliothek.

Contents

Contents I

Abstract III

Kurzfassung IV

Acknowledgment V

Introduction 1

1 Fundamentals 3
- 1.1 Electric field transducer . . . 4
- 1.2 Michelson interferometer . . . 8
- 1.3 Modulation of light . . . 10
- 1.4 Measurement system . . . 19

2 Stabilization 23
- 2.1 Control theory . . . 24
- 2.2 Actuator . . . 30
- 2.3 Feedback . . . 32
  - 2.3.1 Hybrid demodulation approach . . . 37
  - 2.3.2 Double quadrature demodulation approach . . . 39
- 2.4 Synchronization . . . 41

3 Implementation 45
- 3.1 Digital circuit . . . 45
  - 3.1.1 Data acquisition . . . 45
  - 3.1.2 Hybrid demodulation . . . 49
- 3.2 Double quadrature demodulation . . . 56
- 3.3 Analogue circuit . . . 59
- 3.4 Measurement results . . . 66

Conclusion and Outlook 73
- 3.5 Outlook, generation of a FM signal . . . 73
- 3.6 Conclusion . . . 78

Die approbierte gedruckte Originalversion dieser Diplomarbeit ist an der TU Wien Bibliothek verfügbar.
The approved original version of this thesis is available in print at TU Wien Bibliothek.
TU WIEN Bibliothek Your knowledge hub

Die approbierte gedruckte Originalversion dieser Diplomarbeit ist an der TU Wien Bibliothek verfügbar.
The approved original version of this thesis is available in print at TU Wien Bibliothek.

Abstract

In this thesis different methods have been developed and tested to stabilize an optical readout for a micro-electrical-mechanical-system (MEMS) electric field sensor. The optical readout is used because it does not interfere with the electric field the system measures. Due to its inherent high resolution of 10^{-10} m a Michelson interferometer is used.

For the stabilization an piezoelectric mirror is placed in the reference arm of the interferometer. With the piezoelectric actuator an oscillating signal is introduced with a known frequency and modulation index. Via a feedback mechanism the signal is detected and the instantaneous working point of the interferometer is calculated. A controller, that is connected to the piezoelectric mirror, adjusts the mirror position.

We implemented two types of stabilization mechanisms with different level of complexity and functional flexibility. They both showed similar performance and established a very stable working point for the Michelson interferometer.

Three tests were executed. The first one was done without a stabilization which delivered only useless, noisy measurements. The second test was done on a piezoelectric buzzer, to determine its transfer function. In the third test we used the electric field transducer, to determine the maximum sensitivity that could be achieve.

Die approbierte gedruckte Originalversion dieser Diplomarbeit ist an der TU Wien Bibliothek verfügbar.
The approved original version of this thesis is available in print at TU Wien Bibliothek.
TU Bibliothek WIEN Your knowledge hub

Kurzfassung

In dieser Arbeit wurden verschiedene Methoden für ein optisches Readout eines Sensors für die elektrische Feldstärke entwickelt und getestet. Der Sensor basiert auf mikro-elektromechanischen Strukturen (MEMS), die im elektrischen Feld geringfügig ausgelenkt werden. Diese kleinen Auslenkungen einerseits und die leichte Störbarkeit des elektrischen Feldes andererseits erfordern ein Readout, das nicht auf die Struktur zurückwirkt. Dies und die hohe erforderliche Auflösung von 10^{-10} m erklärt die Wahl des optischen Prinzips im Allgemeinen und des Michelson-Interferometers im Speziellen. Das Interferometer kann allerdings leicht durch Vibrationen und thermische Ausdehnungen gestört werden. Dem wird mit einer Stabilisierung begegnet, in den Referenzarm des Interferometers wird ein piezoelektrisch verstellbarer Spiegel platziert. Mit dem Piezoaktuator wird ein Schwingungssignal mit bekannter Frequenz und bekannten Modulationsindex erzeugt. Über einen Rückkopplungsmechanismus wird das Signal erfasst und der aktuelle Arbeitspunkt des Interferometers berechnet. Über eine Steuerung, die mit dem piezoelektrischen Spiegel verbunden ist, wird die Spiegelposition eingestellt. Zwei unterschiedliche Arten von Stabilisierungsmechanismen mit unterschiedlicher Komplexität und funktionaler Flexibilität wurden implementiert. Beide zeigten, ähnliche Funktionalität und es gelang mit ihnen, einen hinreichend stabilen Arbeitspunkt des Interferometers zu erzeugen. Es wurden drei prinzipielle Messungen durchgeführt. Die erste, ohne Stabilisierung zeigte das Grundproblem und lieferte die Vergleichsbasis. Die zweite Messung wurde an einem piezoelektrischen Buzzer durchgeführt, um dessen Übertragungsfunktion zu bestimmen. Für die dritte Messung haben wir den elektrischen Feld-Sensor verwendet, um die maximale Empfindlichkeit zu bestimmen, die wir so erreichen konnten.

Die approbierte gedruckte Originalversion dieser Diplomarbeit ist an der TU Wien Bibliothek verfügbar.
The approved original version of this thesis is available in print at TU Wien Bibliothek.
TU Bibliothek WIEN Your knowledge hub

Acknowledgment

I would like to thank my professor Franz Keplinger for the generous opportunity to work on this project. I would also like to thank Andreas Kainz for his supervision and guidance.

Special thanks goes to my parents who invested in me and made my studies possible. Also thanks to my brother for the support and for being helpful whenever I needed him.

My deepest thanks to my lovely wife for the mental support, for always believing in me and for pushing me in hard times.

Die approbierte gedruckte Originalversion dieser Diplomarbeit ist an der TU Wien Bibliothek verfügbar.
The approved original version of this thesis is available in print at TU Wien Bibliothek.
TU WIEN Bibliothek Your knowledge hub

Die approbierte gedruckte Originalversion dieser Diplomarbeit ist an der TU Wien Bibliothek verfügbar.
The approved original version of this thesis is available in print at TU Wien Bibliothek.

Die approbierte gedruckte Originalversion dieser Diplomarbeit ist an der TU Wien Bibliothek verfügbar.
The approved original version of this thesis is available in print at TU Wien Bibliothek.

Introduction

Measurement of electric fields provides still many difficulties, since the measurement instrument itself can cause interference with the electric field that is being measured. Surface charges of dielectric bodies, conducting materials and connections to potentials all cause distortions to the measurement [16, 17]. To avoid these effects optical readouts, such as an Michelson interferometer, can be used.

To use the Michelson interferometer the Electric field needs to be transformed into a mechanical displacement. Therefore, a MEMS (Microelectromechanical system) transducer is used on the measuring arm of the interferometer. It transforms the electric field into a mechanical oscillation. This oscillation will cause an oscillating intensity on the photodiode of the interferometer.

The challenge in such a system is that different noise sources like thermal fluctuations and airflow can cause that the working point of the interferometer drifts.That makes the measurement highly susceptible to errors.

The drifting of the working point caused the need for a stabilization of the working point at a fixed value.

Die approbierte gedruckte Originalversion dieser Diplomarbeit ist an der TU Wien Bibliothek verfügbar.
The approved original version of this thesis is available in print at TU Wien Bibliothek.
TU Bibliothek Your knowledge hub WIEN

Die approbierte gedruckte Originalversion dieser Diplomarbeit ist an der TU Wien Bibliothek verfügbar.
The approved original version of this thesis is available in print at TU Wien Bibliothek.

Die approbierte gedruckte Originalversion dieser Diplomarbeit ist an der TU Wien Bibliothek verfügbar.
The approved original version of this thesis is available in print at TU Wien Bibliothek.

Chapter 1

Fundamentals

The detection of low-frequency and static electric fields was always challenging. In this work a possible solution for the detection of the electric field (E-Field) and method for the stabilization of the measurement system will be presented.
For the detection of the electric field, a transducer will be used which converts the electric field into a spatial displacement. With the help of a Michelson interferometer, the displacement can be converted into an electric signal which is extracted and evaluated by a readout circuit [9, 10, 16].
A system built like this is not resistant to noise that causes a drift of the working point. There are many noise sources like thermal noise, vibrations, air movement and other that can affect the measurement and lead to inaccurate results. To make the system more resilient to noise, a stabilization mechanism is introduced. This is achieved by placing a piezoelectric mirror on the reference arm of the interferometer. An AC voltage drives this mirror. This oscillation is picked up by the photodetector of the interferometer. A signal processing system then reads the phase of the signal . If the phase is shifted due to noise, a feedback control mechanism will compensate this shift.
Figure 1.1 shows a graphical representation of the system.

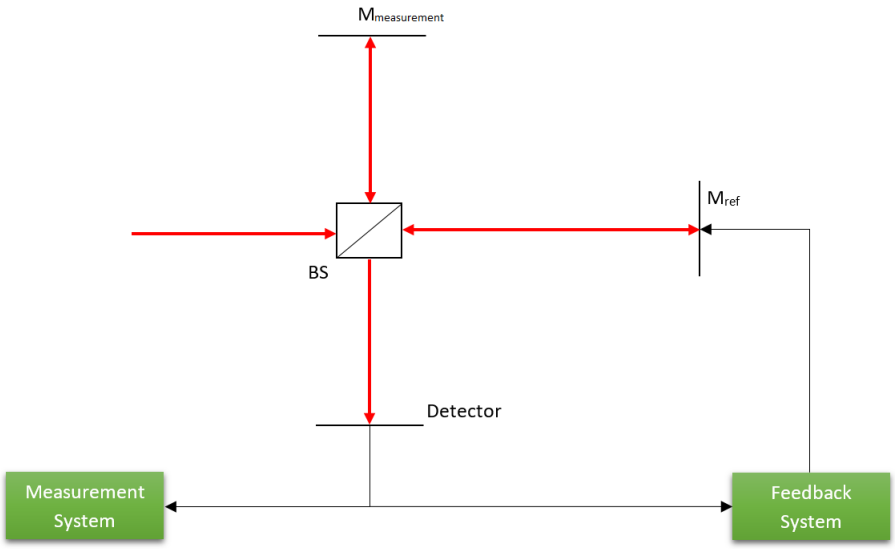

Figure 1.1: Principle setup of the measurement system with stabilization

In the following sections the individual components are described in detail.

1.1 Electric field transducer

To transform the electric field into a spatial displacement, a transducer is used [16]. It is is made of two parts (Figure 1.2): the first part is stationary and the second one can move in the z-direction. These two parts are made of a conductive material and are connected via an insulating layer. Both parts are connected to an AC-voltage source supplying a voltage

$$U(t) = \hat{U}\cos(\omega t). \tag{1.1}$$

Both conductors form a capacitor with the capacitance C. The corresponding charge on the moving part of the transducer is:

$$Q(t) = U(t)C = \hat{U}C\cos(\omega t). \tag{1.2}$$

If a transducer is placed into the electric field E, a force

$$F(t) = EQ(t) = EC\hat{U}\cos(\omega t), \tag{1.3}$$

acts on the transducer, which will lead to a displacement of the moving part of. The displacement can be described with the classic equation of a damped driven harmonic

Die approbierte gedruckte Originalversion dieser Diplomarbeit ist an der TU Wien Bibliothek verfügbar.
The approved original version of this thesis is available in print at TU Wien Bibliothek.
TU Bibliothek Your knowledge hub WIEN

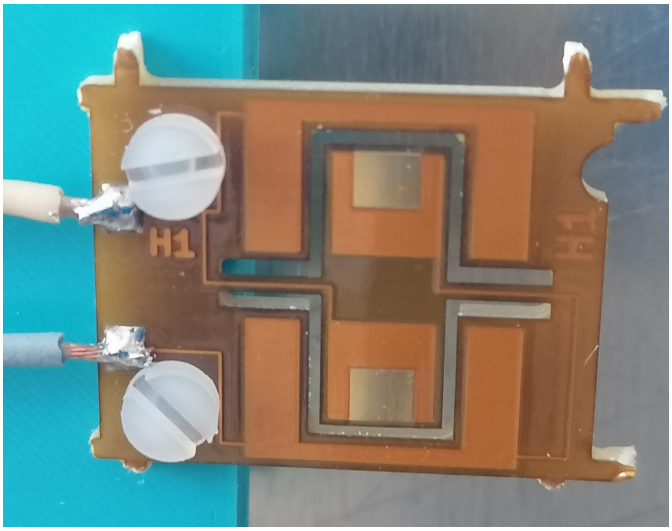

Figure 1.2: A picture of the electric field transducer. The moving part is located in the middle and is anchored to the stationary part over two bars

oscillator [1, 2]

$$m\ddot{x}(t) + c\dot{x}(t) + kx(t) = F(t), \tag{1.4}$$

where c is the damping coefficient, k is the elastic coefficient of the springs, m the mass of the moving part and x the displacement of the moving part (Figure 1.3).

Because the system is a linear time-invariant system, the mass oscillates with the same frequency as the voltage, so we can write the voltage and displacement in complex form

$$U(t) = \hat{U}\cos(\omega t) = Re\left\{\underline{U}\mathrm{e}^{\mathrm{j}\omega t}\right\}, \quad \underline{U} = \hat{U} \tag{1.5}$$

$$x(t) = \underline{X}\mathrm{e}^{\mathrm{j}\omega t}. \tag{1.6}$$

If we transform the equation to the frequency domain, substitute F with Eq. (1.3) and divide by m, we get

$$-\omega^2\underline{X} + \mathrm{j}\omega\frac{c}{m}\underline{X} + \frac{k}{m}\underline{X} = \frac{EC\hat{U}}{m}. \tag{1.7}$$

After solving for $\underline{X}$ yields

$$\underline{X} = \frac{\frac{EC\hat{U}}{m}}{\left(\frac{k}{m} - \omega^2\right) + \mathrm{j}\frac{c}{m}\omega_0\omega}, \tag{1.8}$$

where $\underline{X}$ is the complex amplitude of the oscillation. The resonant frequency of the oscillator

Die approbierte gedruckte Originalversion dieser Diplomarbeit ist an der TU Wien Bibliothek verfügbar.
The approved original version of this thesis is available in print at TU Wien Bibliothek.
TU WIEN Bibliothek Your knowledge hub

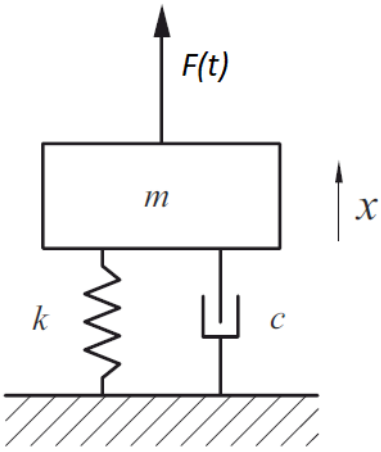

Figure 1.3: Model of a damped driven harmonic oscillator

is defined by

$$\omega_0 = \sqrt{\frac{k}{m}}, \tag{1.9}$$

and the damping coefficient

$$D = \frac{c}{2\omega_0 m}. \tag{1.10}$$

For low damping coefficients the largest magnitude of the amplitude is at the resonance frequency (Figure 1.4). Consequently, for best sensitivity we want to drive the transducer at the resonant frequency. For this system we can define the Q-factor. It is described as the ratio of the peak energy stored in a system to the energy lost per radian cycle. It can be calculated as

$$Q = \frac{\sqrt{mk}}{D}. \tag{1.11}$$

High Q means less energy loss which results in larger amplitude of the oscillation.

Die approbierte gedruckte Originalversion dieser Diplomarbeit ist an der TU Wien Bibliothek verfügbar.
The approved original version of this thesis is available in print at TU Wien Bibliothek.

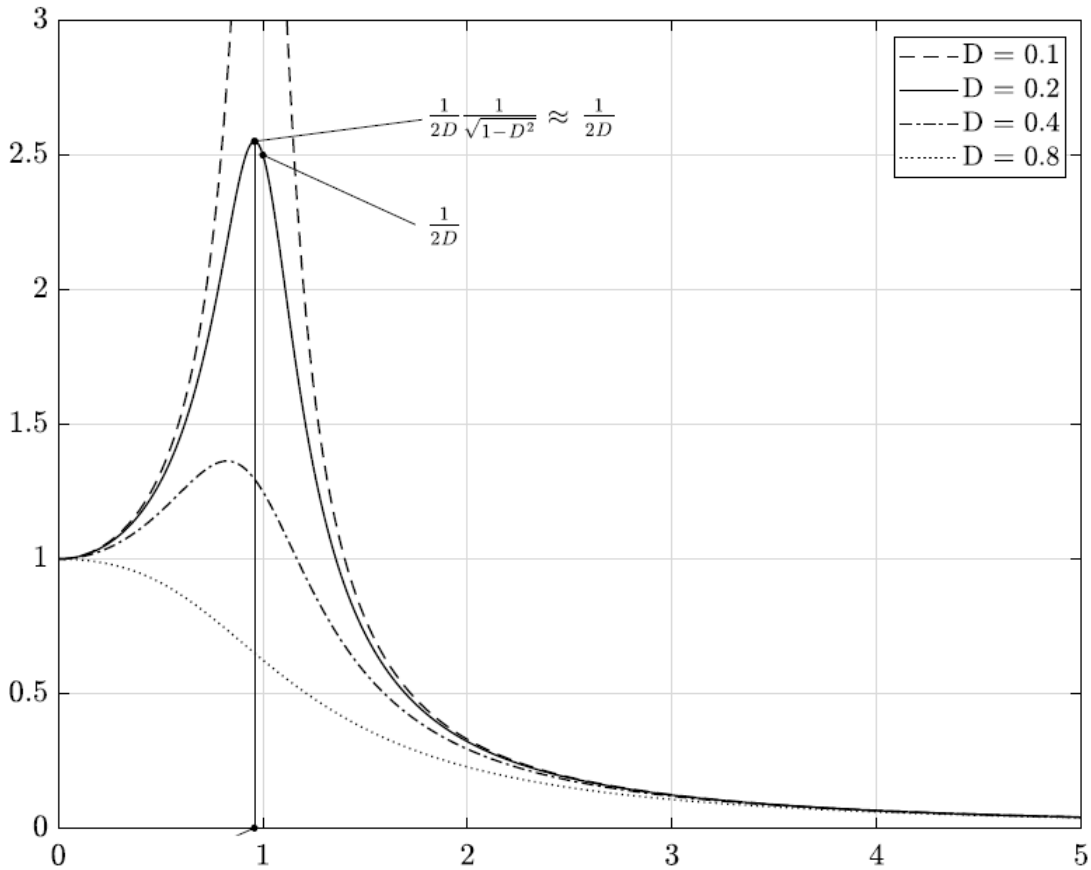

Figure 1.4: Frequency characteristic of a damped driven harmonic oscillator

Die approbierte gedruckte Originalversion dieser Diplomarbeit ist an der TU Wien Bibliothek verfügbar.
The approved original version of this thesis is available in print at TU Wien Bibliothek.

1.2 Michelson interferometer

The Michelson interferometer is an instrument that uses the superposition principle of two fields [3]. The resulting field is measured with an optical detector (usually a photodiode). These detectors don't measure the electric field strength directly, but its intensity, which is the square of the field strength. Because of this nonlinearity, the intensity of the resulting field is not equal to the sum of the intensities of the two fields. This phenomen is called interference. Two fields with same frequency and a complex field amplitude $\underline{U}$ is introduced. The intensity is calculated as

$$I(x) = \underline{U}(x) \cdot \underline{U}^*(x), \tag{1.12}$$

with * denoting the complex conjugate. The superposition of two fields U_1 and U_2 is

$$I(x) = (\underline{U}_1 + \underline{U}_2) \cdot (\underline{U}_1 + \underline{U}_2)^* = I_1 + I_2 + 2\mathrm{Re}\left[\underline{U}_1(x)\underline{U}_2^*(x)\right]. \tag{1.13}$$

The first two terms represent the individual intensities of the two waves. The third one is the interference term that can be positive or negative depending on the relative phase of the waves. Polarization can influence the interference when we assume that all waves have the same polarization. Because we work in this thesis with monochromatic electromagnetic waves, we assume that all waves have the same frequency. For a defined spatial point the two waves differ only in amplitude and phase.

$$U_{1,2} = A_{1,2}\mathrm{e}^{\mathrm{j}\varphi_{1,2}}. \tag{1.14}$$

For the superposition of the two waves, the resulting intensity is

$$I(x) = I_1(x) + I_2(x) + 2\sqrt{I_1(x)I_2(x)}\cos(\varphi_2 - \varphi_1). \tag{1.15}$$

For waves with same intensity $I_{1,2} = I_0$ it is

$$I(x) = 2I_0(x)[1 + \cos(\Delta\varphi)], \tag{1.16}$$

with $\Delta\varphi = \varphi_2 - \varphi_1$. The resulting intensity, depending on the phase difference, will be between $0 \leq I \leq 4I_0$. The maximum intensity $I_{\max} = 4I_0$ occurs at $\Delta\varphi = 2m\pi$, where m is an integer number. In the case of the Michelson interferometer in (Figure 1.5) a laser beam is directed at a beam splitter where it is split into two beams. Those two beams

Die approbierte gedruckte Originalversion dieser Diplomarbeit ist an der TU Wien Bibliothek verfügbar.
The approved original version of this thesis is available in print at TU Wien Bibliothek.
TU Bibliothek Your knowledge hub WIEN

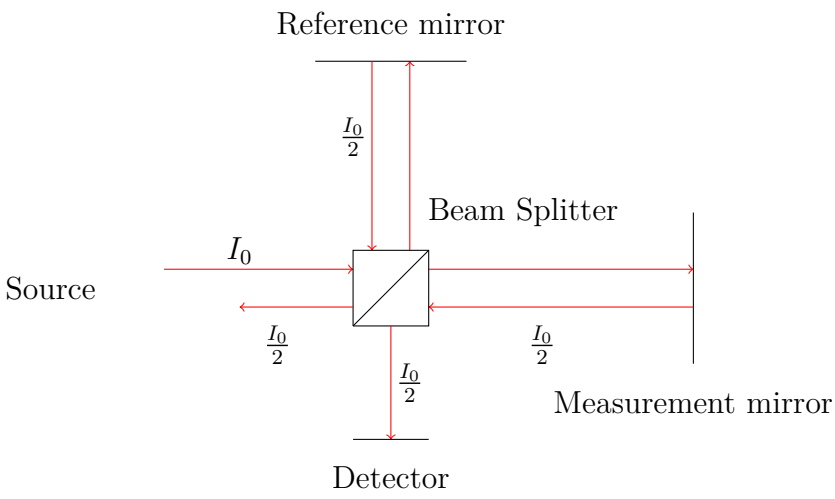

Figure 1.5: Schematic representation of the Michelson interferometer

are reflected from two mirrors back to the beam splitter. In this process the beams travel the paths L_1 and L_2. After passing the beam splitter again, the beams interfere at the detector. The phase difference of the waves depends on the path difference the waves have travelled. Because the wave goes through the beam splitter two times, the intensity of a single wave is $\frac{I_0}{4}$. If we say that the path difference of the two arms of the interferometer is $\Delta l = L_2 - L_1$, the phase difference of the two waves is $\Delta\varphi = 2k\Delta l$. here, $k = \frac{2\pi}{\lambda}$ the wave number of the wave, where lambda is the wave length.

$$k = \frac{2\pi}{\lambda}, \tag{1.17}$$

Depending on the path difference, the equation of the resulting wave on the detector is:

$$I = \frac{I_0}{2}\left[1 + \cos(\Delta\varphi))\right]. \tag{1.18}$$

Figure 1.6 shows the intensity measured on the detector depending on the difference in path lengths. If one of the mirrors is stationary (reference arm) and the other is moving (measurement arm) we can measure the position of the moving mirror.

Die approbierte gedruckte Originalversion dieser Diplomarbeit ist an der TU Wien Bibliothek verfügbar.
The approved original version of this thesis is available in print at TU Wien Bibliothek.

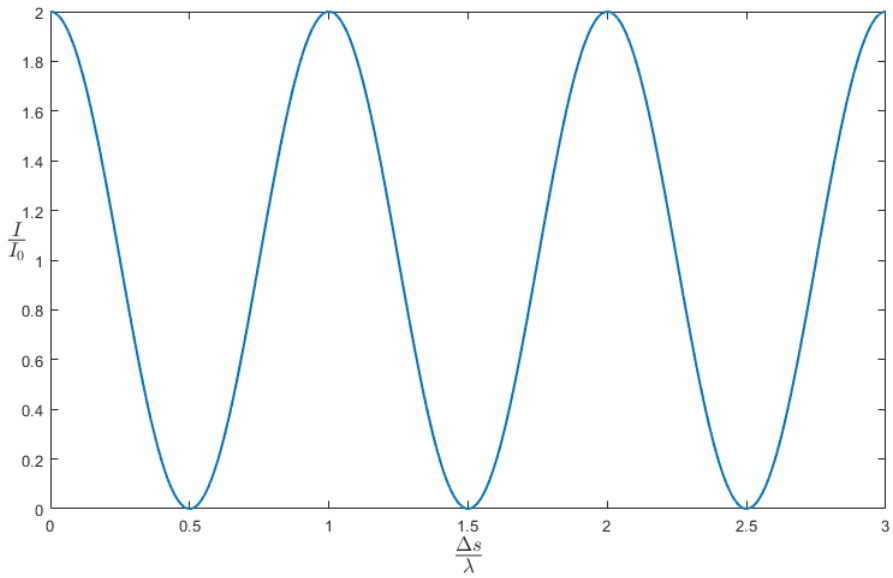

Figure 1.6: Function of the intensity in regard to the path difference

1.3 Modulation of light

Now, the working principles of the transducer and Michelson interferometer are described, we need to describe how they work together. The transducer used for this system will be the measuring mirror. If an electric field is applied to the transducer, it will start oscillating. Consequently, the arm length of the interferometer will change, in this case, will oscillate. If light reflects of a moving object its frequency will change. There are two ways to describe this phenomena, as a modulation of the phase or modulation of the frequency, which are tightly coupled [4, 8]. First we look at a phase modulated signal

$$s_{\mathrm{PM}}(t) = A\sin(\omega_0 t + \psi + \psi_{\mathrm{d}} M(t)). \tag{1.19}$$

Here, ω_0 is the carrier frequency, A is the amplitude, ψ is a constant phaseshift, ψ_{d} modulation strength and $M(t)$ is the modulating function or modulator. We can write the phase of the sine function as

$$p(t) = \omega_0 t + \psi + \psi_{\mathrm{d}} M(t). \tag{1.20}$$

The phase modulation, mathematically, is straight forward.

A frequency modulation requires a changing frequency. That means that a changing

Die approbierte gedruckte Originalversion dieser Diplomarbeit ist an der TU Wien Bibliothek verfügbar.
The approved original version of this thesis is available in print at TU Wien Bibliothek.
TU Bibliothek Your knowledge hub WIEN

frequency term besides $\omega_0 t$ is required. The instantaneous angular frequency is defined as the derivative of the phase

$$\omega(t) = \frac{\mathrm{d}}{\mathrm{d}t} p(t). \tag{1.21}$$

This is the relationship between phase modulation and frequency modulation. Again we assume that we have an unmodulated phase

$$p(t) = \omega_0 t + \psi. \tag{1.22}$$

The time derivative is therefore

$$\omega(t) = \frac{\mathrm{d}}{\mathrm{d}t}(\omega_0 t + \psi) = \omega_0. \tag{1.23}$$

We can see that in the unmodulated case we have a constant frequency ω_0. Now, to get a frequency modulated signal we need to add an additional changing frequency term. Our instantaneous frequency then reads

$$\omega(t) = (\omega_0 + \omega_\mathrm{d} M(t))\, t, \tag{1.24}$$

where ω_0 is the constant frequency and ω_d the frequency modulation strength. Now if we want to calculate the phase, the angular frequency needs to be integrated

$$p(t) = \int \omega(t)\mathrm{d}t, \tag{1.25}$$

therefore:

$$p(t) = \int (\omega_0 + \omega_\mathrm{d} M(t))\mathrm{d}t = \omega_0 t + \psi + \omega_\mathrm{d} \int M(t)\mathrm{d}t. \tag{1.26}$$

We can write the frequency-modulated signal as

$$s_\mathrm{FM}(t) = \omega_0 t + \psi + \omega_\mathrm{d} \int M(t)\mathrm{d}t. \tag{1.27}$$

In our case the signal will be modulated with a sine function $M(t) = \sin(\Omega t)$ with the frequency Ω. Our frequency- and phase-modulated signal are

$$s_\mathrm{FM}(t) = \sin(\omega_0 t + \psi - \frac{\omega_\mathrm{d}}{\Omega}\cos(\Omega t)), \quad \text{and} \tag{1.28}$$

$$s_\mathrm{PM}(t) = \sin(\omega_0 t + \psi + \psi_\mathrm{d}\sin(\Omega t)). \tag{1.29}$$

Die approbierte gedruckte Originalversion dieser Diplomarbeit ist an der TU Wien Bibliothek verfügbar.
The approved original version of this thesis is available in print at TU Wien Bibliothek.
TU Bibliothek WIEN Your knowledge hub

The phase-hub for the phase-modulation is ψ_d and for the frequency-modulation $-\frac{\omega_d}{\Omega}$. The instantaneous frequency for phase-modulation is $\omega_0 + \psi_\mathrm{d}\Omega\cos(\Omega t)$ and for the frequency-modulation $\omega_0 + \omega_\mathrm{d}\sin(\Omega t)$. In our case the phase modulation is used, because the displacement of the mirror is directly changing the phase difference of the resulting wave on the detector. An oscillating position of the mirror results in an oscillating phase difference

$$\Delta\varphi = k(\Delta l_0 + x_\mathrm{d}\sin(\Omega t)), \tag{1.30}$$

where Δl_0 is the path length difference of the two beams in the resting position. Therefore, we can write the intensity as

$$I = I_1 + I_2 + 2\sqrt{I_1 I_2}\cos(\psi + \psi_\mathrm{d}\sin(\Omega t)), \tag{1.31}$$

where ψ_d is the modulation index of the signal, which is directly proportional to the oscillation amplitude of the mirror, and ψ is the phase difference of the two mirrors caused by Δl_0. Figure 1.7 shows a phaser diagram of the phase modulated signal. The phase is oscillating with an angular frequency Ω and amplitude ψ_d around a constant phase ψ.

The relation between I and ψ is not linear, so the phase modulation results in a number of harmonic terms. These terms are described by Bessel functions [8, 10, 16, 18, 19]. The Bessel-functions split the non-linear sinusoid function into an infinite number of linear sinusoids (side bands) (Figure 1.8). First we need to rewrite the intensity as

$$I = I_1 + I_2 + 2\sqrt{I_1 I_2}[\cos(\psi)\cos(\psi_\mathrm{d}\sin(\Omega t)) - \sin(\psi)\sin(\psi_\mathrm{d}\sin(\Omega t))]. \tag{1.32}$$

Now we have two terms with non-linear behaviour that can be transformed into Bessel coefficients:

$$\cos(\psi_\mathrm{d}\sin(\Omega t)) = J_0(\psi_\mathrm{d}) + 2J_2(\psi_\mathrm{d})\cos(2\Omega t) + \ldots \tag{1.33}$$

$$\sin(\psi_\mathrm{d}\sin(\Omega t)) = 2J_1(\psi_\mathrm{d})\sin(\Omega t) + 2J_3(\psi_\mathrm{d})\sin(\Omega t) + \ldots \tag{1.34}$$

Because we are working with modulation indices $\psi_\mathrm{d} < 1$ only terms with $J_{\mathrm{i}<2}$ relevant. By putting those terms back into the intensity equation we get:

$$\begin{aligned} I = I_1 + I_2 + 2\sqrt{I_1 I_2}J_0(\psi_\mathrm{d})\cos(\psi) - 4\sqrt{I_1 I_2}J_1(\psi_\mathrm{d})\sin(\psi)\sin(\Omega t) \\ + 4\sqrt{I_1 I_2}J_2(\psi_\mathrm{d})\cos(\psi)\cos(2\Omega t) \end{aligned} \tag{1.35}$$

Die approbierte gedruckte Originalversion dieser Diplomarbeit ist an der TU Wien Bibliothek verfügbar.
The approved original version of this thesis is available in print at TU Wien Bibliothek.
TU Bibliothek WIEN Your knowledge hub

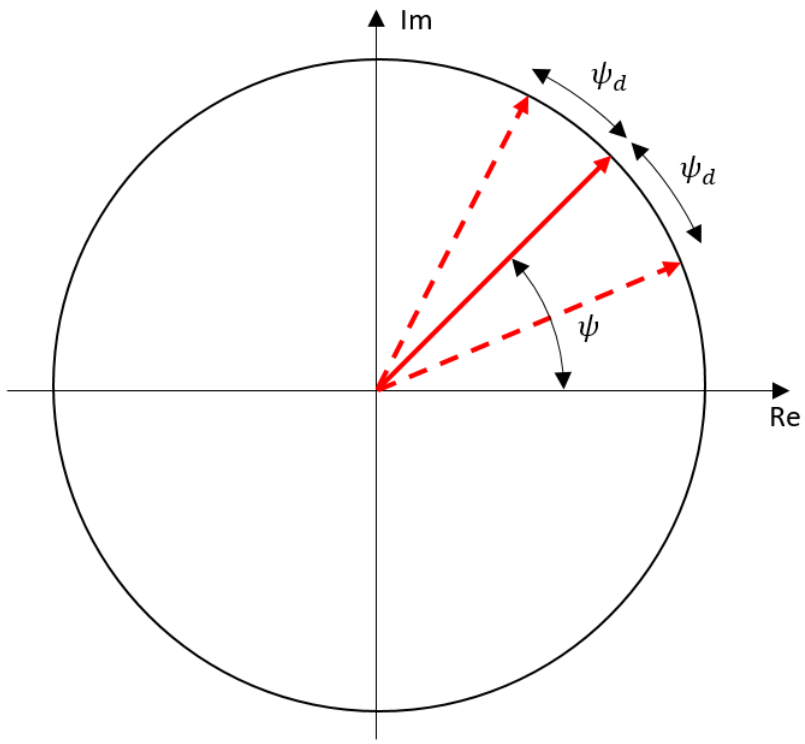

Figure 1.7: Phaser diagram of the phase modulated signal. The phase is oscillating with an angular frequency Ω and amplitude ψ_d around a constant phase ψ

Die approbierte gedruckte Originalversion dieser Diplomarbeit ist an der TU Wien Bibliothek verfügbar.
The approved original version of this thesis is available in print at TU Wien Bibliothek.

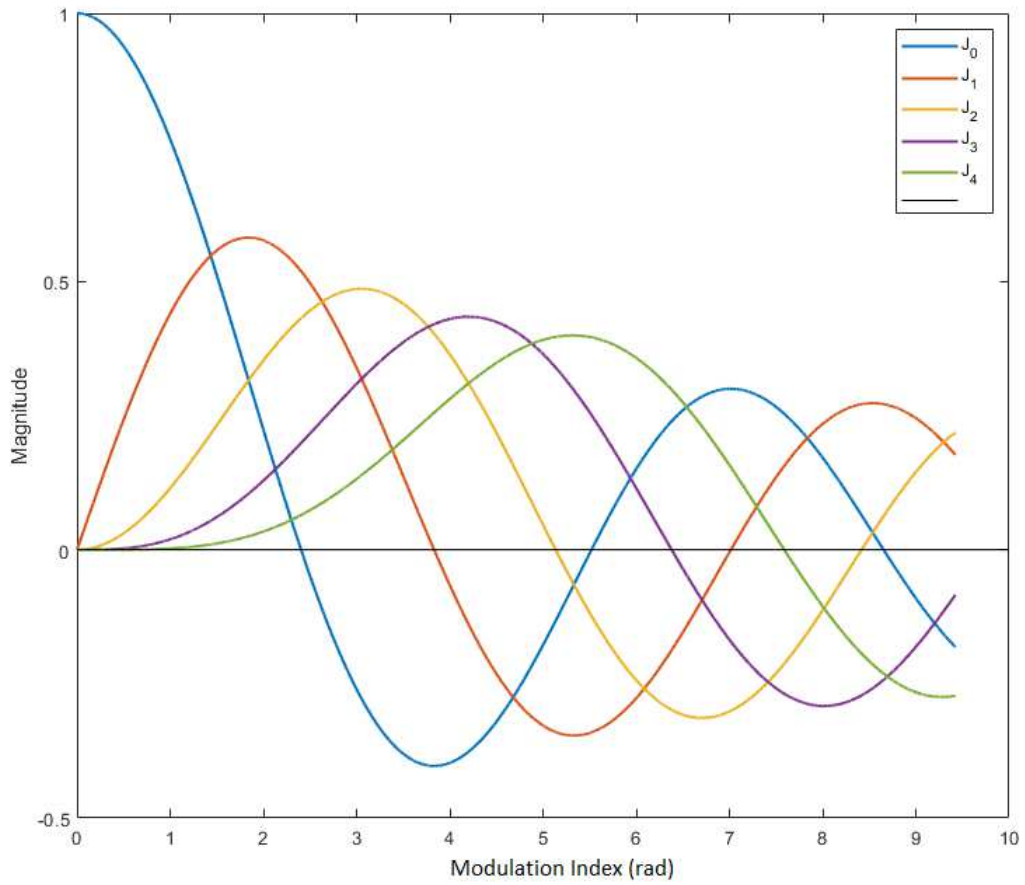

Figure 1.8: Amplitudes of the Bessel-functions for different modulation indices

Die approbierte gedruckte Originalversion dieser Diplomarbeit ist an der TU Wien Bibliothek verfügbar.
The approved original version of this thesis is available in print at TU Wien Bibliothek.

The amplitudes of the side bands can be calculated as

$$J_n(\psi_\mathrm{d}) = \frac{2}{\pi}\int_0^{\frac{\pi}{2}} \sin(\psi_\mathrm{d}\sin(\Omega))\sin(n\Omega)\mathrm{d}\Omega \quad (n \text{ odd}) \tag{1.36}$$

$$J_n(\psi_\mathrm{d}) = \frac{2}{\pi}\int_0^{\frac{\pi}{2}} \cos(\psi_\mathrm{d}\sin(\Omega))\cos(n\Omega)\mathrm{d}\Omega \quad (n \text{ even}) \tag{1.37}$$

For better visualization and understanding of this phenomenon, we can simulate the intensity function in the frequency domain. For simplicity we will assume that the constant phase term $\psi = \frac{\pi}{4}$, so $\sin(\psi) = \cos(\psi) = \frac{1}{\sqrt{2}}$. We also assume that $I_1 = I_2 = I_0$ which delivers

$$I = 2I_0\left[1 + \cos\left(\frac{\pi}{4} + \psi_\mathrm{d}\sin(\Omega t)\right)\right]. \tag{1.38}$$

We divide by $2I_0$ and get

$$\frac{I}{2I_0} = 1 + \cos\left(\frac{\pi}{4} + \psi_\mathrm{d}\sin(\Omega t)\right). \tag{1.39}$$

As the simulation program LabView is chosen. Figure 1.9 shows the block diagram of the simulation process used for the calculation of the spectrum of the function $1 + \cos(\psi + \psi_\mathrm{d}\sin(\Omega t))$. The "Simulate Signal" box generates a signal $\psi_\mathrm{d}\sin(\Omega t)$. A constant phase ψ is added to the signal and now we have the phase $\psi + \psi_\mathrm{d}\sin(\Omega t)$. Because the "Cosine" block, that returns the cosine of the input function, has the input defined in radians, we need to transform our phase into radians first. Now we need to add 1 to the cosine function to get the function from equation (1.39). To get a frequency domain power spectrum of our signal we use the "Spectral measurement" block of LabView that transforms the time domain signal into the frequency domain and calculates its power. The output is connected to an oscilloscope block to visualize the results.

The Parseval-Theorem [4] brings the definition of the signal power from the time domain in the frequency domain. The power definition of a time signal is brought into the frequency domain by defining a new parameter of the time signal, namely the mean (normalized) power. That is the power, the signal $s(t)$ would transform into heat in a resistance R. We regard the signal $s(t)$ as a voltage signal $u(t)$. The mean power, per definition of the effective voltage, is defined as the square of the effective voltage. The mean normalized (to 1 Ohm) power is defined as

Die approbierte gedruckte Originalversion dieser Diplomarbeit ist an der TU Wien Bibliothek verfügbar.
The approved original version of this thesis is available in print at TU Wien Bibliothek.
TU WIEN Bibliothek Your knowledge hub

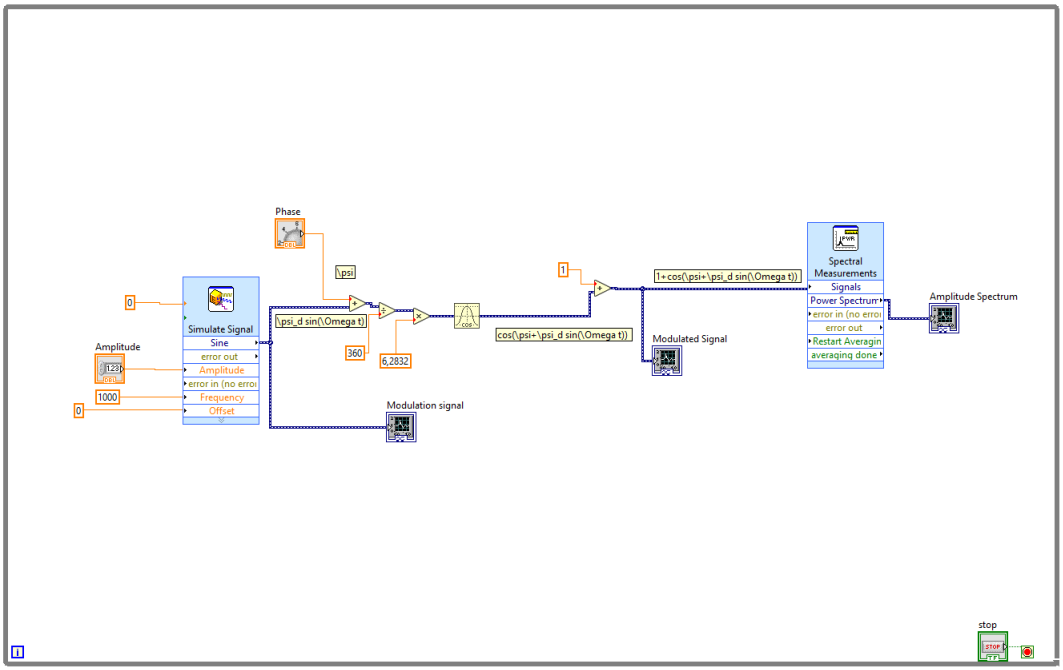

Figure 1.9: Block diagram of a simulation that calculates the spectrum of the function $f(t) = 1 + \cos(\psi + \psi_\mathrm{d} \sin(\Omega t))$

$$P_\mathrm{s} = R \cdot \left[\frac{1}{T}\int_0^T u(t) \cdot i(t)\mathrm{d}t\right] = R \cdot \left[\frac{1}{T}\int_0^T s(t) \cdot \frac{s(t)}{R}\mathrm{d}t\right] = \left[\frac{1}{T}\int_0^T s^2(t)\mathrm{d}t\right]. \tag{1.40}$$

We are working with a periodic signal so that it can be represented as a Fourier-series (single sided)

$$s(t) = C_0 + \sum_{n=1}^{\infty} C_n \cdot \cos(\Omega_n t), \tag{1.41}$$

where C_0 is the DC value and calculated as

$$C_0 = \frac{1}{T}\int_0^T s(t)\mathrm{d}t. \tag{1.42}$$

The power in the frequency domain is the sum of powers of all its components

$$P_\mathrm{s} = C_0^2 + \sum_{n=1}^{\infty} P_n = C_0^2 + \sum_{n=1}^{\infty} \frac{C_n^2}{2} = C_0^2 + \frac{C_1^2}{2} + \frac{C_2^2}{2} + \ldots \tag{1.43}$$

Now we can start the simulation for different ψ_d. As said, we set $\psi = \frac{\pi}{4}$ so that splitting up Eq. (1.9) into the Bessel coefficients yields

Die approbierte gedruckte Originalversion dieser Diplomarbeit ist an der TU Wien Bibliothek verfügbar.
The approved original version of this thesis is available in print at TU Wien Bibliothek.
TU Bibliothek Your knowledge hub WIEN

$$\frac{I}{2I_0} = 1 + \frac{1}{\sqrt{2}}\left(J_0(\psi_\mathrm{d}) - 2J_1(\psi_\mathrm{d})\sin(\Omega t) + 2J_2(\psi_\mathrm{d})\cos(2\Omega t) + ...\right), \tag{1.44}$$

which means for the signal power:

$$\frac{P_\mathrm{s}}{P_0} = \left(1 + \frac{1}{\sqrt{2}}J_0(\psi_\mathrm{d})\right)^2 + \frac{J_1^2(\psi_\mathrm{d})}{2} + \frac{J_2^2(\psi_\mathrm{d})}{2} + ... \tag{1.45}$$

This shows us that, as a result, we should get peaks at the zero frequency and at he multiple of the modulation frequency Ω depending on the modulation index ψ_d. Figure 1.10 shows the results of the spectral analysis of the equation. We can see that for $\psi_\mathrm{d} = 0°$ there is only one peak at the zero point of the spectrum. With increasing modulation index ψ_d, the first peak appears at $f = 1000\,\mathrm{Hz}$. With further increasing of ψ_d the second peak at $f = 2000\,\mathrm{Hz}$ appears. We can also see that the J_0 value is decreasing. At around $\psi_\mathrm{d} = 100°$, J_1 reaches its maximum. At around $\psi_\mathrm{d} = 150°$, J_1 and J_2 are equal. With higher ψ_d, peaks at frequencies of integer multiples of $1000\,\mathrm{Hz}$ start appearing. Because we are working with J_1 and J_2 we want to make them as high as possible. The target modulation index would be around 150° (2.62 rad) where $J_1 = J_2$. However, this is not possible, because of instrumental limitations so a different value needs to be chosen.

Die approbierte gedruckte Originalversion dieser Diplomarbeit ist an der TU Wien Bibliothek verfügbar.
The approved original version of this thesis is available in print at TU Wien Bibliothek.

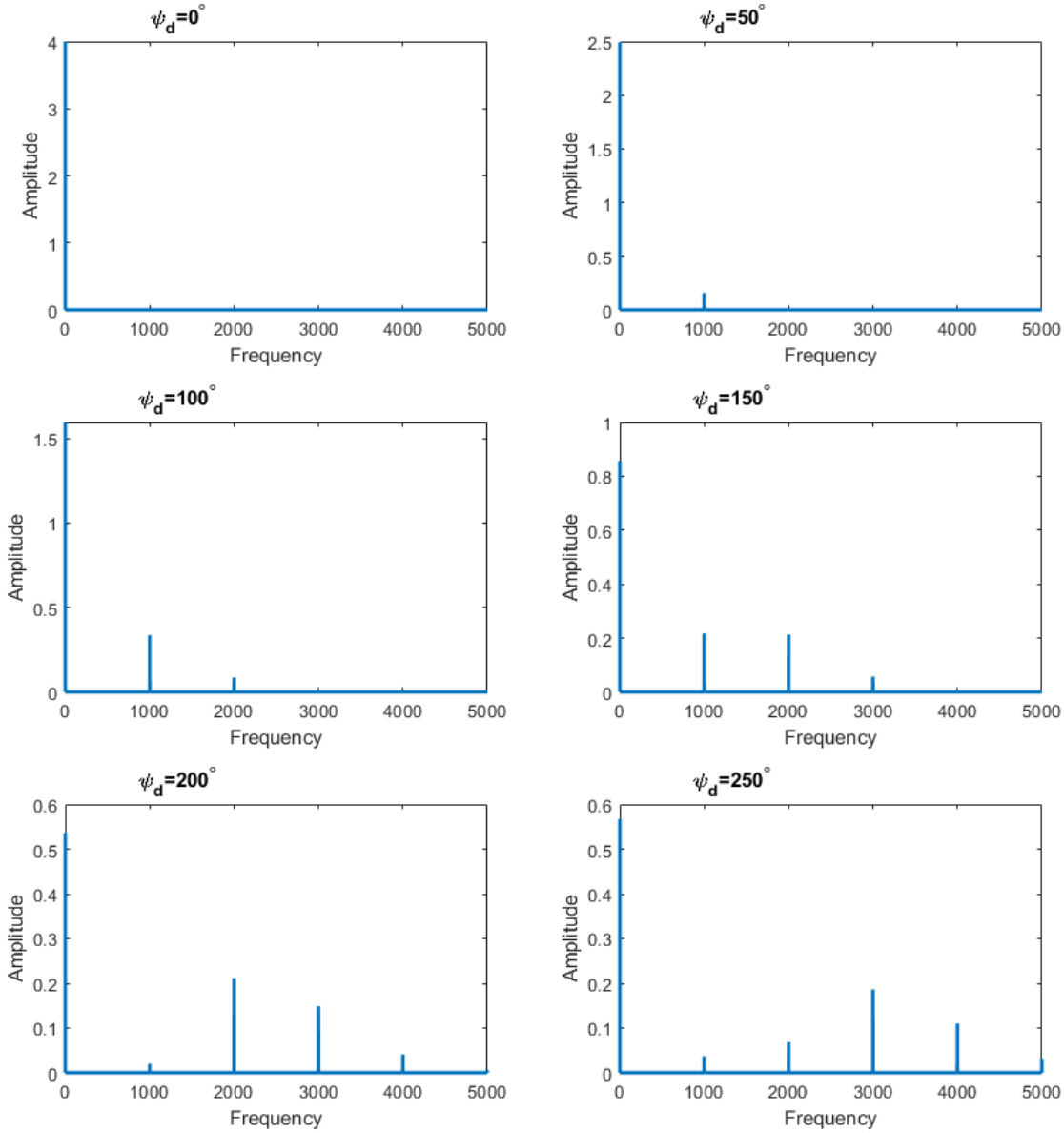

Figure 1.10: Results of the frequency domain simulation of the equation $f(t) = 1 + \cos(\psi + \psi_{\mathrm{d}} \sin(\Omega t))$ for different modulation strengths.

Die approbierte gedruckte Originalversion dieser Diplomarbeit ist an der TU Wien Bibliothek verfügbar.
The approved original version of this thesis is available in print at TU Wien Bibliothek.

1.4 Measurement system

The measurement system takes the signal from the photodiode and converts it into an information about the amplitude of the electric field to be measured. First the photodiode converts the intensity of the light into current which is treansformed into a voltage via a transimpedance amplifier [9]. It is described as

$$U(t) = KI(t), \tag{1.46}$$

where K is a proportionality constant. As mentioned in the previous chapters the intensity at the photodiode is described with the equation

$$I = I_1 + I_2 + 2\sqrt{I_1 I_2}\cos(\Delta\varphi). \tag{1.47}$$

For $\Delta\varphi = 0$ the maximum intensity at the detector is

$$I_{\max} = I_1 + I_2 + 2\sqrt{I_1 I_2} = (\sqrt{I_1} + \sqrt{I_2})^2, \tag{1.48}$$

and for $\Delta\varphi = \pi$ the minimum intensity

$$I_{\min} = I_1 + I_2 + 2\sqrt{I_1 I_2} = (\sqrt{I_1} - \sqrt{I_2})^2. \tag{1.49}$$

We now can rewrite Eq. (1.47) and yield

$$I = \frac{1}{2}(I_{\max} - I_{\min})[1 + \cos(\Delta\varphi)] + I_{\min}. \tag{1.50}$$

After the intensity is transformed into voltage by the photo diode we get:

$$U = \frac{\Delta U}{2}[1 + \cos(\Delta\varphi)] + U_{\min}, \tag{1.51}$$

where $\Delta U = U_{\max} - U_{\min}$. If an electric field is applied to the transducer it will start oscillating which will result in a modulation of the phase as described in section 1.3. This leads us to the final equation for the voltage

$$U(t) = \frac{\Delta U}{2}[1 + \cos(\psi + \psi_{\mathrm{d}}\sin(\Omega t))] + U_{\min}. \tag{1.52}$$

Analysing this equation in time domain, as in Figure 1.7, that we get an oscillation signal around a constant DC value which is called the working point. To achieve the best results out of the measurement we want to set our working point to region of the highest sensitivity.

Die approbierte gedruckte Originalversion dieser Diplomarbeit ist an der TU Wien Bibliothek verfügbar.
The approved original version of this thesis is available in print at TU Wien Bibliothek.
TU WIEN Bibliothek Your knowledge hub

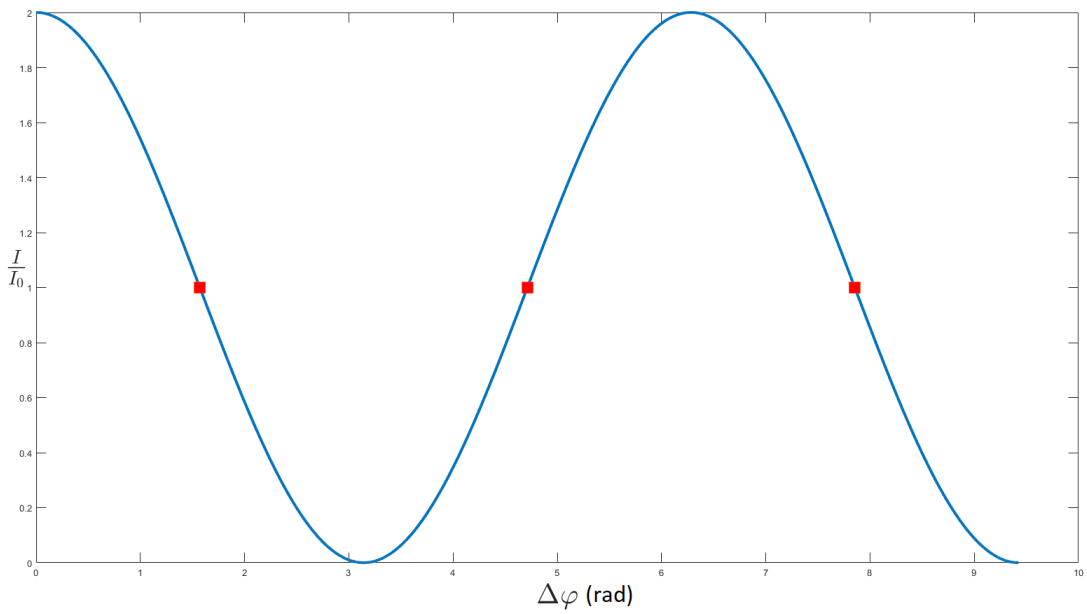

Figure 1.11: Points on the intensity diagram with highest sensitivity

The interferometer will be most sensitive to changes in phase when $\frac{\mathrm{d}U}{\mathrm{d}\Delta\varphi}$ is maximum, as shown in Fig. 1.11. Since

$$\frac{\mathrm{d}U}{\mathrm{d}\Delta\varphi} = -\frac{\Delta U}{2}\sin(\Delta\varphi), \tag{1.53}$$

The best measuring sensitivity is reached for $\Delta\varphi = \left(n + \frac{1}{2}\right)\pi$ where $n = 1, 2, 3...$. To express the relation between change in voltage and change in mirror position we need to convert the change in phase to change in position with

$$\Delta\varphi = 2k\Delta l = \frac{4\pi\Delta l}{\lambda}. \tag{1.54}$$

For very small changes in δlwe can assume that $\sin(\Delta\varphi) \approx \Delta\varphi$. Inserting this into Eq. (1.53), the magnitude of the maximum is

$$\left|\frac{\mathrm{d}U}{\mathrm{d}\Delta l}\right|_{\max} = \frac{2\pi\Delta U}{\lambda}. \tag{1.55}$$

Rewriting this equation to express the dependence of voltage regarding the displacement gives us

Die approbierte gedruckte Originalversion dieser Diplomarbeit ist an der TU Wien Bibliothek verfügbar.
The approved original version of this thesis is available in print at TU Wien Bibliothek.
TU Bibliothek Your knowledge hub WIEN

$$\mathrm{d}U = \frac{2\pi\Delta U}{\lambda}\mathrm{d}\Delta l. \tag{1.56}$$

For λ in in the nanometer or micrometer region it will be possible to measure displacements in these orders of magnitude and get reasonable changes in voltage.

Die approbierte gedruckte Originalversion dieser Diplomarbeit ist an der TU Wien Bibliothek verfügbar.
The approved original version of this thesis is available in print at TU Wien Bibliothek.
TU WIEN Bibliothek Your knowledge hub

Die approbierte gedruckte Originalversion dieser Diplomarbeit ist an der TU Wien Bibliothek verfügbar.
The approved original version of this thesis is available in print at TU Wien Bibliothek.

Chapter 2

Stabilization

As seen in Chapter 1, there are three variables describing the measurement system: mirror position described by the phase ψ, the modulation index of the transducer ψ_d and the modulation frequency Ω. For the measurement system to work properly we need to know the position of the phase ψ and the frequency Ω. The only variable left is the modulation index ψ_d which contains the information about the electric field strength we want to measure. In a perfect system without noise, we would need to measure the intensity of the interferometer to move the mirrors to the desired positions so that we get the phase ψ. The relation between the phase and the intensity (without the modulation) is related in the equation

$$I = I_1 + I_2 + 2\sqrt{I_1 I_2}\cos(\psi). \tag{2.1}$$

If we introduce noise from different sources (temperature, vibrations, air movement and etc.), the position of the mirrors can change. Now that a stochastic process determines the position of the mirrors, the measurement loses its quality or the measurement is made impossible depending on the power of the noise. Figure 2.1 shows a block diagram of the system, where $x(t)$ and $n(t)$ are the input variables of the Michelson interferometer and $I(t)$ is the output parameter, in this case the intensity at the detector, which is then converted with a photodiode into a voltage $U(t)$, the input of the measuring system.

The first input variable $x(t)$ is the length difference between the 2 arms of the interferometer Δl, or in other words the position of the measuring mirror relative to the reference mirror

$$\Delta l = L_2 - L_1 = L + x(t) - L = x(t), \tag{2.2}$$

where L is the distance of the reference mirror to the beam splitter. The second variable

Die approbierte gedruckte Originalversion dieser Diplomarbeit ist an der TU Wien Bibliothek verfügbar.
The approved original version of this thesis is available in print at TU Wien Bibliothek.
TU WIEN Bibliothek Your knowledge hub

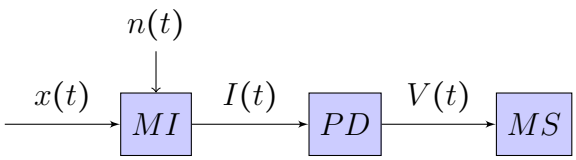

Figure 2.1: Block diagram of the interferometer with the measurement system. Input of the interferometer are the position of the mirror $x(t)$ and the noise $n(t)$. MI-Michelson interferometer, PD-Photo diode, MS-Measurement system

$n(t)$ is the random noise introduced to the system. It will cause changes in the position of the mirrors. Consequently $x(t)$ and $n(t)$ have an additive relation. Therefore resulting position of the mirror is

$$x_{\mathrm{r}}(t) = x(t) + n(t). \tag{2.3}$$

Since the relation between the displacement and phase is linear for small displacements the resulting phase is

$$\psi_{\mathrm{r}} = \frac{4\pi x_{\mathrm{r}}(t)}{\lambda} = \frac{4\pi x(t)}{\lambda} + \frac{4\pi n(t)}{\lambda} = \psi + \psi_{\mathrm{n}}, \tag{2.4}$$

where ψ is the displacement caused by our movement of the mirror and ψ_{n} the phase caused by random noise.

2.1 Control theory

One way to overcome the problem with the noise generated phase drift is to measure the drift and to subtract it from the input via a feedback loop [5, 10]. Hence, the resulting input for the displacement of the mirror is

$$x_{\mathrm{r}}(t) = x(t) - n(t) + n(t) = x(t). \tag{2.5}$$

However, since after compensating the deviation, the system will measure no deviation in the next iteration step and will drift back to the previous state. We can prove this mathematically and with a simulation. Figure 2.2 depicts the simulation set up in Simulink of a simplified and linearised version of our system where the transfer function of the interferometer is set to $G_{\mathrm{I}} = 1$. We have u as the input of the system, n as the noise and y as the output. The output and input are coupled with a feedback as described before that

Die approbierte gedruckte Originalversion dieser Diplomarbeit ist an der TU Wien Bibliothek verfügbar.
The approved original version of this thesis is available in print at TU Wien Bibliothek.
TU Bibliothek Your knowledge hub WIEN

only measures the noise n so it subtracts the input value from the output. Putting this system into equations we get for the output

$$y = e + n, \tag{2.6}$$

where e is the output of the subtracter. We can calculate e as

$$e = u - y + u = 2u - y, \tag{2.7}$$

and insert it into the equation for y and yielding

$$y = 2u - y + n. \tag{2.8}$$

The final equation for the output is therefore

$$y = u + \frac{n}{2}. \tag{2.9}$$

It is obvious that we compensated the error only by the half but did not eliminate it. Figure 2.3 shows the simulation results for $u = 3\varepsilon(t)$ and $n = \varepsilon(t-1)$, where ε represents the step function. We can see that before introducing noise $y = 3$ and after noise introduction $y = 3.5$ which validates our equations. This problem is called steady-state problem of the proportional controller. It is characteristic of systems with just a proportional controller. The proportional controller has a transfer function

$$G_{\mathrm{C}} = K_{\mathrm{P}}, \tag{2.10}$$

where K_{P} is the gain. For the the calculations we have done we can imagine that we had a proportional controller with a transfer function $G_{\mathrm{C}} = 1$.

A solution for this problem would be to introduce a PI controller. The PI controller has a proportional and integrating element in parallel. The transfer function of the PI controller will be

$$G_{\mathrm{C}} = K_{\mathrm{P}} + K_{\mathrm{I}}\frac{1}{s}, \tag{2.11}$$

where K_{I} is the gain of the integrating element and s the complex angular frequency. The integrating element has the property to accumulate the error over time so the output of the system system will stay at the same point after it equalizes with the input. For our system to work we will need to make a slight change. Now with the integrating element the

Die approbierte gedruckte Originalversion dieser Diplomarbeit ist an der TU Wien Bibliothek verfügbar.
The approved original version of this thesis is available in print at TU Wien Bibliothek.
TU Bibliothek WIEN Your knowledge hub

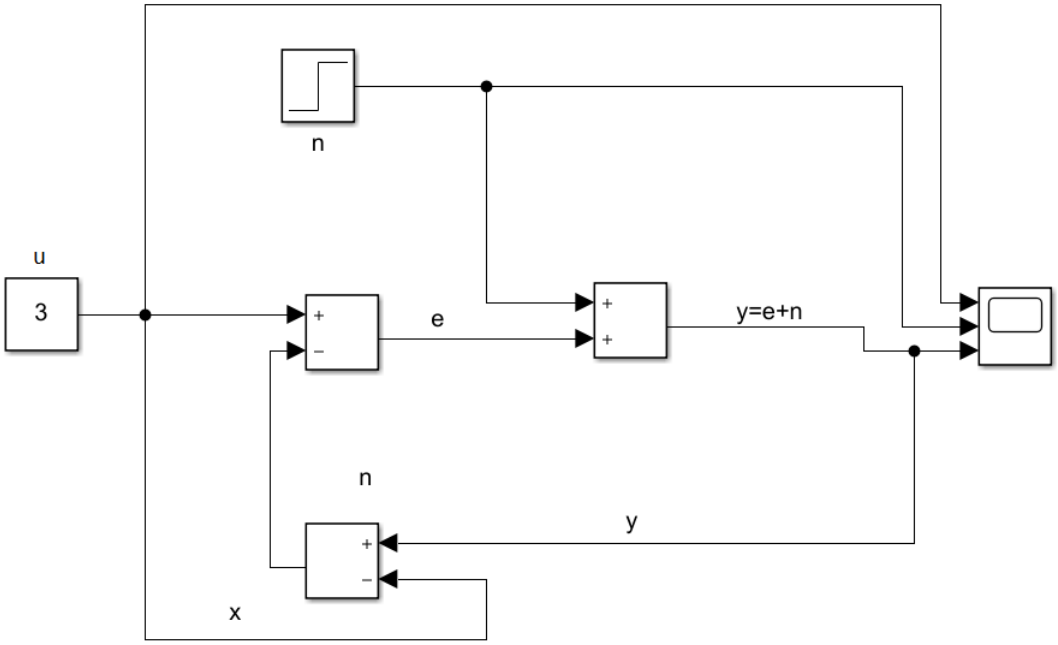

Figure 2.2: Simulink model of the feedback where the noise source is a step function and the mirror position is a constant value.

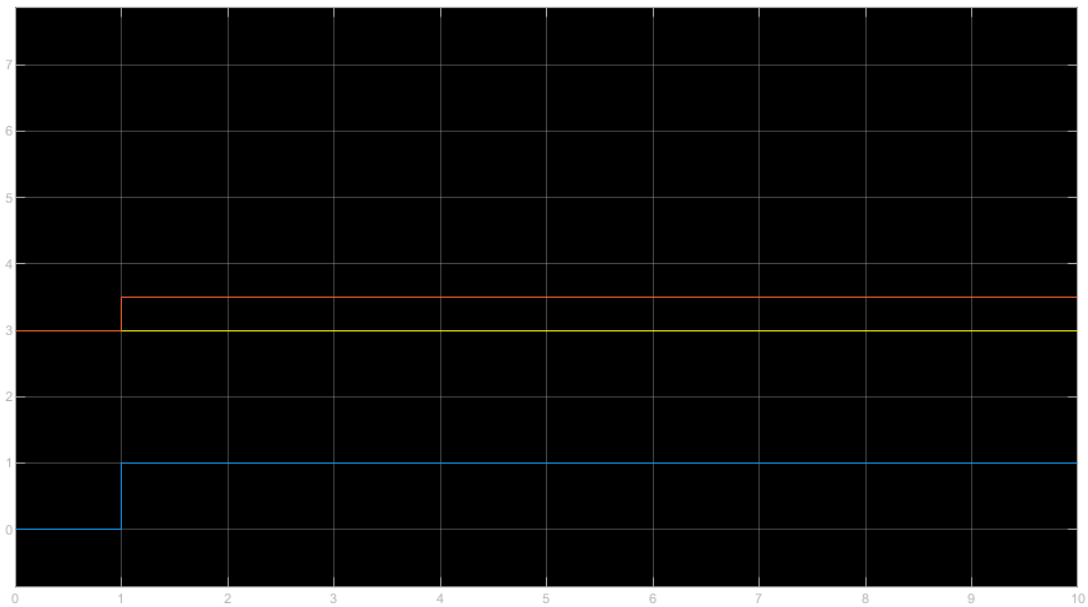

Figure 2.3: Results of the Simulink simulation. It shows that a feedback alone will reduce the noise but not cancel it all the way out. Yellow line represents the input, orange the output and the blue line the noise

Die approbierte gedruckte Originalversion dieser Diplomarbeit ist an der TU Wien Bibliothek verfügbar.
The approved original version of this thesis is available in print at TU Wien Bibliothek.

output will settle to a steady state only when $e = 0$. Because for our previous configuration $e = 2u - y + n$, e will be zero for $y = 2u$. We will remove the subtraction of u in the feedback. Now the system in our simulation in Simulink will look like in Fig. 2.4. The input of the system u is the output of the controller and the output of the system is subtracted from the a value which is called the set point r. It is the desired value or target value of an essential variable, in this case the output of the system y. Note that for demonstration purposes we have set the transfer function of the interferometer to $G_I = 1$ for now, which will be evaluated in the following chapter. In this chapter the focus is on the controller. To validate our assumptions mathematically we will use a more sophisticated and general method than before. We will use the final value theorem of the Laplace transformation, [5], that says

$$e_\infty = \lim_{t\to\infty} e(t) = \lim_{s\to 0} sE(s). \tag{2.12}$$

Because we are working with an LTI (linear time invariant) system we can look at the output of the system as a superposition of the two inputs. In the first case we assume that $r(t) = 3\varepsilon(t)$ and $n(t) = 0$. Our measurement error in Laplace domain will be

$$E(s) = R(s) - Y(s), \tag{2.13}$$

and the output

$$Y(s) = E(s)G_\mathrm{C}(s)G_\mathrm{I}(s), \tag{2.14}$$

Solving this two equations for $E(s)$ gives us

$$E(s) = \frac{1}{1 + G_\mathrm{C}G_\mathrm{I}} R(s). \tag{2.15}$$

Inserting it back to Eq. (2.12) will give us the final value

$$e_\infty = \lim_{s\to 0} s \frac{1}{1 + \frac{1}{s}G_\mathrm{I}} 3\frac{1}{s} = 0. \tag{2.16}$$

This proves that for a step function in the input, our output will reach a steady state value that is equal to the input. In the second case, we set $x(t) = 0$ and $n(t) = \varepsilon$. Now we have slightly different equations, because the noise is added behind the controller. Our measurement error in Laplace domain will be

Die approbierte gedruckte Originalversion dieser Diplomarbeit ist an der TU Wien Bibliothek verfügbar.
The approved original version of this thesis is available in print at TU Wien Bibliothek.
TU Bibliothek WIEN Your knowledge hub

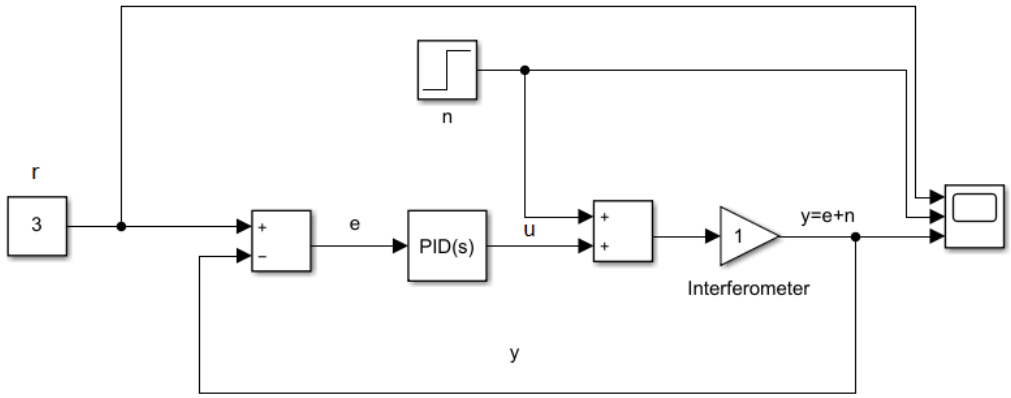

Figure 2.4: Simulink model of the feedback where the noise source is a step function and the mirror position is a constant value with added PI controller. The transfer function of the interferometer is for now set to $G_I = 1$ and will be evaluated in the following chapters (PI controller in simulink can be obtained by defining the differential coefficient of a PID controller to zero.

$$E(s) = -Y(s), \tag{2.17}$$

and the output

$$Y(s) = E(s)G_{\mathrm{C}}(s)G_{\mathrm{I}}(s) + N(s)G_{\mathrm{I}}(s). \tag{2.18}$$

Solving this equations for $E(s)$ and inserting them back to equation (2.12) will give us

$$e_\infty = \lim_{s\to 0} s \frac{G_{\mathrm{I}}}{1 + \frac{1}{s}G_{\mathrm{I}}} \frac{1}{s} = 0. \tag{2.19}$$

This means that for the input value equal to zero and added noise, the output will come to a steady state also equal to zero. Figure 2.5 shows the simulation of the system that verifies our mathematical model. The noise is added at an offset of $T_0 = 20\,\mathrm{s}$ for better visualization. Now that we know that for our feedback system a controller is needed, a more complete system block diagram can be drawn. For the system to work two new blocks need to be introduced: An actuator that will convert a voltage signal of the output of the PID to a movement of the mirror and a feedback measurement system that can measure the phase ψ that needs to be stabilized. Figure 2.6 shows the system with the added blocks.

Die approbierte gedruckte Originalversion dieser Diplomarbeit ist an der TU Wien Bibliothek verfügbar.
The approved original version of this thesis is available in print at TU Wien Bibliothek.
TU Bibliothek Your knowledge hub WIEN

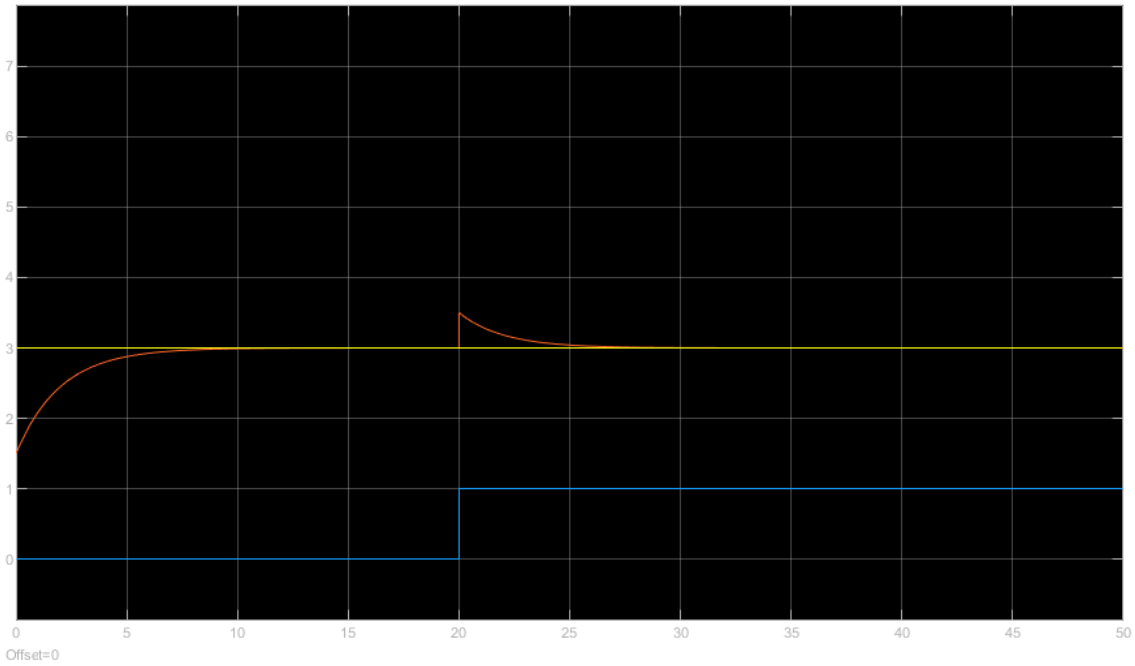

Figure 2.5: Results of the simulink simulation with PI controller. It shows that the integrating element solves the steady state problem of the proportional element. Yellow line represents the set point, orange the output and the blue line the noise

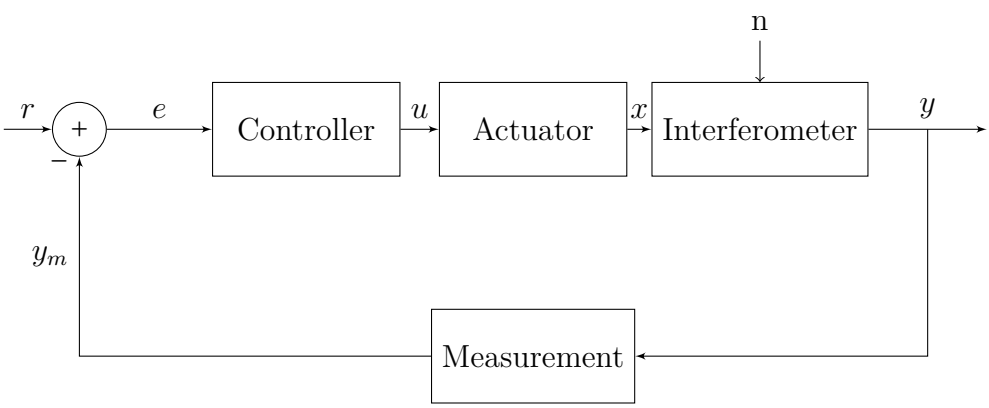

Figure 2.6: Representation of the system with feedback and controller

Die approbierte gedruckte Originalversion dieser Diplomarbeit ist an der TU Wien Bibliothek verfügbar.
The approved original version of this thesis is available in print at TU Wien Bibliothek.
TU WIEN Bibliothek Your knowledge hub

2.2 Actuator

An actuator is a component of a system to allow the controller to act on a system upon an environment. In our case, it transforms the low-energy control signal from the controller into via mechanical motion. To perform this operation the actuator needs to be connected to an energy source, because the low-energy signal from the controller is not enough. The actuator system used for our measurements consists of a high-voltage amplifier and a piezoelectric element [10] as shown in Fig. 2.7. The piezoelectric element is used for the reference mirror of our system. By applying a voltage $V(t)$ to the piezoelectric element, the mirror moves by the distance $x(t)$. We have determined empirically that the piezo is linear in the voltage range we drive it. Therefore, the displacement of the mirror is

$$x(t) = K_{\mathrm{AC}} V(t), \tag{2.20}$$

where $K_{\mathrm{AC}} = 16,4\,\frac{\mathrm{nm}}{\mathrm{V}}$ is the proportionality constant of the piezo actuator. It is important to know that the piezoelectric element cannot tolerate negative voltages. If we want to drive it with a sinusoid voltage we need to make sure that the DC offset V_{DC} is larger than the amplitude of the driving voltage. The high-voltage amplifier converts the low-power control signal into a high-power signal that can drive the piezoelectric element. The three signals (DC voltage, driving AC voltage and the feedback voltage) and have to be added and feed the piezoelectric element.

The circuit required is an adder circuit [7]. Left part of Fig. 2.8 (first op-amp circuit) shows an inverting adder circuit. The output voltage of the adder is

$$V_{\mathrm{out}} = -\left(V_{\mathrm{in1}}\frac{R_4}{R_1} + V_{\mathrm{in2}}\frac{R_4}{R_2} + V_{\mathrm{in3}}\frac{R_4}{R_3}\right). \tag{2.21}$$

As we can see the result is a negative voltage. Since the voltage needs to be positive, an additional inverting amplifier is added, which is shown in the right part of Fig. 2.8. The output voltage of the inverter will be

$$V_{\mathrm{out}} = V_{\mathrm{in}}\frac{R_6}{R_5}. \tag{2.22}$$

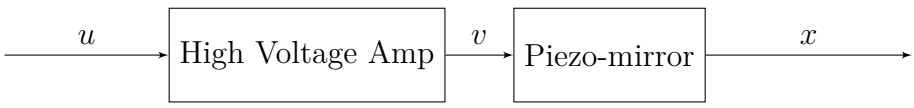

Figure 2.7: Block diagram representation of the actuator system

Die approbierte gedruckte Originalversion dieser Diplomarbeit ist an der TU Wien Bibliothek verfügbar.
The approved original version of this thesis is available in print at TU Wien Bibliothek.
TU Bibliothek Your knowledge hub WIEN

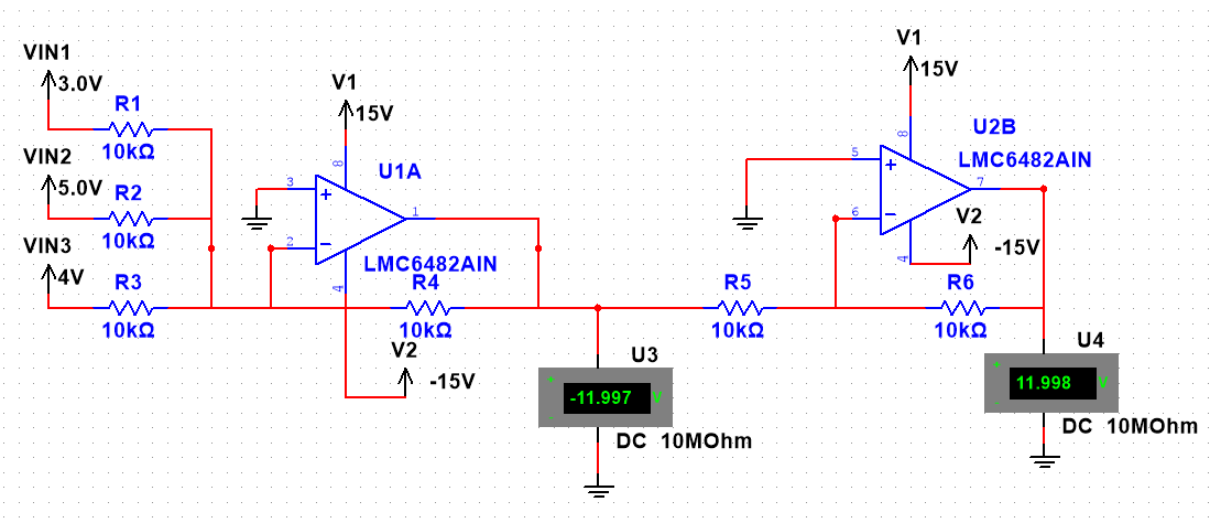

Figure 2.8: A Multisim schematic of the inverting adder circuit

Simulating the circuit in Multisim we get the results from Fig. 2.9. It shows us that the circuit has in the low frequency ranges linear behaviour with a negligible phase shift. Consequently we can describe our actuator system fully with a transfer function. For the input $u_\mathrm{i}(t)$ and output $x(t)$ the transfer function is

$$G_{\mathrm{AC,i}}(s) = \frac{X(s)}{U_\mathrm{i}(s)} = K_\mathrm{AC}\frac{R_4 R_6}{R_i R_5}, \tag{2.23}$$

or if we transform the displacement into phase

$$G_{\mathrm{AC,i}}(s) = \frac{\psi(s)}{U_\mathrm{i}(s)} = K_\mathrm{AC}\frac{4\pi R_4 R_6}{\lambda R_i R_5}. \tag{2.24}$$

Die approbierte gedruckte Originalversion dieser Diplomarbeit ist an der TU Wien Bibliothek verfügbar.
The approved original version of this thesis is available in print at TU Wien Bibliothek.

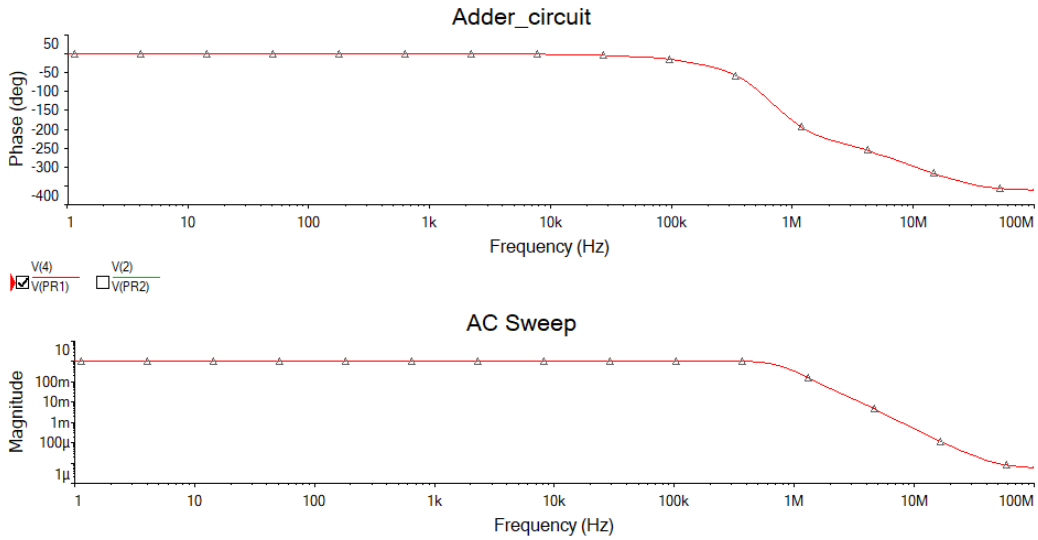

Figure 2.9: Magnitude and phase bode plots of the adder circuit showing a linear behaviour in the low-voltage range. Phase shift caused by the circuit is negligible, at 1 kHz we have a phase shift of −0.15° and at 10 kHz a phase shift of −1.5°

2.3 Feedback

For being able to compensate the phase shift caused by the noise, we need to measure the phase of the signal. As said in the beginning of the chapter, we have three variables we are dealing with: the phase shift of the mirror ψ, modulation index ψ_d and modulation frequency Ω. To be able to measure the phase ψ we need to have a signal in our system with known modulation index and frequency. We can generate this signal artificially by driving one of the inputs of the actuator system with a sinusoid signal. The actuator system is an LTI system. With an input $u(t)$ that can be described by a linear operation of e^{st}, the particular solution of the output can be described by the same linear operation applied on $G(s)\mathrm{e}^{st}$ [6],

$$u(t) = L\left[\mathrm{e}^{st}\right] \rightarrow y_\mathrm{p}(t) = L\left[G(s)\mathrm{e}^{st}\right]. \tag{2.25}$$

If we drive our actuator with a voltage

$$V = \hat{V}\cos(\Omega t + \theta) = \mathrm{Re}\left\{\underline{V}\mathrm{e}^{\mathrm{j}\Omega t}\right\}, \tag{2.26}$$

the output described in phase will be

$$\psi_\mathrm{AC} = \mathrm{Re}\left\{G_\mathrm{AC}(\mathrm{j}\Omega)\underline{V}\mathrm{e}^{j\Omega t}\right\} = \psi_\mathrm{d}\cos(\Omega t + \theta). \tag{2.27}$$

Die approbierte gedruckte Originalversion dieser Diplomarbeit ist an der TU Wien Bibliothek verfügbar.
The approved original version of this thesis is available in print at TU Wien Bibliothek.
TU Bibliothek WIEN Your knowledge hub

We now can calculate the modulation index as

$$\psi_{\mathrm{d}} = \mathrm{Re}\left\{G_{\mathrm{AC}}(\mathrm{j}\Omega)\underline{V}\right\} = \hat{V} K_{\mathrm{AC}} \frac{4\pi R_4 R_6}{\lambda R_1 R_5}, \tag{2.28}$$

assuming the voltage is connected to the first input of the adder. As discussed in the previous chapter, the oscillation of the reference mirror will result in a phase modulation of the signal. The signal at the detector is described by the Bessel functions Eq. (1.35). The peaks we will use in our feedback system will be at Ω and 2Ω. Their intensities at the detector will be

$$I_{\Omega} = 4J_1(\psi_{\mathrm{d}})\sqrt{I_1 I_2}\sin(\psi)\sin(\Omega t) \tag{2.29}$$

$$I_{2\Omega} = 4J_2(\psi_{\mathrm{d}})\sqrt{I_1 I_2}\cos(\psi)\cos(2\Omega t). \tag{2.30}$$

The optical element of the detector has a gain $G_{\mathrm{O}} = K_{\mathrm{O}}$, where K_{O} is a constant characteristic for the detector. We can define the voltages of the two signals coming out of the detector as

$$V_1 = K_{\mathrm{O}} 4J_1(\psi_{\mathrm{d}})\sqrt{I_1 I_2}\sin(\psi)\sin(\Omega t) = \hat{V}_1 \sin(\psi)\sin(\Omega t) \tag{2.31}$$

$$V_2 = K_{\mathrm{O}} 4J_2(\psi_{\mathrm{d}})\sqrt{I_1 I_2}\cos(\psi)\cos(2\Omega t) = \hat{V}_2 \cos(\psi)\cos(2\Omega t). \tag{2.32}$$

These equations show us that now the information about the phase lies in amplitude of our signals and not in the phase. Such signals can be generated by multiplying an amplitude with a carrier signal

$$s(t) = A(t)\cos(\Omega t). \tag{2.33}$$

In order to reconstruct the amplitude on the receiver end, we need to multiply the signal with a reference signal of the same frequency as the carrier [4, 8]

$$s_r = s(t) * \cos(\Omega t) = \frac{1}{2}[A(t) + A(t)\cos(2\Omega t)]. \tag{2.34}$$

The doubled frequency part of the signal is eliminated by a low-pass filter, so we get a signal with the half amplitude

Die approbierte gedruckte Originalversion dieser Diplomarbeit ist an der TU Wien Bibliothek verfügbar.
The approved original version of this thesis is available in print at TU Wien Bibliothek.
TU WIEN Bibliothek Your knowledge hub

$$\overline{s}_r = \frac{1}{2}A(t). \tag{2.35}$$

This principle is simple, but the down side of it is that it can not tolerate phase differences between the carrier and the reference signal at the receiver. Considering such a phase difference θ, we get a more general definition of our signal

$$s(t) = A(t)\cos(\Omega t + \theta(t)). \tag{2.36}$$

Writing this signal as the real part of a rotating phaser and isolating the information carrying parts we get

$$s(t) = A(t)\cos(\Omega t + \theta(t)) = \mathrm{Re}\left\{A(t)\mathrm{e}^{\mathrm{j}\Omega t + \mathrm{j}\theta(t)}\right\} = \mathrm{Re}\left\{\underline{\tilde{s}}\mathrm{e}^{\mathrm{j}\Omega t}\right\}, \tag{2.37}$$

with the complex envelope of the signal

$$\underline{\tilde{s}} = A(t)\mathrm{e}^{\mathrm{j}\theta(t)}. \tag{2.38}$$

Figure 2.10 shows a visual representation of a signal with its complex envelope. Applying Euler's formula $\mathrm{e}^{\mathrm{j}\theta} = \cos(\theta) + \mathrm{j}\sin(\theta)$ we get

$$\underline{\tilde{s}} = A(t)e^{j\theta} = A(t)\cos(\theta(t)) + jA(t)\sin(\theta(t)) = s_{\mathrm{I}}(t) + js_{\mathrm{Q}}(t). \tag{2.39}$$

This splits the signal into two orthogonal components which are called quadrature components. The real part is called the in-phase component I and the imaginary form the quadrature component Q. A phaser diagram using these components is often called an I/Q-Diagram. Now we can express our signal in the I/Q-representation as

$$s(t) = \mathrm{Re}\left\{[s_{\mathrm{I}}(t) + \mathrm{j}s_{\mathrm{Q}}(t)] \cdot [\cos(\Omega t) + \mathrm{j}\sin(\Omega t)]\right\} = s_{\mathrm{I}}(t)\cos(\Omega t) - s_{\mathrm{Q}}(t)\sin(\Omega t). \tag{2.40}$$

This expression shows how a general Modulator/Demodulator structure for amplitude and phase modulated signals looks like. Figure 2.11 shows us from the I/Q-representation resulting modulator and demodulator which is also known as the quadrature modulator. The quadrature demodulator splits the signal into its quadrature components. If the detection is coherent (the carrier and the reference signals are in phase) $s_{\mathrm{I}} = A$ and $s_{\mathrm{Q}} = 0$. Therefore, the signal can be described with only the I-part of the modulator. For incoherent detection s_{I}

Die approbierte gedruckte Originalversion dieser Diplomarbeit ist an der TU Wien Bibliothek verfügbar.
The approved original version of this thesis is available in print at TU Wien Bibliothek.
TU Bibliothek Your knowledge hub WIEN

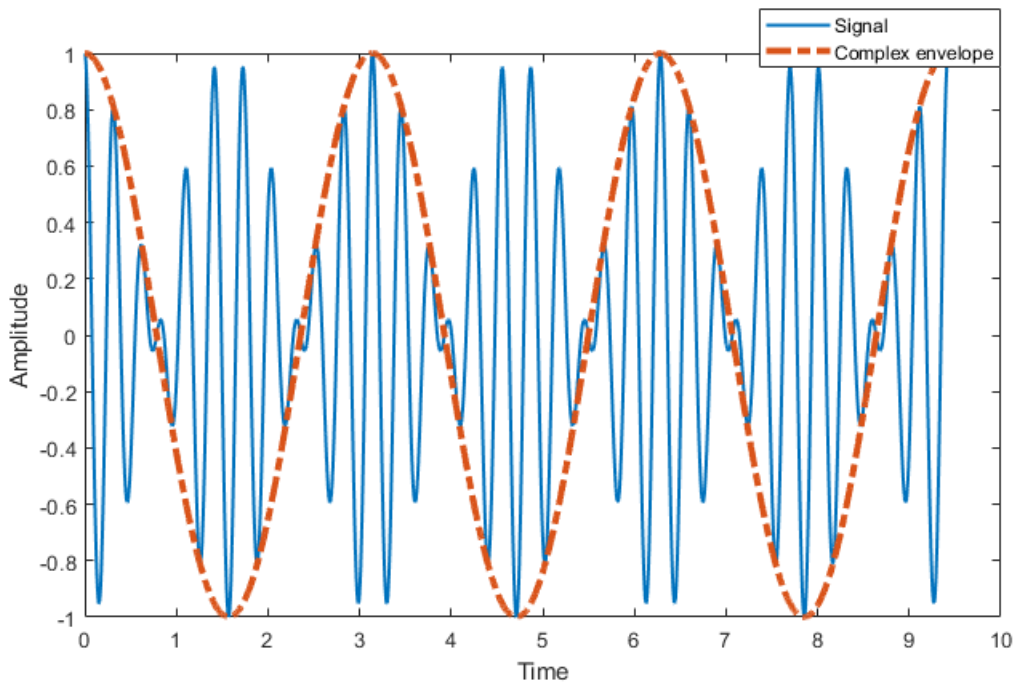

Figure 2.10: The complex envelope of a signal with a sinusoid amplitude $A(t) = \cos(2t)$ and a carrier $\cos(20t)$.

represents the amplitude projection on the I-axis and s_Q represents the amplitude projection on the Q-axis. By squaring those signals and adding them together we get

$$(A\cos(\theta))^2 + (A\sin(\theta))^2 = A^2. \tag{2.41}$$

Applying this method to V_1 Eq. 2.31 yields

$$A^2 = (\hat{V}_1 \sin(\psi))^2, \tag{2.42}$$

from which the signal amplitude follows by taking the square root.

Building such a feed back and connecting it to the input of the controller would bring some limitations with it. The output of the feedback is a nonlinear sinusoid function, and we need to linearise it around a certain working point of our choice. The working point will be the reference of the controller and will have the form $\sin(\theta)$. The sensitivity of our feedback is defined as

$$\frac{\mathrm{d}V_1}{\mathrm{d}\psi} = \hat{V}_1 \cos(\psi). \tag{2.43}$$

Die approbierte gedruckte Originalversion dieser Diplomarbeit ist an der TU Wien Bibliothek verfügbar.
The approved original version of this thesis is available in print at TU Wien Bibliothek.
TU Bibliothek Your knowledge hub WIEN

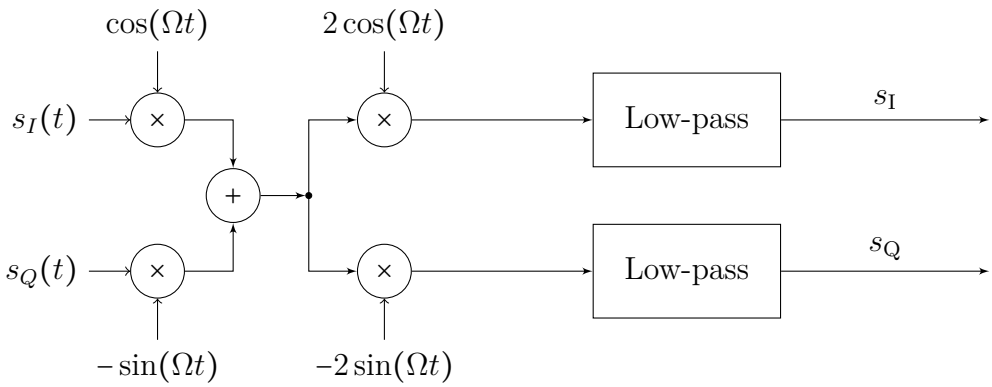

Figure 2.11: Block diagram representation of the Modulator/Demodulator system in quadrature representation

Thus, the maximum sensitivity of our feedback lies at $\psi = 0$ and the minimum at $\psi = \frac{\pi}{2}$. Therefore, setting our working point to be at $\psi = \frac{\pi}{2}$ would result in a strong reduction in sensitivity and instability of the system due to the highly nonlinear behaviour of the sine function. The solution of this problem would be to measure the error (deviation of the working point) and not the phase so that the output of the feedback would be $\sin(\psi - \theta)$. This approach has the benefit that the reference point of the controller is set to zero which for the sine function is the point of highest sensitivity and linearity. We can linearise a nonlinear function around a working point according to reference [5] with the expression

$$y_\mathrm{R} + \Delta y = h(x_\mathrm{R} + \Delta x, u_\mathrm{R} + \Delta u), \tag{2.44}$$

where y is the output, x the inner states of the system and u the input. Index R indicates the values of the variables in the working point. Expanding h into a Taylor series up to first order yields

$$y_\mathrm{R} + \Delta y = h(x_\mathrm{R}, u_\mathrm{R}) + \frac{\mathrm{d}}{\mathrm{d}x} h(x_\mathrm{R}, u_\mathrm{R}) \Delta x + \frac{\mathrm{d}}{\mathrm{d}u} h(x_\mathrm{R}, u_\mathrm{R}) \Delta u. \tag{2.45}$$

Since our system does not contain internal dynamic states, so we can set $x = 0$ and $x_\mathrm{R} = 0$. Because $y_\mathrm{R} = h(x_\mathrm{R}, u_\mathrm{R})$, we get the relation

$$\Delta y = \frac{\mathrm{d}}{\mathrm{d}u} h(u_\mathrm{R}) \Delta u. \tag{2.46}$$

Applying this to our feedback we will get

Die approbierte gedruckte Originalversion dieser Diplomarbeit ist an der TU Wien Bibliothek verfügbar.
The approved original version of this thesis is available in print at TU Wien Bibliothek.
TU Bibliothek WIEN Your knowledge hub

$$\Delta V_1 = \hat{V}_1 \cos\left(\frac{\pi}{2}\right) \Delta(\psi - \theta), \tag{2.47}$$

this results in a transfer function of the feedback

$$G_{\mathrm{F}}(s) = \frac{\Delta Y(s)}{\Delta U(s)} = \hat{V}_1. \tag{2.48}$$

Now the feedback needs to be redesigned to obtain our desired function as output. In this work two approaches will be covered. Both of them have their strengths and weaknesses depending on the use cases.

2.3.1 Hybrid demodulation approach

In the first approach, called hybrid demodulation approach.We demodulate the in-phase component of V_1 and the quadrature component of V_2. Figure 2.12 shows a block diagram of the system.

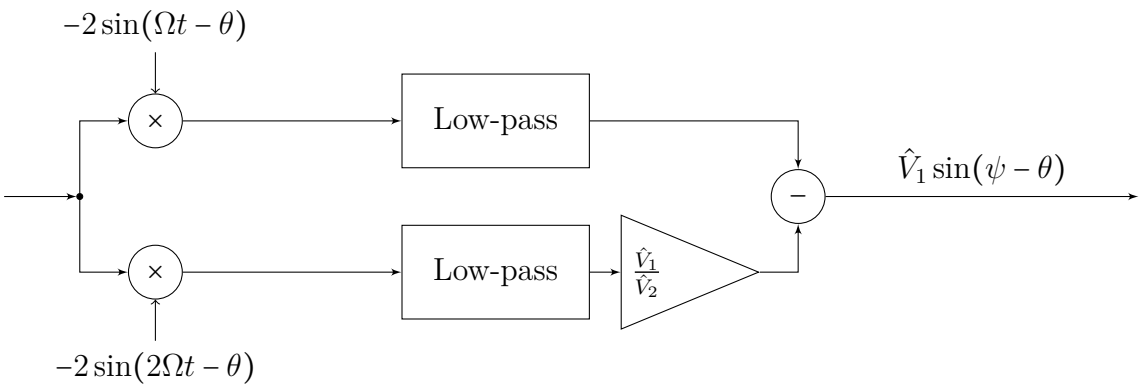

Figure 2.12: Block diagram representation of the hybrid demodulator system

Note that the first signal has the form

$$V_1 = -\hat{V}_1 \sin(\psi)\sin(\Omega t) = -\hat{V}_1 \sin(\psi)\cos\left(\Omega t - \frac{\pi}{2}\right). \tag{2.49}$$

By demodulation of the quadrature component of V_1 we will get at the output of the low-pass filter the signal

$$V_{\mathrm{L1}} = -\hat{V}_1 \sin(\psi)\sin\left(-\frac{\pi}{2} + \theta\right) = \hat{V}_1 \sin(\psi)\cos(\theta). \tag{2.50}$$

Die approbierte gedruckte Originalversion dieser Diplomarbeit ist an der TU Wien Bibliothek verfügbar.
The approved original version of this thesis is available in print at TU Wien Bibliothek.
TU Bibliothek WIEN Your knowledge hub

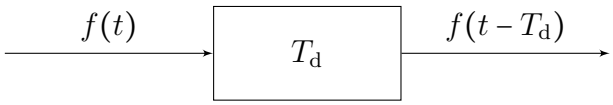

Figure 2.13: Block diagram of a time delay element with an input function $f(t)$ and output $f(t-T_\mathrm{d})$

Demodulation of the quadrature component of V_2 and then low pass filtering and amplifying it by $\frac{\hat{V}_1}{\hat{V}_2}$ will give us

$$V_{\mathrm{L2}} = \hat{V}_1 \cos(\psi)\sin(\theta). \tag{2.51}$$

Subtracting V_{L2} from V_{L1} will give us the desired signal

$$V_{\mathrm{out}} = \hat{V}_1 \sin(\psi - \theta), \tag{2.52}$$

where θ is the reference phase we want to achieve. The upsides of this approach are that it is simple and that it can be implemented as an analogue circuit relatively easy. If it is implemented digitally it needs low processing power because of the simplicity. The downside is that the demodulation happens at two different frequencies and we introduce the phase θ via a phase delay. Thus, in order to have the same phase difference on both frequencies we need the delays to be

$$T_\Omega = 2T_{2\Omega}. \tag{2.53}$$

Another limitation of this system is that the signal of the laser needs to be detected by the photodiode and then travel trough the circuitry of the detector system and is then measured by our feedback system. This process takes time and causes a delay of the signal. Figure 2.13 shows the input and output relation of a time delay element. If we put two sinusoid signals with different frequencies at the input, we will get as outputs

$$s_1 = \cos(\Omega(t-T_\mathrm{d})) = \cos(\Omega t + \Omega T_\mathrm{d}) = \cos(\Omega t + \varepsilon_1) \tag{2.54}$$

$$s_1 = \cos(2\Omega(t-T_\mathrm{d})) = \cos(2\Omega t + 2\Omega T_\mathrm{d}) = \cos(2\Omega t + \varepsilon_2). \tag{2.55}$$

The phase delay caused by the circuitry is not the same for different frequencies. This phenomenon can lead to inaccuracies in our measurements, if $\varepsilon = \Omega T_\mathrm{d}$ is sufficiently large. Hence, the error caused by the delay is proportional to the frequency and inverse proportional to the delay. This means that for our system to work ε must be negligible.

Die approbierte gedruckte Originalversion dieser Diplomarbeit ist an der TU Wien Bibliothek verfügbar.
The approved original version of this thesis is available in print at TU Wien Bibliothek.
TU Bibliothek Your knowledge hub WIEN

2.3.2 Double quadrature demodulation approach

For systems in which the hybrid demodulation approach reaches its limits, a more complex method can be used. It is called it double quadrature demodulation approach, because the quadrature demodulation method will be used on both frequencies Ω and 2Ω.

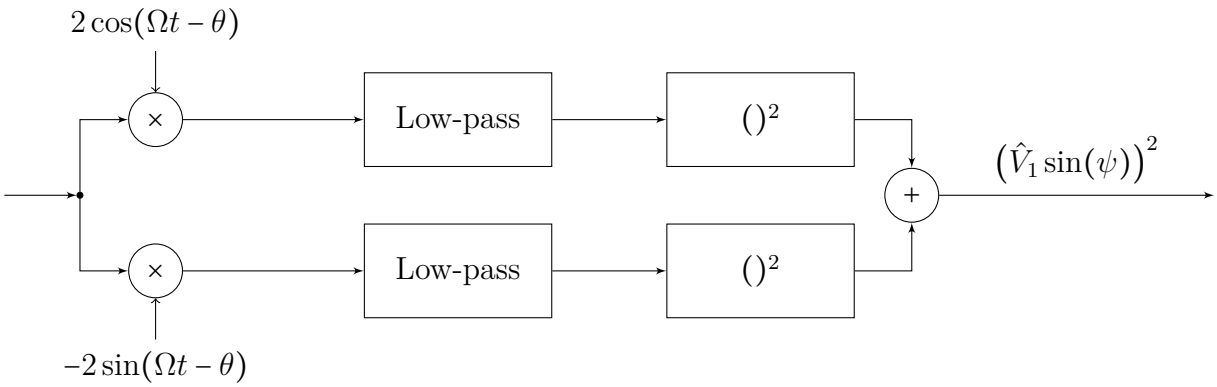

Figure 2.14: Block diagram representation of a quadrature modulator for incoherent amplitude detection for V_1

Figure 2.14 shows a quadrature demodulator slightly different from the one in figure 2.11. At the exit of our low-pass filters we have the quadrature components of our signal

$$V_{1,\mathrm{I}} = -\hat{V}_1 \sin(\psi) \cos\left(\frac{\pi}{2} + \theta\right) = \hat{V}_1 \sin(\psi) \sin(\theta) \tag{2.56}$$

$$V_{1,\mathrm{Q}} = \hat{V}_1 \sin(\psi) \sin\left(\frac{\pi}{2} + \theta\right) = \hat{V}_1 \sin(\psi) \cos(\theta). \tag{2.57}$$

The signal has an initial phase shift of $\frac{\pi}{2}$ because

$$\sin(\Omega t) = -\cos\left(\Omega t + \frac{\pi}{2}\right). \tag{2.58}$$

By squaring $V_{1,\mathrm{I}}$ and $V_{1,\mathrm{Q}}$ then adding them together we will get

$$\left[\hat{V}_1 \sin(\psi) \sin(\theta)\right]^2 + \left[\hat{V}_1 \sin(\psi) \cos(\theta)\right]^2 = \left[\hat{V}_1 \sin(\psi)\right]^2, \tag{2.59}$$

which is the square of the amplitude of V_1. Is is not dependent on θ anymore, which makes this method superior compared to the hybrid demodulation. This also means we do not need the demodulator system to share the same signal generator reference with the actuator system. We now have the possibility to introduce a local signal generator or a separate

Die approbierte gedruckte Originalversion dieser Diplomarbeit ist an der TU Wien Bibliothek verfügbar.
The approved original version of this thesis is available in print at TU Wien Bibliothek.
TU Bibliothek Your knowledge hub WIEN

signal generator, because the phase difference between them does not matter anymore. The only thing that matters is that the reference signal has the same frequency as the crier. Applying the same process for the signal V_2 yields its amplitude $\left[\hat{V}_2 \cos(\psi)\right]^2$. Knowing the phase of the quadrature components can be helpful, but it is lost during the squaring. However, it can be reconstructed measuring the phase of the quadrature components before squaring. The phase is calculated

$$\theta = \arctan\left(\frac{V_{1,\mathrm{I}}}{V_{1,\mathrm{Q}}}\right). \tag{2.60}$$

To get the desired function of our output signal $\hat{V}_1 \sin(\psi - \theta)$ we need to introduce new local variables $\sin(\theta)$ and $\cos(\theta)$ where θ is the desired phase we want to achieve. Figure 2.15 shows the second stage of the demodulation process in which the variable θ is introduced. First, we need to take take the square root of the square of the amplitude. For the amplitude of the signal V_2 we need an additional multiplication with $\frac{\hat{V}_1}{\hat{V}_2}$. By multiplying the first signal with $\cos(\theta)$ and the second with $\sin(\theta)$ and subtracting them, we get the desired signal at the output $\sin(\psi - \theta)$. Although the double quadrature method solves the limitations of the hybrid demodulation method, the drawback is much higher complexity. It is relatively easy to realize digitally in a program like LabView but hard coding it would be a much bigger challenge than the hybrid demodulation method. Building an analogue circuit would be also more complex for this method.

Die approbierte gedruckte Originalversion dieser Diplomarbeit ist an der TU Wien Bibliothek verfügbar.
The approved original version of this thesis is available in print at TU Wien Bibliothek.
TU Bibliothek WIEN Your knowledge hub

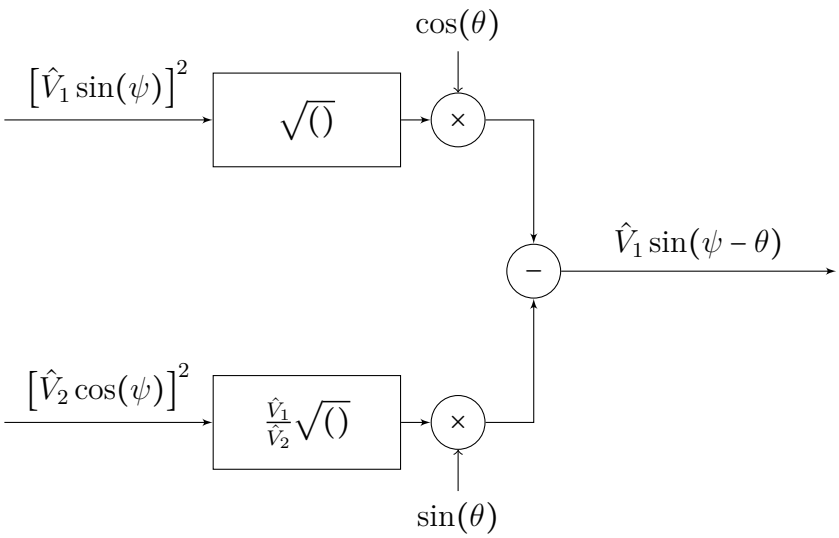

Figure 2.15: Block diagram of the second stage of the double quadrature demodulation method. Square rooting and multiplying with local variables gives us the desired output

2.4 Synchronization

Receiver systems that use local oscillators need their phase to be synchronized with that of the transmitter. There are multiple levels of synchronisation, but for our system the physical level of synchronisation is important. This process is also called carrier recovery (CR) [4, 8]. Figure 2.16 shows the block diagram with the CR system. It generates a local copy of the carrier signal which is synchronous with the carrier signal is or it has a constant phase shift.

The most intuitive realisation of this system would be to measure the the phase of the quadrature components and to control the phase of the local oscillator via feedback. The problem for this method is that our information lies in the amplitude of the signal. If the amplitude is negative, it will be interpreted as a 180° phase shift of the carrier signal and

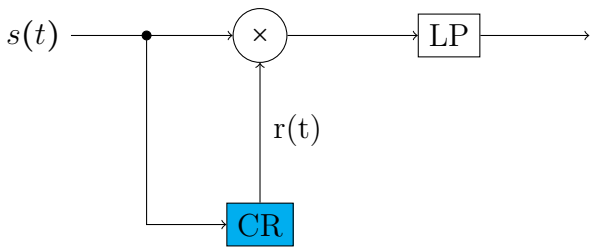

Figure 2.16: Position of the carrier recovery system in the block diagram

Die approbierte gedruckte Originalversion dieser Diplomarbeit ist an der TU Wien Bibliothek verfügbar.
The approved original version of this thesis is available in print at TU Wien Bibliothek.

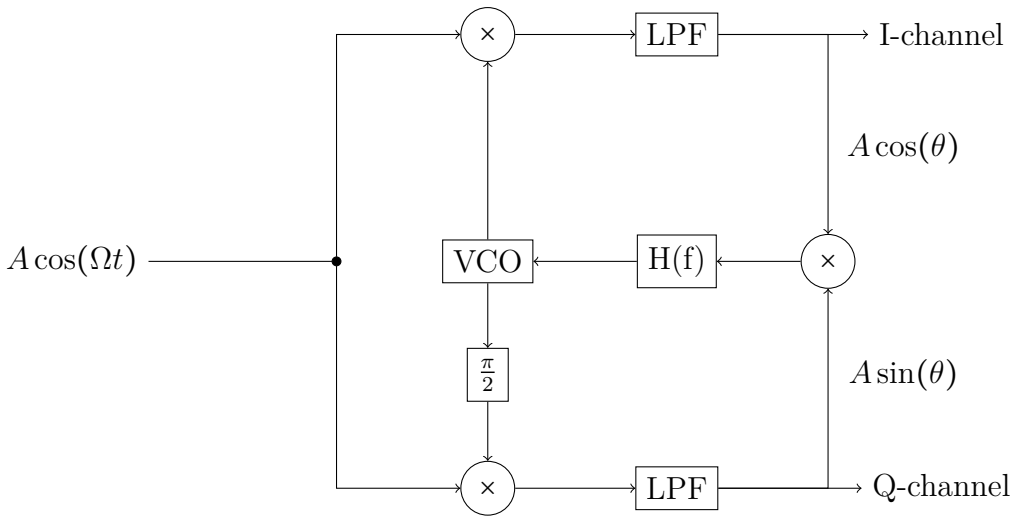

Figure 2.17: Block diagram of Costas loop

not as a movement of the mirror in the negative direction. The solution for this problem is a mechanism called Costas loop. It consists of two phase-locked loops that are forming the quadrature demodulator with a feedback. Figure 2.17 shows the block diagram of the configuration. The I- and Q-channel carry the phase information in the form

$$s_{\mathrm{I}} = A\cos(\theta) \tag{2.61}$$

$$s_{\mathrm{Q}} = A\sin(\theta). \tag{2.62}$$

Multiplication of these signals results in

$$s_{\mathrm{I}} \cdot s_{\mathrm{Q}} = A^2 \sin(\theta)\cos(\theta) = \frac{1}{2}A^2 \sin(2\theta). \tag{2.63}$$

The multiplication has two benefits. First, we now have the square of the amplitude (which means we lost the information about the sign of the amplitude of the signal). Second, we have an error signal $\frac{1}{2}A^2\sin(2\theta)$, which gives us information about the phase difference between the carrier and the reference.

The error signal then goes into a loop filter which filters the high frequency noise and contributes to stability. It consists of a low-pass filter and an integrator. In the next step the signal goes into a VCO (Voltage controlled oscillator). A VCO oscillates with a free running frequency f_0 as long as there is no voltage applied to the input. If we apply a voltage on the input it changes its frequency to $f_0 \pm f_{\mathrm{m}}$. For our digital system we will use an NCO (numerically controlled oscillator). It is the digital equivalent for the VCO and uses

Die approbierte gedruckte Originalversion dieser Diplomarbeit ist an der TU Wien Bibliothek verfügbar.
The approved original version of this thesis is available in print at TU Wien Bibliothek.
TU Bibliothek Your knowledge hub WIEN

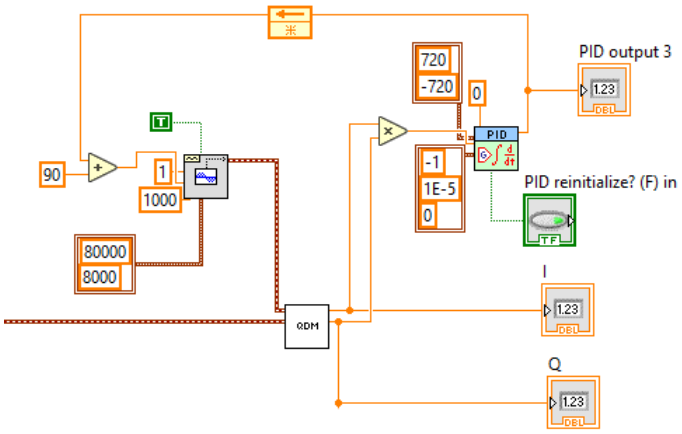

Figure 2.18: Realization of Costas loop in LabView

the frequency, phase and sampling rate as inputs to generate a discrete sine wave. Figure 2.18 shows our algorithm of the Costas loop. The signal enters our quadrature demodulator block. The I- and Q-channel outputs are multiplied and fed into a PID. The reference point of the PID is set to 0. The output of the PID is coupled back to the phase input of the oscillator. Theoretically, we could set the reference point of the PID to any angle, but if we set it to 0, we will get the amplitude directly out of one of the channels, without further signal processing. Depending on whether the proportional element of the controller is positive or negative we can lock our amplitude to come out of the I- or Q-channel.

Figure 2.19 shows the simulation results of the PID output for a $\theta = -45°$ phase delay of the carrier signal. We can observe that the PID output drops from its initial state to $-45°$. Because the PID is connected to the input that defines the phase of the reference signal, it shifts it by $-45°$. The configuration shifts the phase of the reference signal until the phase error is zero, so in the end we get a reference that has the same phase as the carrier.

Die approbierte gedruckte Originalversion dieser Diplomarbeit ist an der TU Wien Bibliothek verfügbar.
The approved original version of this thesis is available in print at TU Wien Bibliothek.

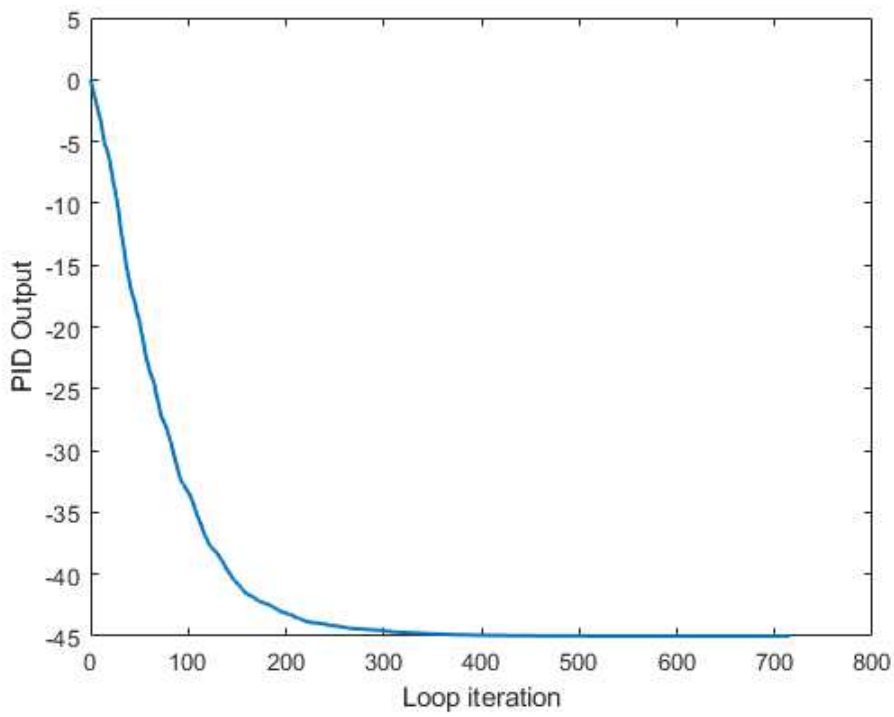

Figure 2.19: Simulation of Costas loop, for a $\theta = -45°$ phase delay of the carrier signal

Die approbierte gedruckte Originalversion dieser Diplomarbeit ist an der TU Wien Bibliothek verfügbar.
The approved original version of this thesis is available in print at TU Wien Bibliothek.

Die approbierte gedruckte Originalversion dieser Diplomarbeit ist an der TU Wien Bibliothek verfügbar.
The approved original version of this thesis is available in print at TU Wien Bibliothek.

Chapter 3

Implementation

Now that the working principles of the subsystems are covered, we can build them together and perform measurements. Here, I present analogue and digital solutions for the implementation of the different methods covered in the previous chapter.

3.1 Digital circuit

Before we discuss the algorithm itself, we first need to introduce how the analogue signal from the interferometer is digitalized.

3.1.1 Data acquisition

The program used for the implementation is LabView, but it can be realized with any other programming language. Our LabView algorithm needs to acquire data from the interferometer. We used a LabView compatible device called MyDaq. It has two analogue inputs and outputs that can be used in this set up. The analogue input of the MyDaq can handle up to 125 $\frac{kS}{s}$ (kilo samples per second). It is connected to an analogue digital converter that converts an analogue signal into a digital signal.

Figure 3.1 shows a block diagram of a standard analogue digital converter (ADC) [4, 8]. However, the ADC of the MyDaq does not have an anti aliasing filter. The aliasing effect appears when the Nyquist sampling criterium is violated. It states that a sine function

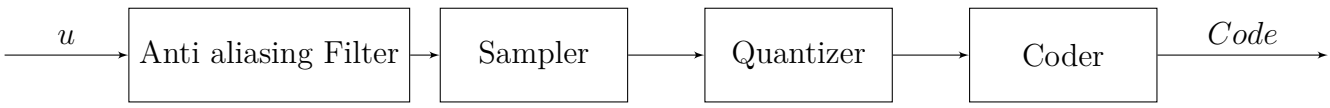

Figure 3.1: Block diagram of a standard analogue digital converter

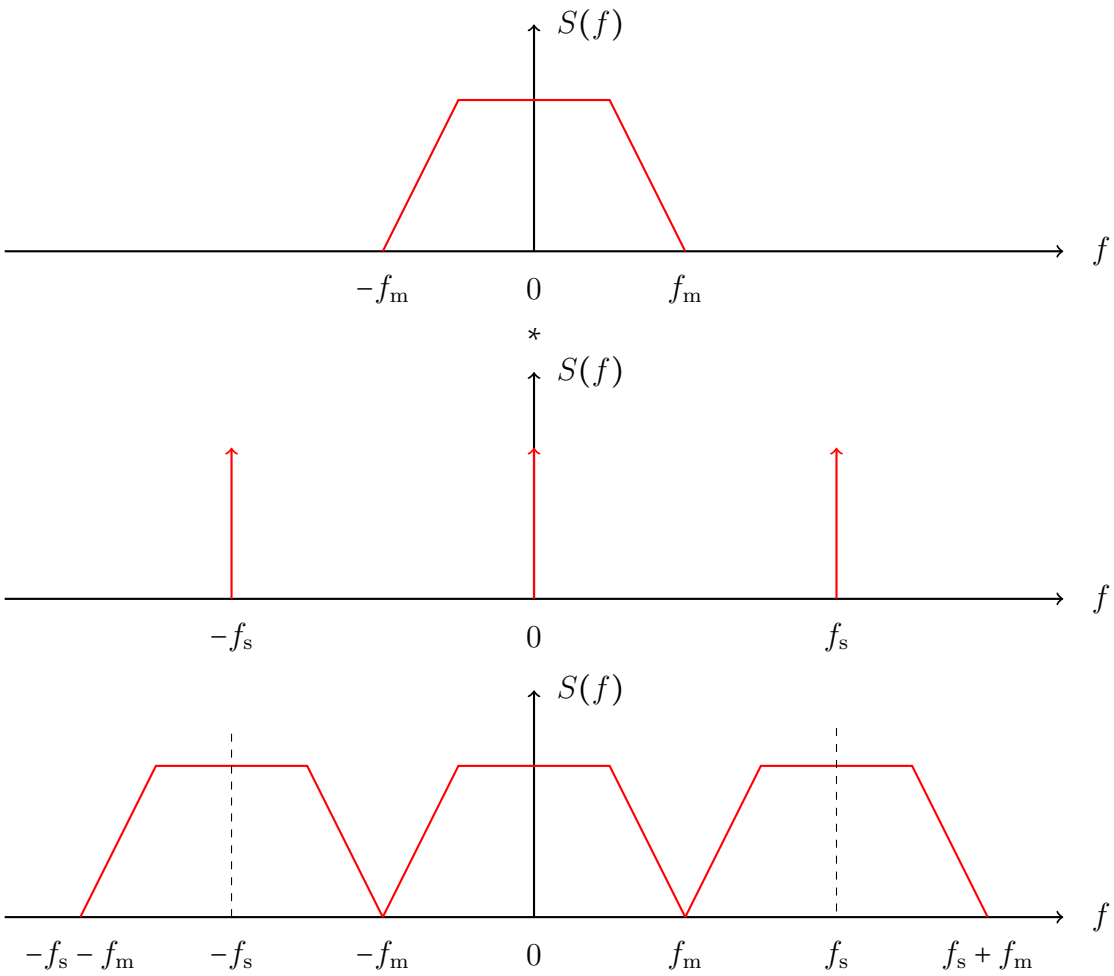

Figure 3.2: Process of getting the spectrum of a sampled signal where $f_s = 2f_m$

can be fully detected, if we sample it at the double of its frequency. If a signal has more than one frequency then the sampling rate f_s needs to be more than or equal to the largest frequency in the signals spectrum

$$f_s \geq f_m, \tag{3.1}$$

where f_m is the largest frequency in the spectrum. To understand this we can visualize the sampling process. The sampling process can be described as multiplying a signal with a series of Dirac impulses with a separation of $\frac{1}{f_s}$. If we switch from time domain, to frequency domain the multiplication becomes a convolution and the series of Dirac impulses has a separation of f_s.

Figure 3.2 shows the process of sampling in the frequency domain for the case where

Die approbierte gedruckte Originalversion dieser Diplomarbeit ist an der TU Wien Bibliothek verfügbar.
The approved original version of this thesis is available in print at TU Wien Bibliothek.
TU Bibliothek Your knowledge hub WIEN

$f_s = 2f_m$. The convolution of the spectrum of a function with a series of Dirac impulses results in a series of copies the original function with the separation of f_s. Figure 3.3 shows the resulting spectrum if the Nyquist criterium is violated. We can observe an overlapping of the signals. This means that higher frequencies will be interpreted as lower frequencies which can cause noise in our signal and inaccuracies.

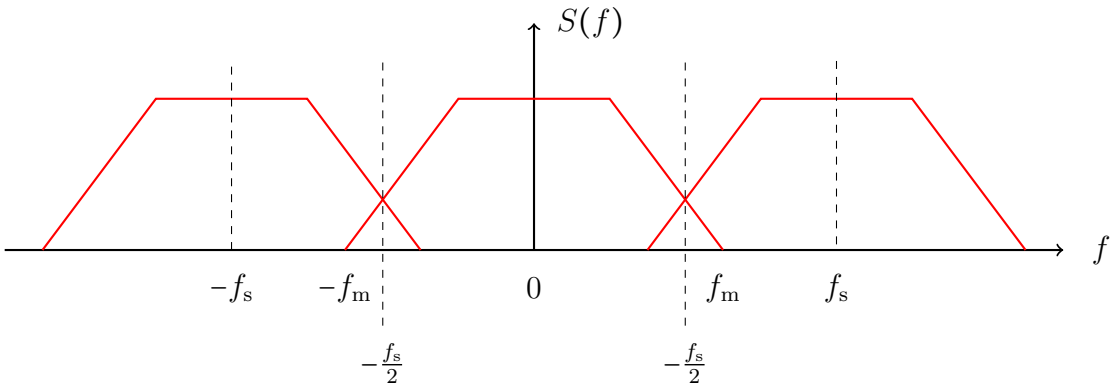

Figure 3.3: Spectrum of a sampled signal where the Nyquist criteria is violated $f_s < 2f_m$

To avoid aliasing we need to implement a low-pass filter that filters all frequencies higher than the half of the sampling rate. We will use our device at a sampling rate of 80 kHz. A simple low-pass filter of first order and cut-off frequency at 40 kHz will be enough to suppress the higher frequencies. By experimenting with the MyDaq device and the interferometer we observed that the interferometer output is altered when it is connected directly to the MyDaq. This happens at the sampling frequency. To avoid this behaviour we need to separate the two devices with a voltage follower (also called unity gain amplifier or buffer amplifier). Because low-pass filtering causes a phase shift and the hybrid demodulation (as discussed in the last chapter) is sensitive to phase shifts of the signal unlike the double quadrature demodulation, we will use the anti-aliasing filter only in dual quadrature demodulation and in the hybrid demodulation only work with just the buffer. Figure 3.4 shows the circuit of the anti aliasing filter with buffer. The filter response is also frequency-dependant, which means that it changes the magnitude of different frequencies differently. This can be corrected in the algorithm by measuring or simulating the circuit for the frequencies used. Figure 3.5 shows a simulation of the circuit with an linear y-axis. By inverting the magnitude function in the software, we can recover the original magnitude of the signal.

After the signal is sampled, it is quantized. This means that the continuous signal

Die approbierte gedruckte Originalversion dieser Diplomarbeit ist an der TU Wien Bibliothek verfügbar.
The approved original version of this thesis is available in print at TU Wien Bibliothek.

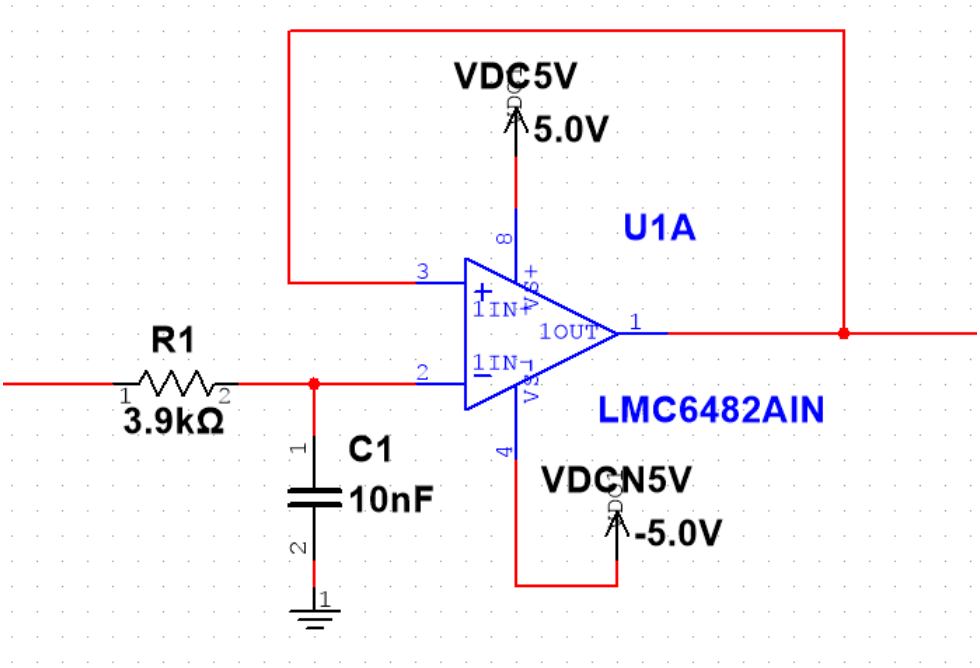

Figure 3.4: Circuit of an anti-aliasing filter with a 40 kHz cut off frequency and a buffer

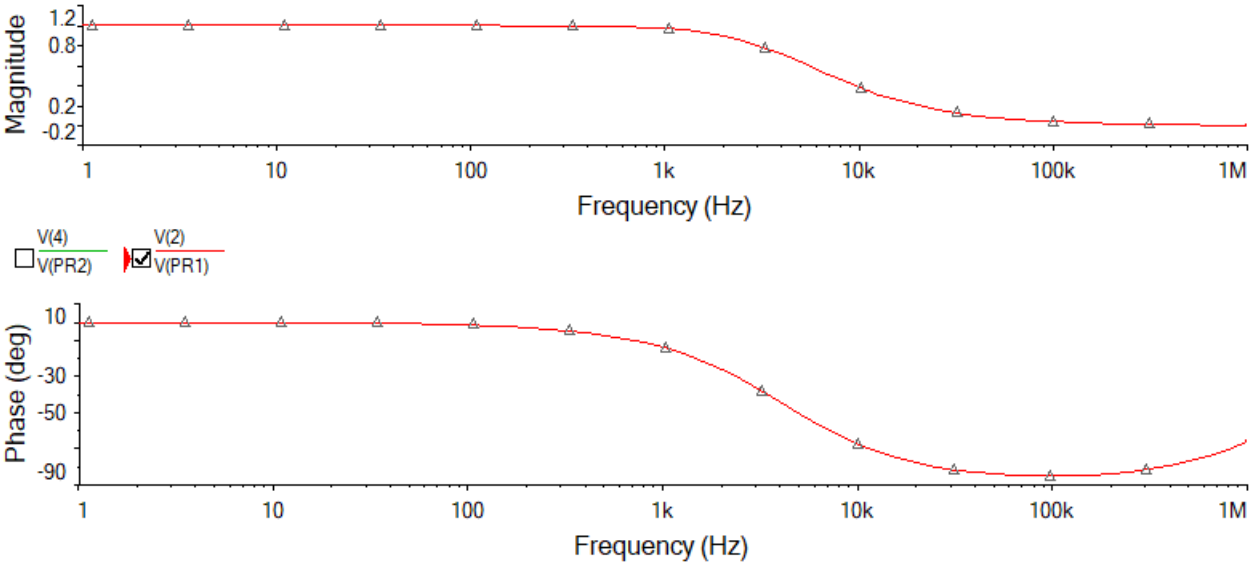

Figure 3.5: Transfere function of an anti-aliasing filter with buffer simulated in Multisim

Die approbierte gedruckte Originalversion dieser Diplomarbeit ist an der TU Wien Bibliothek verfügbar.
The approved original version of this thesis is available in print at TU Wien Bibliothek.

amplitudes will be converted into a signal with discrete amplitude values. The quantizer chooses the nearest quantized amplitude value for the continuous amplitude value. The information loss of this process is called quantization error. In the next step, the quantized amplitude is encoded which is sent via an USB to our PC.

3.1.2 Hybrid demodulation

For the hybrid demodulation we will use the setup shown in Fig. 3.6. The reference signal used for demodulation will be generated by the same source that modulates the signal. It will be connected to one of the analogue inputs of the data acquisition device. On the second of the two inputs the photodiode of the interferometer will be connected. The analogue output of the data acquisition device will be connected to adder circuit where it is combined with the modulation signal and a DC voltage.

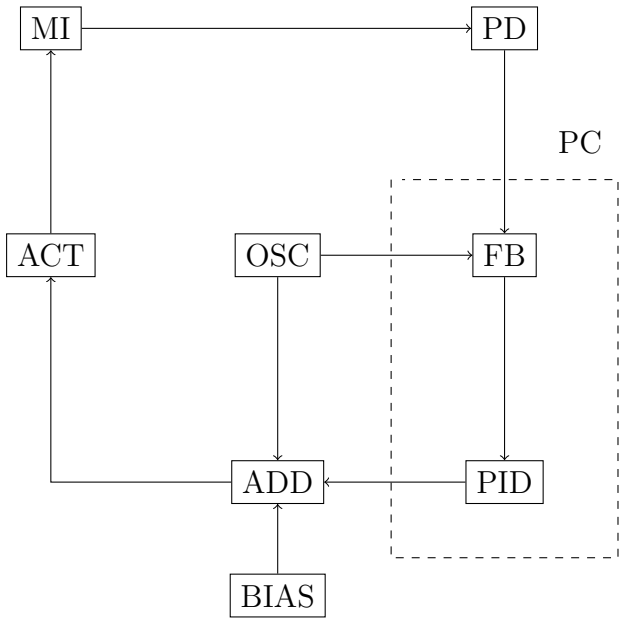

Figure 3.6: Block diagram of our system for hybrid demodulation method.(MI-Michelson interferometer,PD-photo diode, FB-feed back, OSC-Oscillator, PID-Controller, ADD-Adder, BIAS-DC voltage for piezo, ACT-Actuator system

Figure 3.7 shows the LabView algorithm we designed for hybrid demodulation. The first block represents the analogue inputs of the data acquisition device. In this block, we can set up the ADC specifications, such as the sampling rate, expected signal amplitude and buffer size.

Die approbierte gedruckte Originalversion dieser Diplomarbeit ist an der TU Wien Bibliothek verfügbar.
The approved original version of this thesis is available in print at TU Wien Bibliothek.

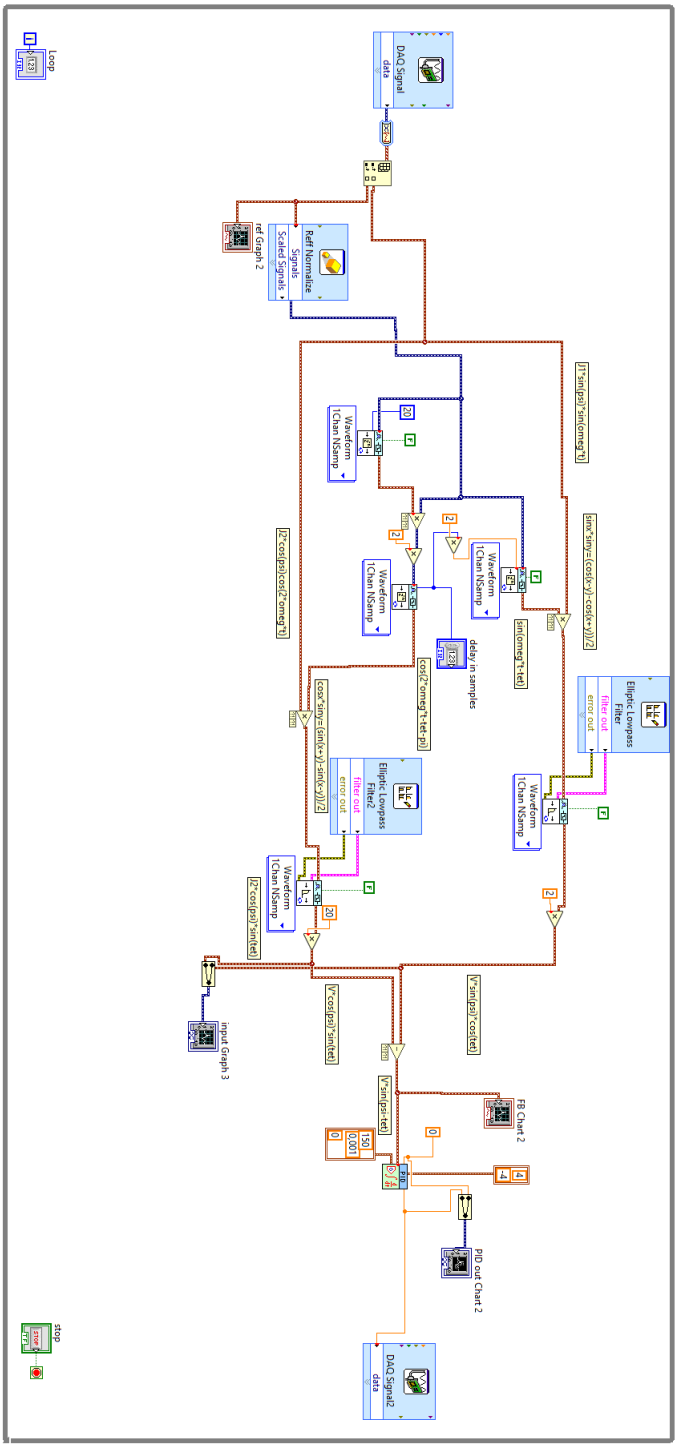

Figure 3.7: LabView algorithm for hybrid demodulation

Die approbierte gedruckte Originalversion dieser Diplomarbeit ist an der TU Wien Bibliothek verfügbar.
The approved original version of this thesis is available in print at TU Wien Bibliothek.

The amplitude settings are important because they can adjust the quantizer to work on a predefined amplitude range which reduces the quantization error of the system. Before the information is sent to our PC, it is filled into a buffer. For large buffers, the MyDaq is capable to send many samples at once, but the tradeoff is that the system is not working in real time. That is the reason why we want our buffer to be as small as possible. After the signal leaves the data acquisition block, it is split in to two signals, one for each input pin. One signal comes from the interferometer photodiode, the other from the oscillator. The signal coming from the oscillator goes into a normalization block, which normalizes the amplitude of the signal to one. This is very important because of the next step. Since we are demodulating for Ω and 2Ω and we only have one signal with the angular frequency Ω, we need a frequency-doubler mechanism. It can be realized if we multiply it by the same signal only $\frac{\pi}{2}$ phase shifted and doubled magnitude

$$\sin(\Omega kT) \cdot 2\cos(\omega kT) = -\sin(2\Omega kT). \tag{3.2}$$

Continuous time needs to be transformed into discrete time for our system

$$t \to kT, \tag{3.3}$$

where k is the discrete time step and T is the time distance between two time steps. It is proportional to the inverse of the sampling frequency

$$T = \frac{1}{f_s}. \tag{3.4}$$

For $\Omega = 1\text{kHz}$ and a sampling rate $f_s = 80\text{kHz}$ a $\frac{\pi}{2}$ phase shift corresponds to

$$k_d = \frac{1}{4}\frac{80\,kHz}{1\,kHz} = 20. \tag{3.5}$$

This means we need a time delay of 20 samples to have the signal $\frac{\pi}{2}$ phase shifted. Now that we have our signals Ω and 2Ω, we need to introduce a phase delay θ which is the phase we want our system to be in. This is done by two delay blocks each on the two reference signals. It is very important to always have twice as much delay on the Ω signal than on the 2Ω signal. This can be seen by

$$\sin(\Omega(k - k_\mathrm{d})T) = \sin(\Omega kT - \Omega k_\mathrm{d}T) = \sin(\Omega kT - \theta) \tag{3.6}$$

$$\sin(2\Omega(k - k_\mathrm{d})T) = \sin(2\Omega kT - 2\Omega k_\mathrm{d}T) = \sin(\Omega kT - 2\theta), \tag{3.7}$$

Die approbierte gedruckte Originalversion dieser Diplomarbeit ist an der TU Wien Bibliothek verfügbar.
The approved original version of this thesis is available in print at TU Wien Bibliothek.
TU Bibliothek WIEN Your knowledge hub

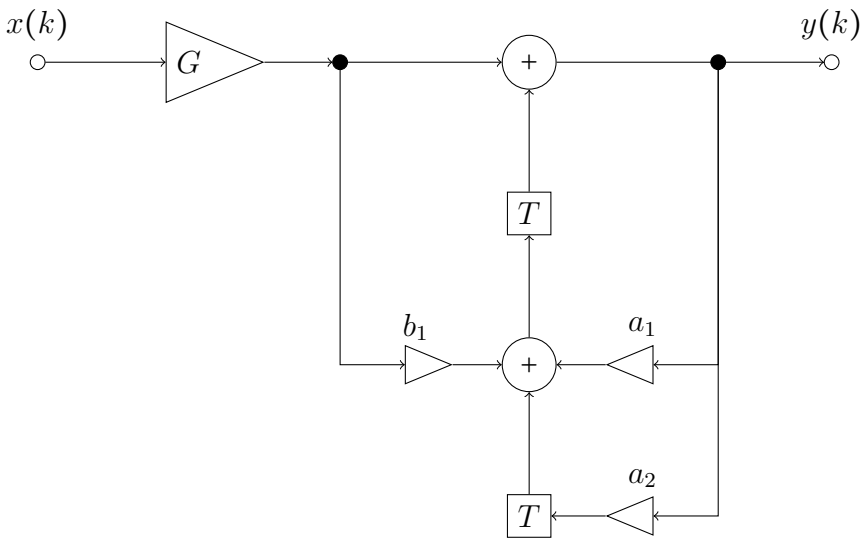

Figure 3.8: Diagram of a simple IIR filter

so the same delay causes the double phase shift on the doubled frequency. After we have set up our references, we can now demodulate the signals by multiplying it with the references. After the multiplication, the signals need to be low-pass filtered and amplified. The filter used is an elliptic IIR (Infinite impulse response) filter, but an FIR (finite impulse response) filter can also be used. The advantage of an FIR filter is that it is stable, but needs more processing power. An IIR filter can be unstable, but needs far less processing power. The used filter design tool of LabView performs the stability checks and makes the IIR filter design reliable. Figure 3.8 shows a simple IIR filter of the second order [13]. By varying the coefficients a_i and b_i we get a change in the transfer function of the filter. After the signals leave the filters and are amplified, we obtain the signals

$$V_1 = \hat{V}_1 \sin(\psi)\cos(\theta) \tag{3.8}$$

$$V_2 = \hat{V}_1 \cos(\psi)\sin(\theta). \tag{3.9}$$

By subtracting V_2 from V_1 we get our final signal

$$V = \hat{V}_1 \sin(\psi - \theta), \tag{3.10}$$

which represents the error signal that is fed into our PID controller.

The parameters of the PID controller could be calculated but it is easier and more

Die approbierte gedruckte Originalversion dieser Diplomarbeit ist an der TU Wien Bibliothek verfügbar.
The approved original version of this thesis is available in print at TU Wien Bibliothek.
TU Bibliothek WIEN Your knowledge hub

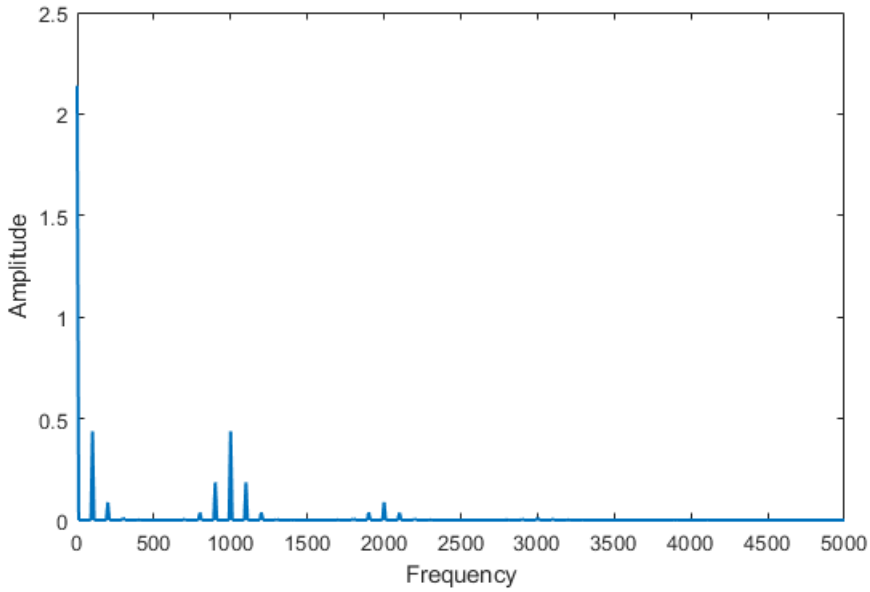

Figure 3.9: Spectrum of the signal when both transducer and piezo are oscillating

accurate to simulate it, because we are dealing with a non-linear system and by simulating the results we can see how the PID behaves. Figure 3.10 shows the simulation algorithm in LabView. The first two blocks represent the oscillations of the piezoelectric element and the transducer. The piezo is oscillating at 1 kHz and the transducer at 100 Hz frequency. They are added together with the phase defined by the position of the mirror.

By putting them trough a cosine block, we get the function $\cos[\psi+\psi_\mathrm{d}\sin(\Omega t)+\psi_\mathrm{m}\sin(\omega t)]$ where ψ_m is the modulation index of the transducer and ω its frequency. Figure 3.9 shows the spectrum of the signal with both transducer and piezo oscillating. We can see from the spectrum that the result is a modulation of the Bessel coefficients with a modulation index ψ_m and frequency ω. Now the signal at the first Bessel frequency of the stabilisation modulation is

$$s_1(t) = J_1(\psi_\mathrm{d})\sin(\psi)\sin(\Omega t)[J_0(\psi_\mathrm{m}) + J_1(\psi_\mathrm{m})\sin(\omega t) + J_2(\psi_\mathrm{m})\cos(\omega t)]. \tag{3.11}$$

By looking at our signal we have two concerns we should consider. The first is the amplitude of the signal at frequency Ω, it will be multiplied with $J_0(\psi_\mathrm{m})$. For modulation indexes where $J_0(\psi_\mathrm{m}) \to 0$ our measurement will be inaccurate. Therefore we want $J_0(\psi_\mathrm{m})$ to be at not too small. This can be obtained by lowering or rising the transducer voltage

Die approbierte gedruckte Originalversion dieser Diplomarbeit ist an der TU Wien Bibliothek verfügbar.
The approved original version of this thesis is available in print at TU Wien Bibliothek.
TU WIEN Bibliothek Your knowledge hub

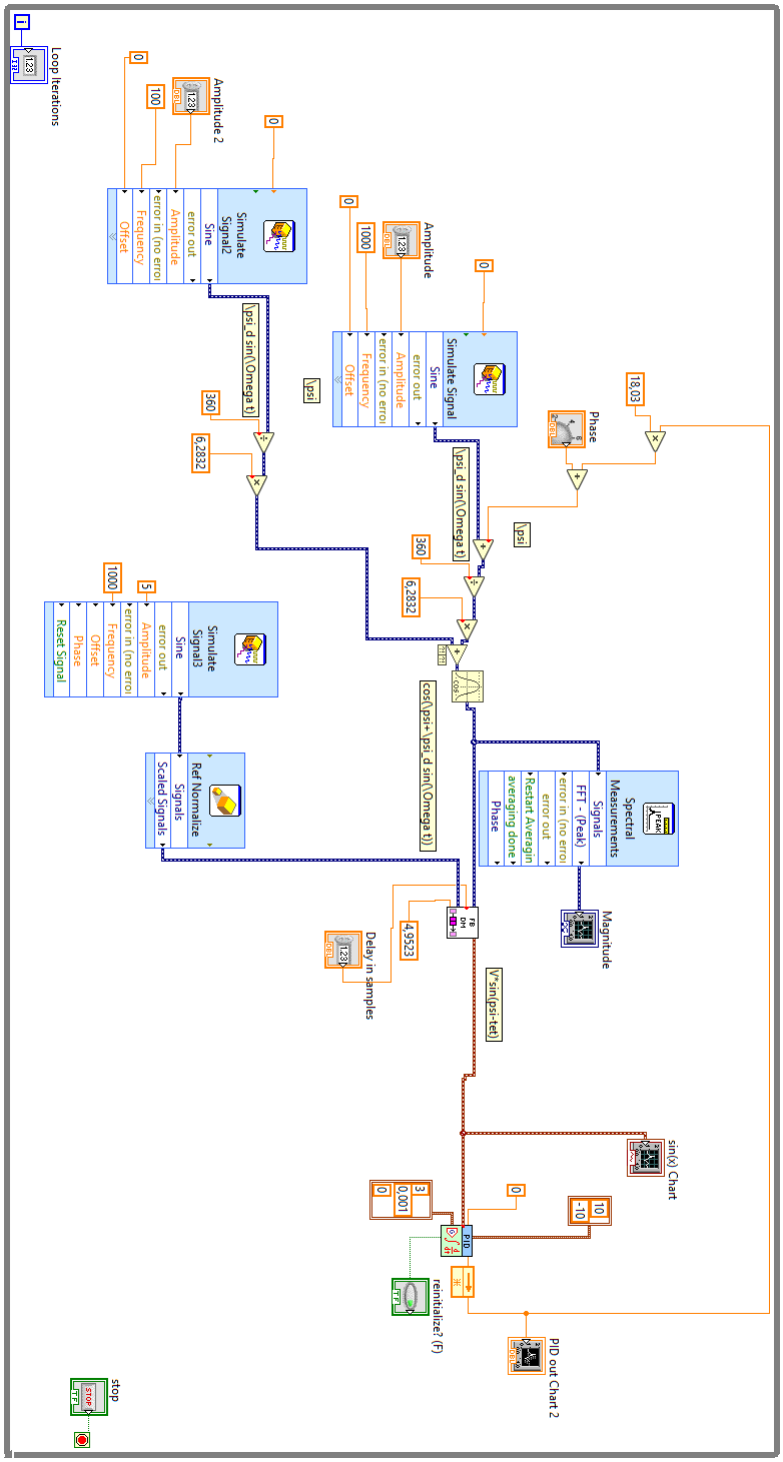

Figure 3.10: LabView algorithm for simulation of the hybrid demodulation set up with PID controller and oscillating transducer

Die approbierte gedruckte Originalversion dieser Diplomarbeit ist an der TU Wien Bibliothek verfügbar.
The approved original version of this thesis is available in print at TU Wien Bibliothek.

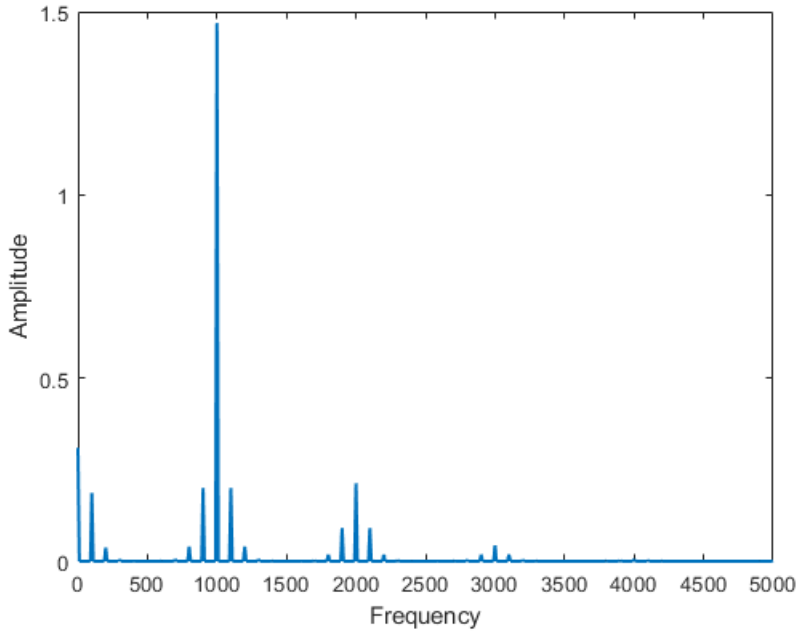

Figure 3.11: Spectrum of the signal at the output of the multiplier of the demodulator at Ω frequency

such that $J_0(\psi_\mathrm{m})$ increases. The second concern are the low pass filters of the demodulators. Without the transducer, we could have the cut-off frequency at Ω. Looking at the spectrum coming out of the multipliers of the demodulator shown in Fig. 3.11, we can see peaks at multiples of ω. This means that now the cut-off frequency of the filters needs to be at ω.

Because of better visualization the hybrid demodulation system is put into one block with four inputs: signal, reference, delay (for θ) and amplification (for $\frac{J_1}{J_2}$). The output of the demodulator is connected to a PID, which is coupled back to the phase and multiplied by the transfer function of the actuator system, in this case $18.03\,\frac{°}{V}$. Depending on the interferometer and the modulation strength of the signal, the parameters of the PID are set. For this particular setup, the parameters $K_\mathrm{P} = 3$ and $K_\mathrm{I} = 0.001$ give good results. Figure 3.12 shows the simulation results of the setup. We used as input variables $\psi_\mathrm{d} = \psi_\mathrm{m} = \theta = 45°$ and we increased the phase ψ from 0° to 90°. By looking at the output of the PID at the beginning it jumps to around $2.5\,V$ which is equal to $-(\psi - \theta) = 45°$. By increasing ψ the output of the PID is decreasing. For $\psi = \theta$ the output of the PID is zero. By further increasing of ψ, the output of the PID has negative values because $\psi > \theta$. We can observe that because of the low cut-off of the filter, there is no interference between the measurement and stabilization signal.

Die approbierte gedruckte Originalversion dieser Diplomarbeit ist an der TU Wien Bibliothek verfügbar.
The approved original version of this thesis is available in print at TU Wien Bibliothek.
TU WIEN Bibliothek Your knowledge hub

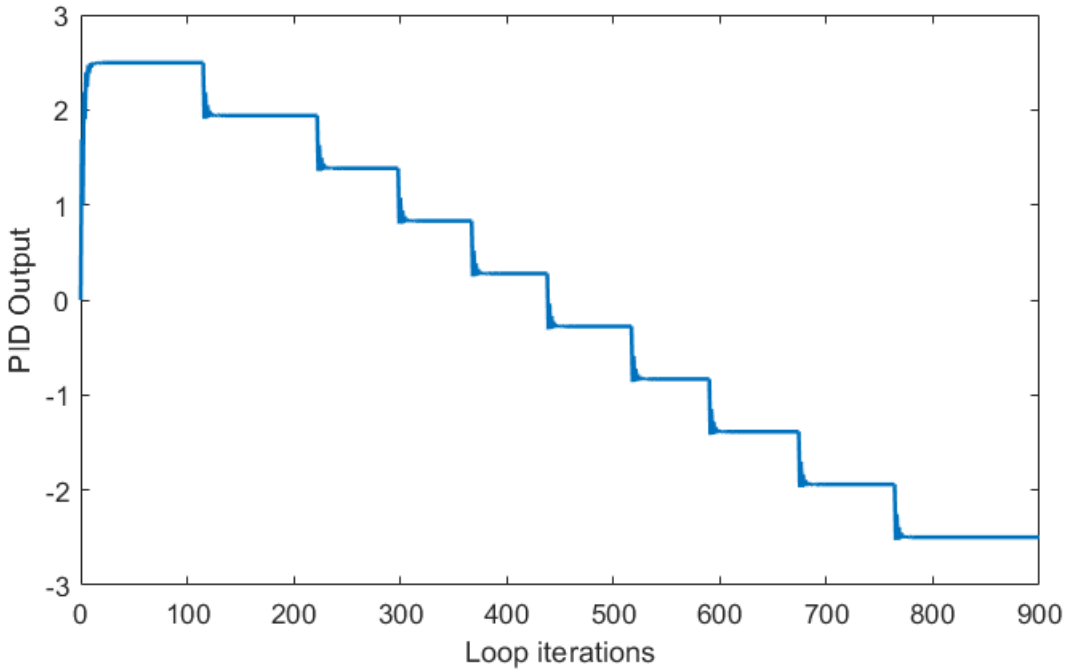

Figure 3.12: Simulation results for $\theta = 45°$ and increasing ψ from 0° to 90° by a step of 10°

3.2 Double quadrature demodulation

For the quadrature demodulation, we will use the setup shown in Fig. 3.13. The reference for the piezo is generated with a signal generator, and the reference for the detector with an intern software-generated oscillator. This means that for this detection method, we will use only one analogue input port. The rest of the setup is the same as for hybrid demodulation.

Figure 3.14 shows the LabView algorithm used for double quadrature demodulation. The signal from the interferometer goes into an input pin of the data acquisition device. The device is represented by the DAQ block on the left side. The signal is split and goes into the two quadrature demodulators. The inside of the quadrature demodulator is shown in Fig. 3.15. It is based on the examples of the official LabView website. The inputs of the block are the reference and the signal. They are fed into the data transformation blocks. The data is transformed from wave to array. Phase shifting of the reference is done by a Hilbert transform block. It causes a $-\frac{\pi}{2}$ phase shift to the reference signal

$$\cos\left(\Omega t - \frac{\pi}{2}\right) = \sin(\Omega t). \tag{3.12}$$

In the next step, the two signals are multiplied with the carrier. Low-pass filtering is then

Die approbierte gedruckte Originalversion dieser Diplomarbeit ist an der TU Wien Bibliothek verfügbar.
The approved original version of this thesis is available in print at TU Wien Bibliothek.
TU Bibliothek WIEN Your knowledge hub

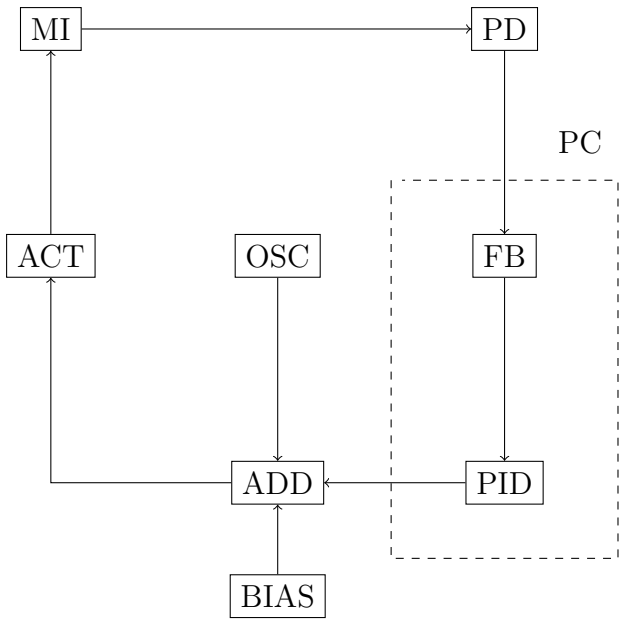

Figure 3.13: Block diagram of our system for double quadrature demodulation method.(MI-Michelson interferometer,PD-photodiode, FB-feedback, OSC-Oscillator, PID-Controller, ADD-Adder, BIAS-DC voltage for piezo, ACT-Actuator system

done by a block that splits the AC from the DC signal component. In the end the I- and Q-component are multiplied by the constants. Now we have I- and Q-components at the output of the quadrature demodulation block. They are split into two paths. One is leading to the PID of Costas loop and then to the signal generator for carrier recovery. The second is used for the regulation of the phase. We use the Q-channel of the first demodulator and the I-channel of the second which contain the full amplitude information of the signal. The first signal is multiplied by $\cos(\theta)$ and the second by $\sin(\theta)$ and $\frac{J_1}{J_2}$ yielding

$$s_1 = V_1 \sin(\psi)\cos(\theta) \tag{3.13}$$

$$s_2 = V_1 \cos(\psi)\sin(\theta). \tag{3.14}$$

By subtracting those two signals, we get our error signal $V_1 \sin(\psi - \theta)$ which is the input of the PID. The PID has also an enable mechanism. We can enable it after the synchronization is finished. The PID is fed back, multiplied by the transfer function of the actuator system and added to the phase.

Figure 3.16 shows the simulation results of the setup. We used the same simulation variables and methodology as in the hybrid demodulation, except we introduced a phase delay of the incoming signal. The phase delay was 5 samples which is equivalent to a phase

Die approbierte gedruckte Originalversion dieser Diplomarbeit ist an der TU Wien Bibliothek verfügbar.
The approved original version of this thesis is available in print at TU Wien Bibliothek.
TU Bibliothek WIEN Your knowledge hub

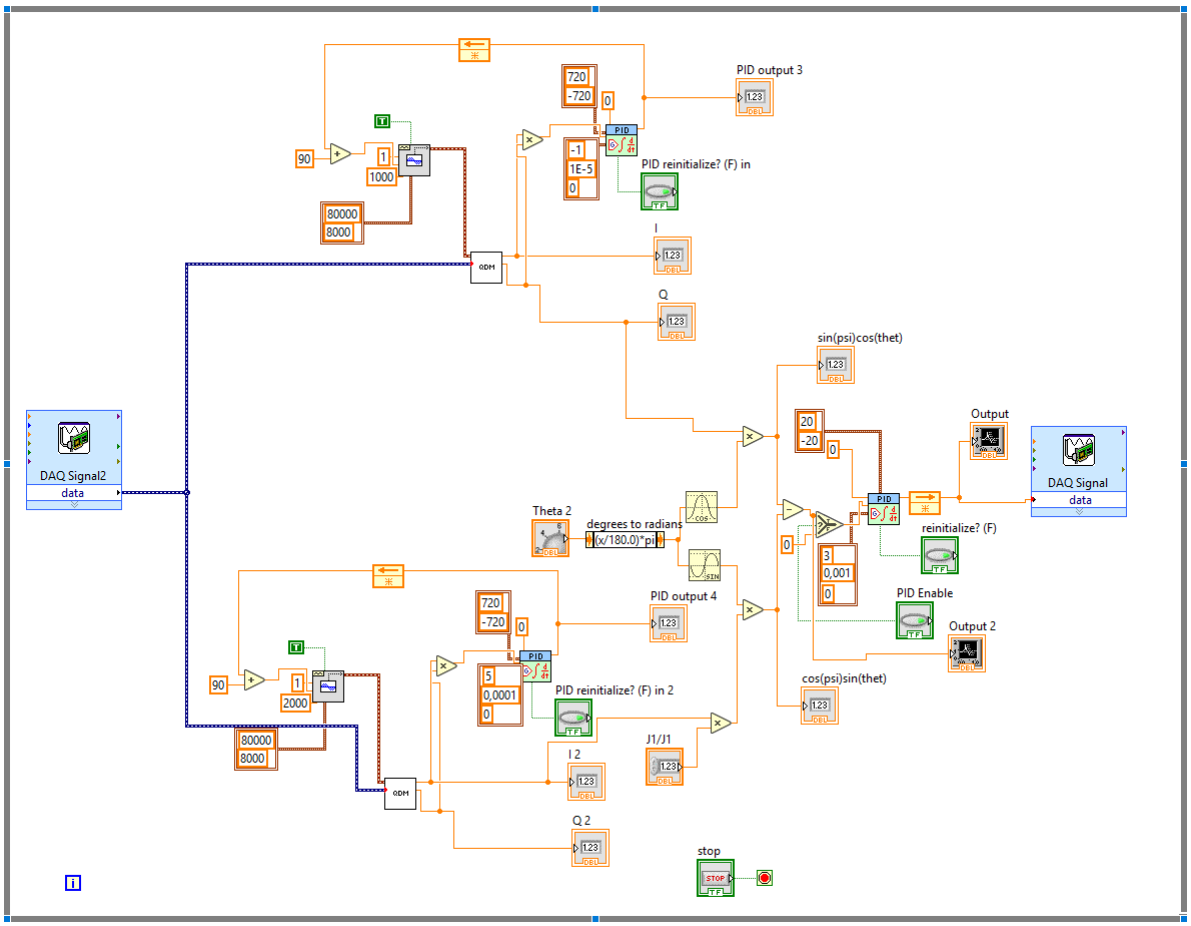

Figure 3.14: Spectrum of the signal at the output of the multiplier of the demodulator at frequency Ω

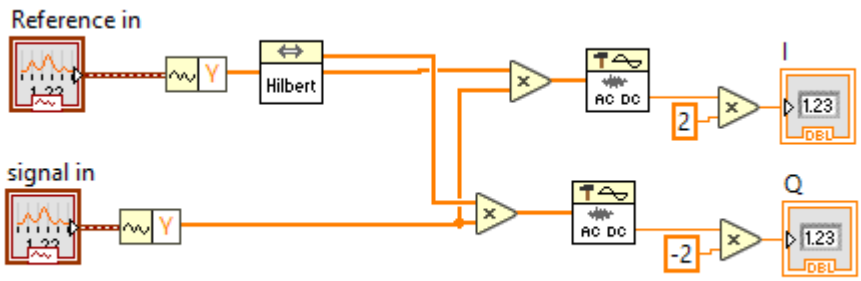

Figure 3.15: LabView implementation of the quadrature demodulator

Die approbierte gedruckte Originalversion dieser Diplomarbeit ist an der TU Wien Bibliothek verfügbar.
The approved original version of this thesis is available in print at TU Wien Bibliothek.
TU Bibliothek Your knowledge hub WIEN

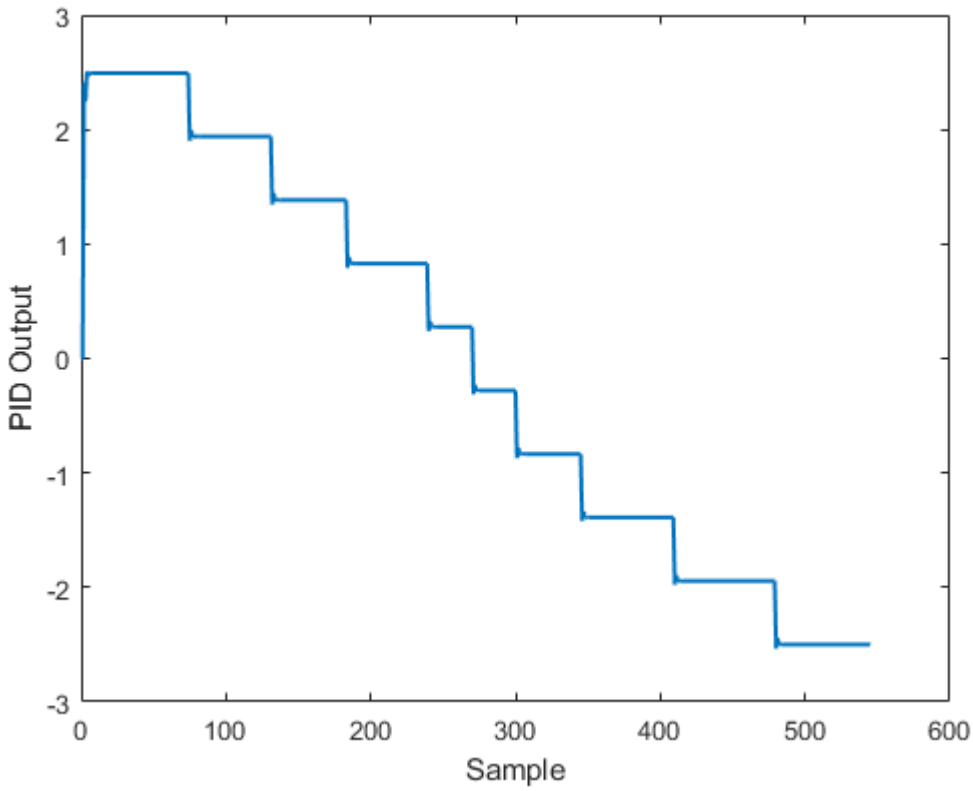

Figure 3.16: Simulation results of the double quadrature demodulator with Costas loop carrier recovery and PID feedback control

shift of $\frac{\pi}{8}$ at Ω and $\frac{\pi}{4}$ at 2Ω. By looking at the results we have the same curve, which means we have the same results as in the hybrid demodulation and have overcome a huge phase shift difference in the two different frequencies.

3.3 Analogue circuit

Building an analogue circuit for our system has it adwantages and disadvantages at the same time. The advantages are that it is cheaper and more simple because no programming and introduction of a microcontroller is needed. The disadvantages are that it is less accurate and it is harder to implement changes. By looking at the block diagram for the hybrid demodulator in Fig. 3.17, we can see that we need seven elements for our analogue circuit: two multipliers, two-low pass filters, two amplifiers and one adder.

Die approbierte gedruckte Originalversion dieser Diplomarbeit ist an der TU Wien Bibliothek verfügbar.
The approved original version of this thesis is available in print at TU Wien Bibliothek.
TU WIEN Bibliothek Your knowledge hub

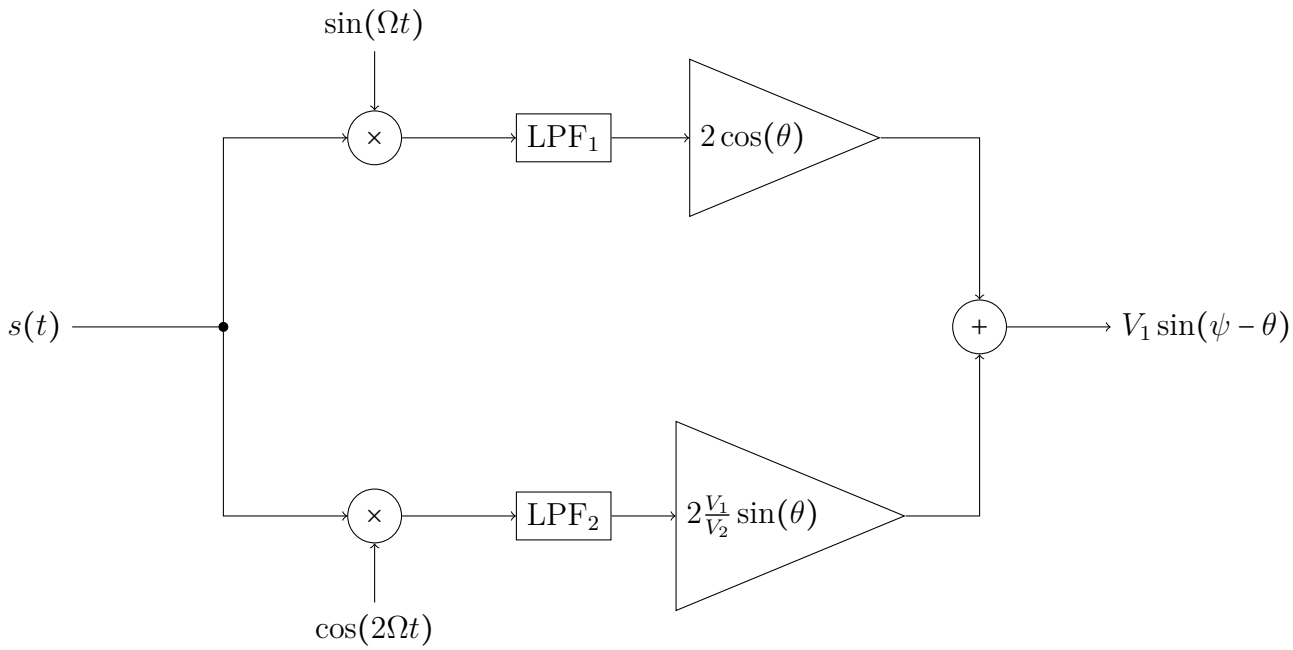

Figure 3.17: Block diagram of the analogue demodulation system

The demodulator is slightly different from the one we used in digital demodulation. Assuming there is no delay between the carrier and reference, the signal coming out of the first low-pass filter will be

$$s_1 = -V_1 \frac{1}{2} \sin(\psi). \tag{3.15}$$

The signal coming out of the second low-pass filter will be

$$s_2 = V_2 \frac{1}{2} \cos(\psi). \tag{3.16}$$

In this circuit we do not introduce the desired angle θ through a delay, but by multiplying the signals s_1 and s_2 with $\cos(\theta)$ and $\sin(\theta)$. Adding the signals together with an inverting adder circuit will result in

$$s_{\text{out}} = V_1 \sin(\psi - \theta) \tag{3.17}$$

For the signal multiplication, we will use an AD33AN IC. For inputs x and y it gives an output of $w = \frac{x \cdot y}{10}$. Figure 3.18 shows a schematic of the circuit with the simulation results. For a $1\,V$ and $1\,kHz$ input and reference we got an output with a DC value of 55 mV, which is a 10 % error rate.

Die approbierte gedruckte Originalversion dieser Diplomarbeit ist an der TU Wien Bibliothek verfügbar.
The approved original version of this thesis is available in print at TU Wien Bibliothek.
TU Bibliothek Your knowledge hub WIEN

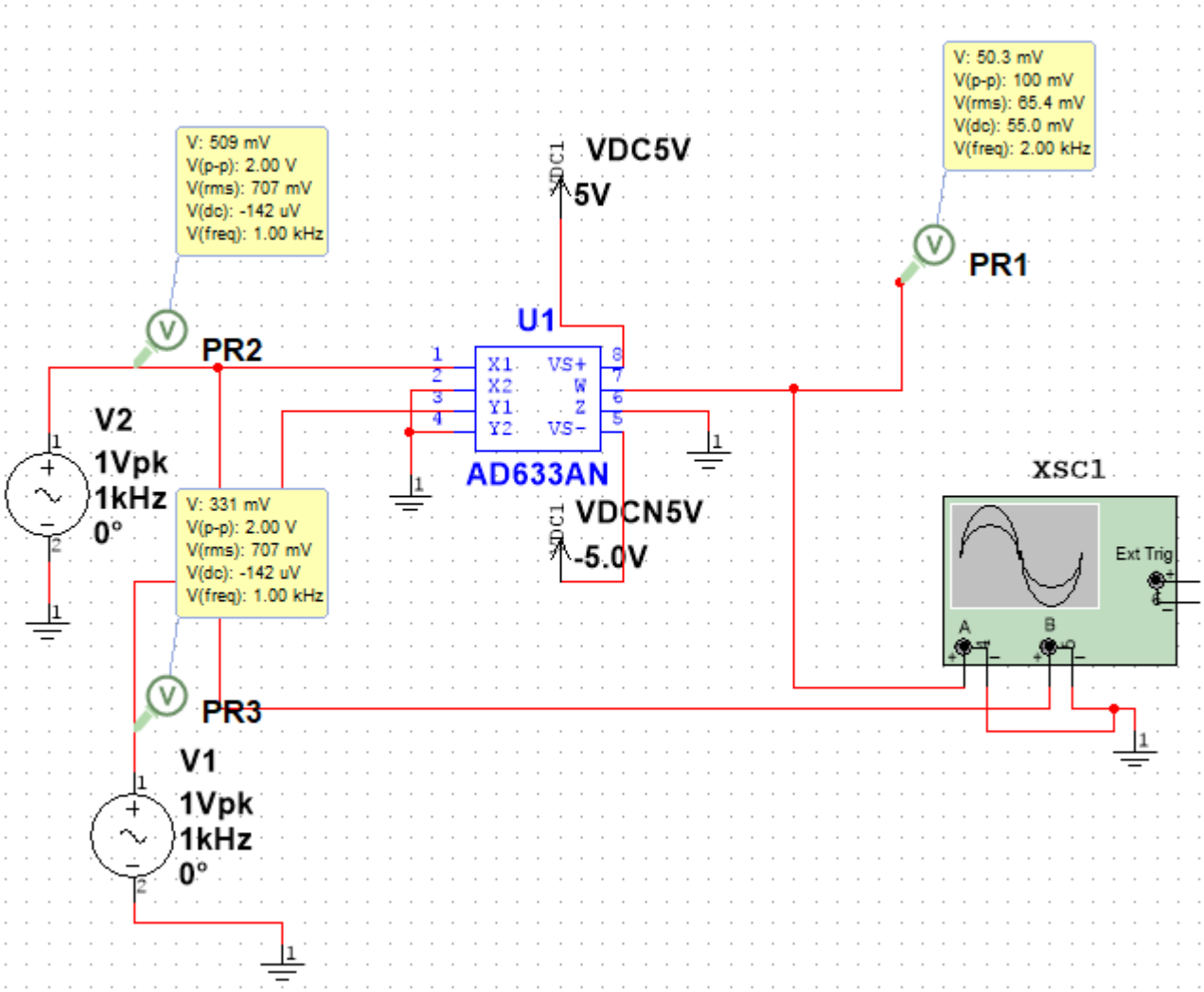

Figure 3.18: AD633AN multiplier schematic with simulation in Multisim

Die approbierte gedruckte Originalversion dieser Diplomarbeit ist an der TU Wien Bibliothek verfügbar.
The approved original version of this thesis is available in print at TU Wien Bibliothek.

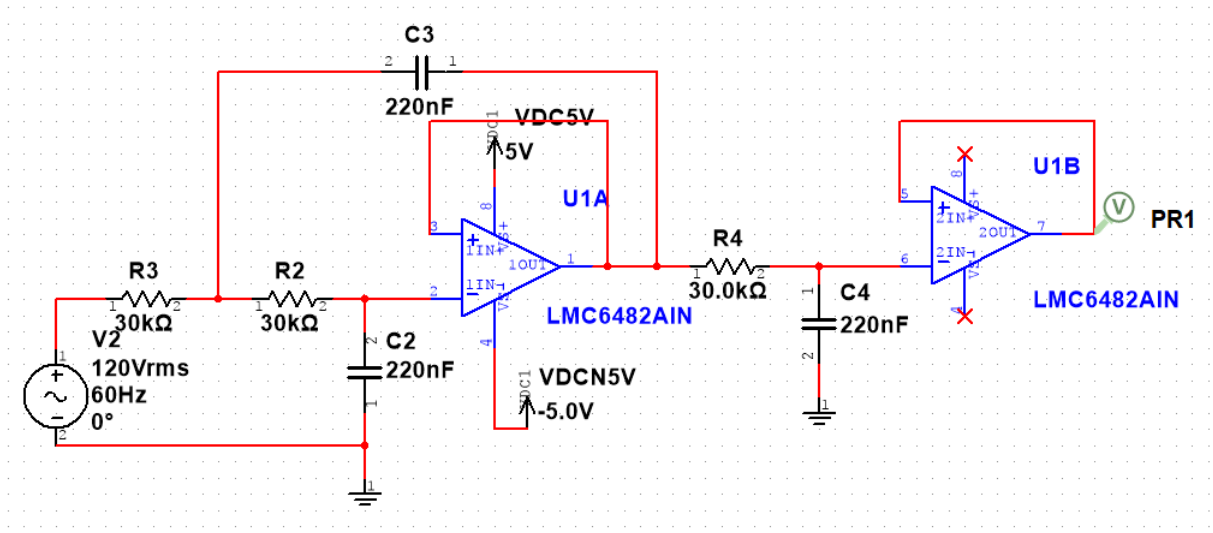

Figure 3.19: Schematic of a third order low-pass filter

The low-pass filtering will be done with a third-order low-pass filter. We will use a Sellen-Key second-order low-pass and a first order low pass connected in series which will result in a third order filter [11, 12]. The values for the resistors and capacitors have been chosen for a cutt-off frequency $f_c = 24\,\text{Hz}$.

Simulating the circuit in Multisim, we get the transfer function shown in Fig. 3.20. We can see that the signal at 100 Hz is attenuated below 1% of its amplitude.

The two amplifiers and the adder can be realized in one circuit. Figure 3.21 shows the schematic of the inverting adder circuit. The output voltage of the circuit will be

$$V_{\text{out}} = -\left(V_{\text{in1}}\frac{R_3}{R_1} + V_{\text{in2}}\frac{R_3}{R_2}\right). \tag{3.18}$$

In order to introduce θ into the signals correctly, we need to make sure that we choose the resistances according to the relations

$$\frac{R_3}{R_1} = 2\cos(\theta) \tag{3.19}$$

$$\frac{R_3}{R_2} = 2\frac{V_1}{V_2}\sin(\theta). \tag{3.20}$$

We can define θ and choose a fixed value for R_3 and then calculate the other two resistances R_1 and R_2.

As we can see, we can only have θ between 0 and $\frac{\pi}{2}$ with this set up. we can fix this with an easy workaround by inserting one inverting amplifier and a mechanical switch on

Die approbierte gedruckte Originalversion dieser Diplomarbeit ist an der TU Wien Bibliothek verfügbar.
The approved original version of this thesis is available in print at TU Wien Bibliothek.
TU Bibliothek Your knowledge hub WIEN

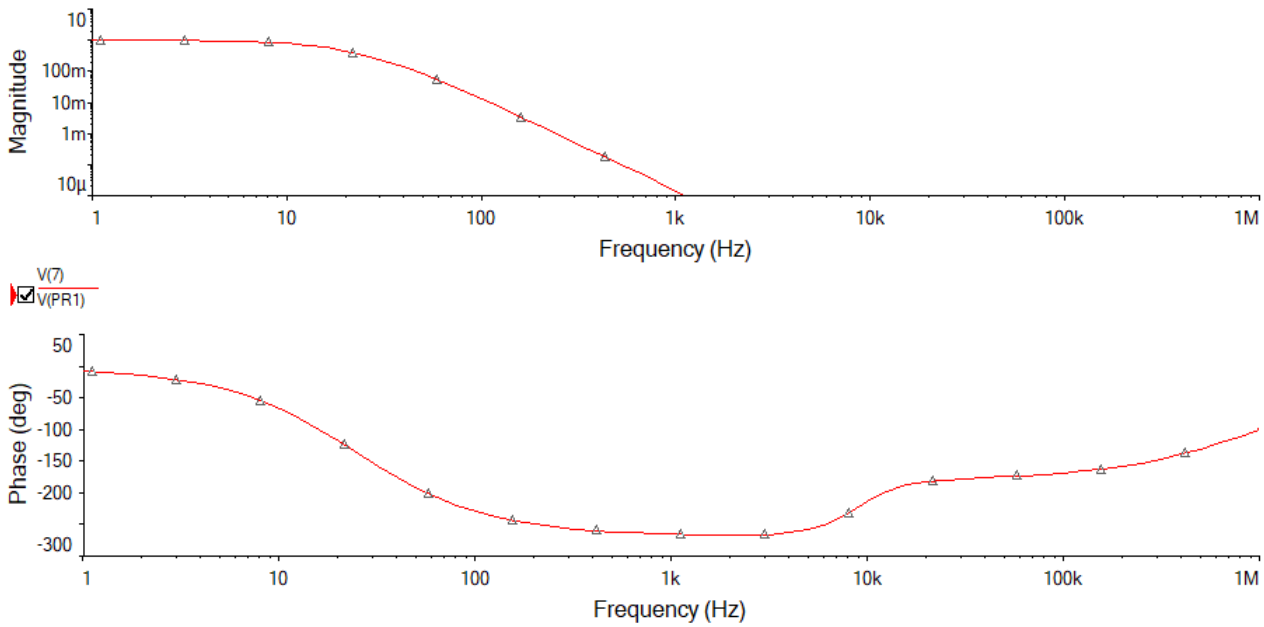

Figure 3.20: Transfer function of the low pass filter

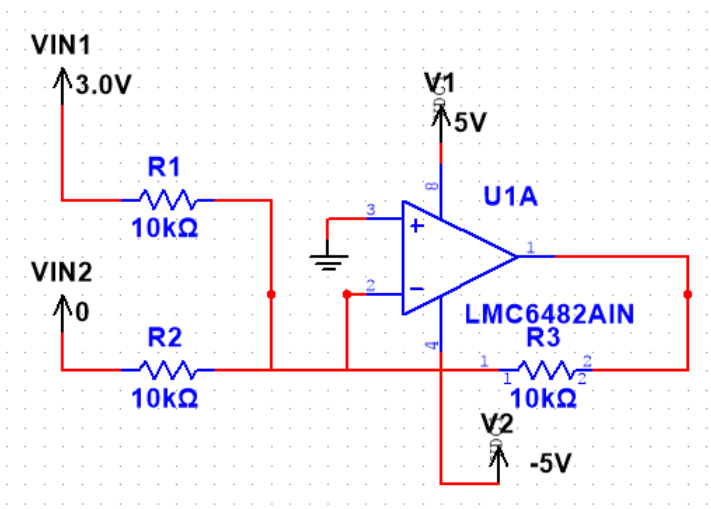

Figure 3.21: Inverting adder circuit

Die approbierte gedruckte Originalversion dieser Diplomarbeit ist an der TU Wien Bibliothek verfügbar.
The approved original version of this thesis is available in print at TU Wien Bibliothek.
TU Bibliothek Your knowledge hub WIEN

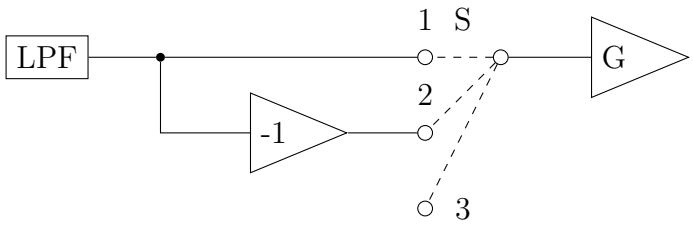

Figure 3.22: Block diagram of the position of the mechanical switch

each signal between the adder and the low-pass filter shown in Fig. 3.22. There are three states the switch can take on. In position 1, we have positive values of $\sin(\theta)$ or $\cos(\theta)$. In position 2, we can have negative values of $\sin(\theta)$ or $\cos(\theta)$. If we switch to position 3, which is disconnected, $\sin(\theta)$ or $\cos(\theta)$will be set to zero.

Now that we have our error signal we can add an analogue PI controller. It consists of three parts, an inverting amplifier, an integrator and an adder. The circuit diagram of the PI controller is shown in figure 3.23.

The transfer function of the PI controller will be the sum of the transfer functions of the integrator and proportional element. The transfer function of the proportional element is

$$G_{\mathrm{P}} = -\frac{R_4}{R_5}. \tag{3.21}$$

To calculate the transfer function of the integrator we need to calculate its output

$$u_{\mathrm{a}}(t) = u_{\mathrm{c}} = -\frac{1}{C_1}\int i_{\mathrm{e}}(t)\mathrm{d}t = -\frac{1}{R_1C_1}\int u_{\mathrm{e}}(t)\mathrm{d}t. \tag{3.22}$$

The Laplace transformation of this equation and dividing with the input, yields the transfer function

$$G_{\mathrm{I}} = -\frac{1}{R_1C_1s}. \tag{3.23}$$

The transfer function of the whole PI circuit will be

$$G_{\mathrm{PI}} = \frac{R_4}{R_5}\frac{R_6}{R_3} + \frac{1}{R_1C_1s}\frac{R_2}{R_3} \tag{3.24}$$

Die approbierte gedruckte Originalversion dieser Diplomarbeit ist an der TU Wien Bibliothek verfügbar.
The approved original version of this thesis is available in print at TU Wien Bibliothek.

Die approbierte gedruckte Originalversion dieser Diplomarbeit ist an der TU Wien Bibliothek verfügbar.
The approved original version of this thesis is available in print at TU Wien Bibliothek.

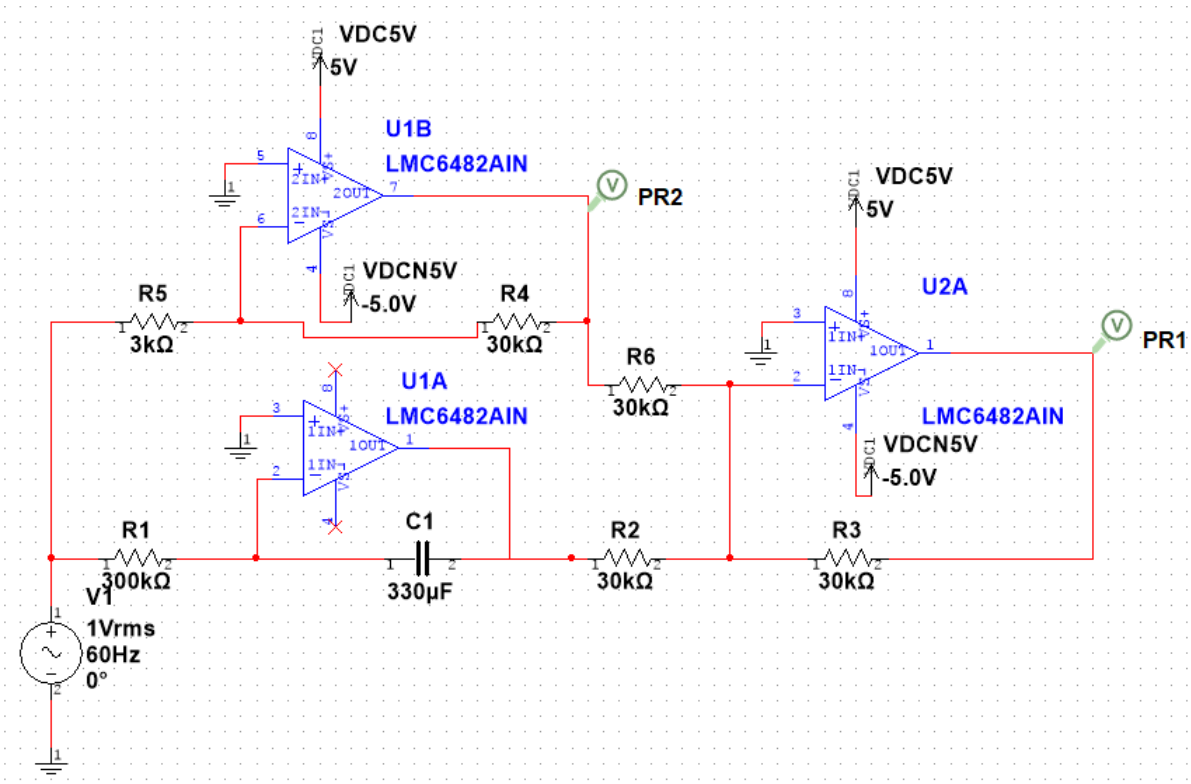

Figure 3.23: Schematic of the analogue PI controller

3.4 Measurement results

To characterize the different stabilization principles the measurement setup depicted in Fig. 3.24 is used. The alignment laser has a wavelength in the visible spectrum and is used for the alignment of the two mirrors. The laser driver generates a laser with a wave length of 1300 μm that is used for the measurement. Via an optical waveguide it is connected to the Michelson interferometer. It splits the laser beam in two and leads them over two optical waveguides to the two lenses. One of them focuses one laser arm at the probe, the second focuses the other at the reference piezoelectric mirror. The characterization of the setup was performed in a three stage manner:

1. Transfer-function of the piezo buzzer without stabilization: A piezo buzzer with a known transfer-function is placed instead of the electric field transducer at the measurement arm of the interferometer. A frequency sweep is performed on the driving voltage of the piezo buzzer for different oscillation amplitudes. Fig. 3.25 shows the measurement results. It turned out, that the noise induced drift impedes a stable working point which causes spikes in the transfer-functions.

2. Transfer-function of the piezo buzzer with stabilization: Similar setup is used as before. The only difference is that the stabilization is performed trough the piezoelectric mirror on the reference arm of the interferometer. By looking at the results shown in Fig. 3.26 we can see that the transfer-function is smooth with the stabilization turned on. At very low amplitudes, of the piezo buzzers driving signal, the SNR (Signal to noise ratio) is very low and a huge amount of noise is measured. In the laboratory where these experiments were performed there are strong noise sources below 150 Hz and at 1 kHz, that cause the spikes at those frequencies. The stabilization mechanism is driven at 1125 Hz which leads to spike at that frequency. For larger amplitudes the SNR raises and less distorted transfer functions could be obtained. By looking at the phase of the signals multiple stable phase points can be observed. Those are the working points on different fringes of the interference pattern discussed in Sec. **1.4.**. Large noise can cause the working point to jump from one to another stable point.

3. Amplitude measurement of the electric filed transducer with stabilization: For this measurement a slightly different setup is used. The piezo buzzer is replaced by the electric field transducer and placed between two plates. To generate the electric field the plates are connected to a 200 V power supply. Due to the transducers low resonant

Die approbierte gedruckte Originalversion dieser Diplomarbeit ist an der TU Wien Bibliothek verfügbar.
The approved original version of this thesis is available in print at TU Wien Bibliothek.
TU Bibliothek Your knowledge hub WIEN

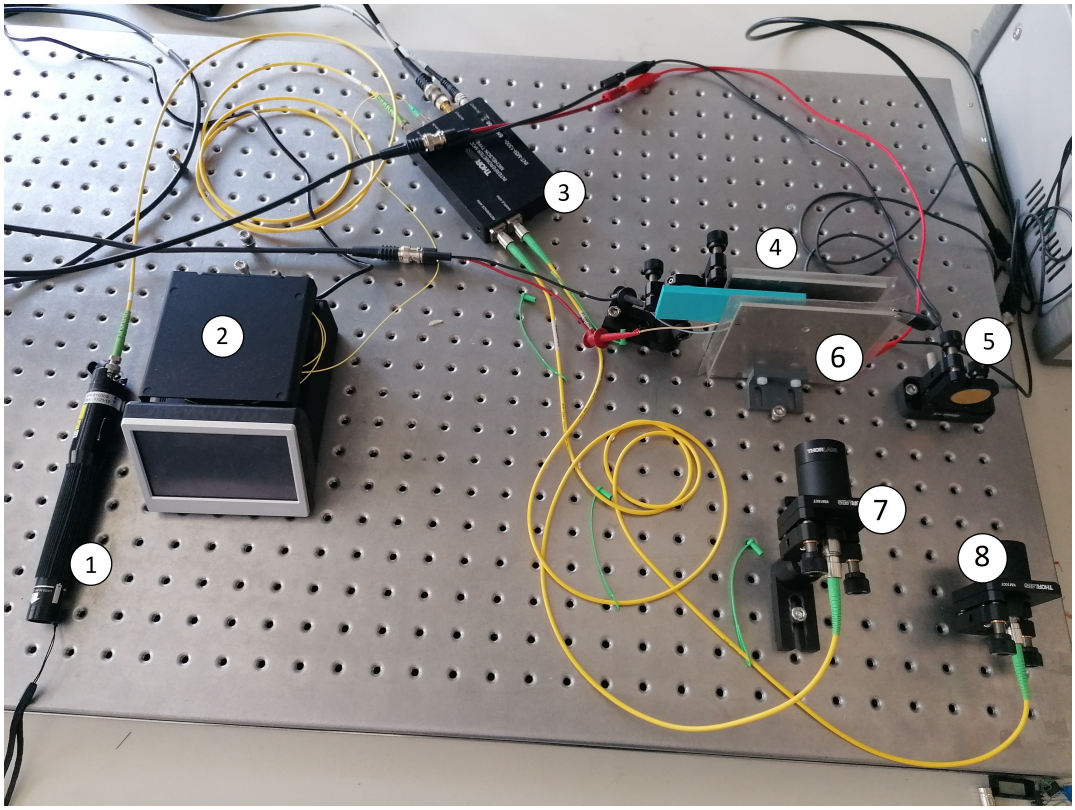

Figure 3.24: Measurement setup: (1)-alignment laser, (2)-laser driver, (3) Thorlabs Michelson interferometer, (4)-measurement probe, (5)-reference piezoelectric mirror, (6)-capacitor plates, (7)-lens of the measurement arm, (8)- lens of the reference arm

Die approbierte gedruckte Originalversion dieser Diplomarbeit ist an der TU Wien Bibliothek verfügbar.
The approved original version of this thesis is available in print at TU Wien Bibliothek.

frequency of 170 Hz an frequency sweep is not performed. Instead an amplitude sweep is performed at the resonant frequency and the amplitude and phase were measured with the stabilization turned on. From the results shown in Fig. 3.27 we can observe that we have a stable amplitude and phase for driving voltages larger than 5 V. Below 1 V the error rate is very high, due to high fluctuations in phase and amplitude.

Die approbierte gedruckte Originalversion dieser Diplomarbeit ist an der TU Wien Bibliothek verfügbar.
The approved original version of this thesis is available in print at TU Wien Bibliothek.
TU WIEN Bibliothek Your knowledge hub

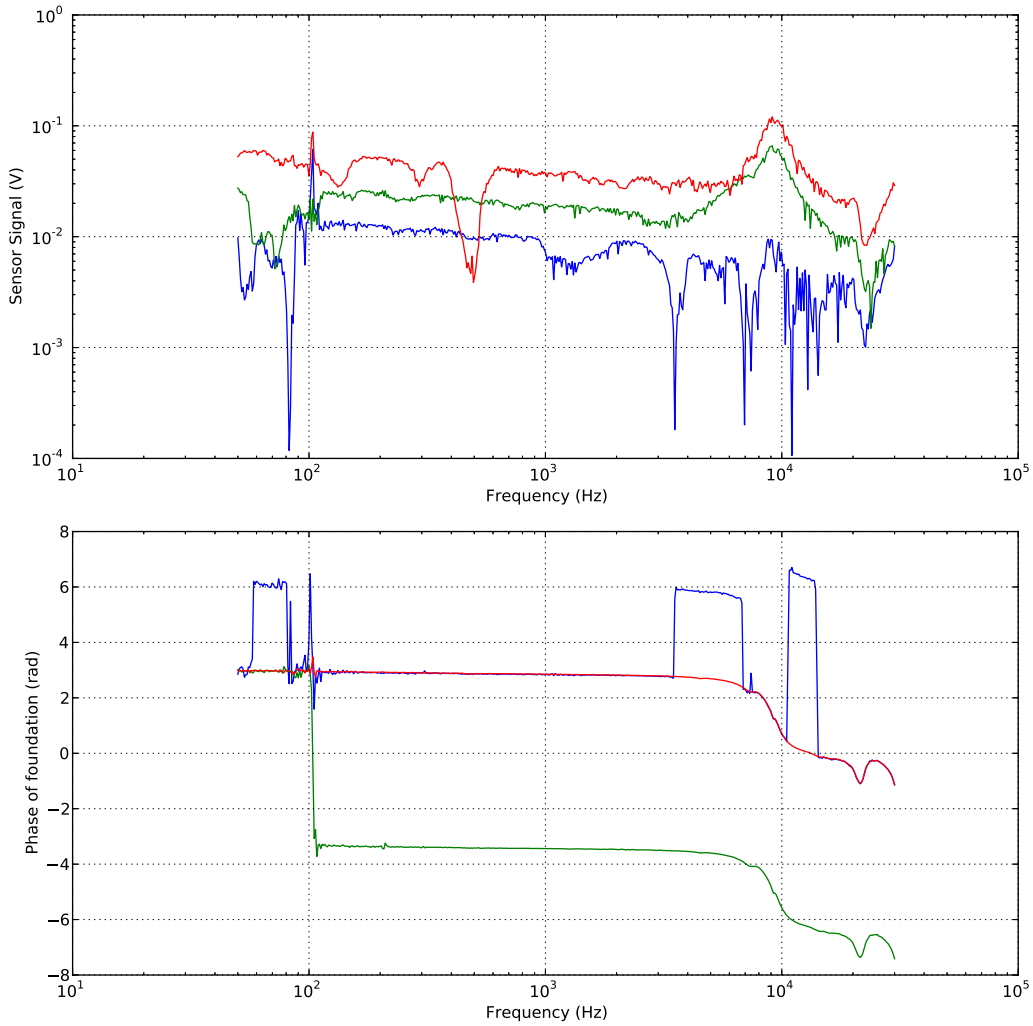

Figure 3.25: Measured transfer function of a piezo buzzer without stabilization, at different driving voltages (Blue - 1 V, Green - 2 V, Red - 5 V)

Die approbierte gedruckte Originalversion dieser Diplomarbeit ist an der TU Wien Bibliothek verfügbar.
The approved original version of this thesis is available in print at TU Wien Bibliothek.

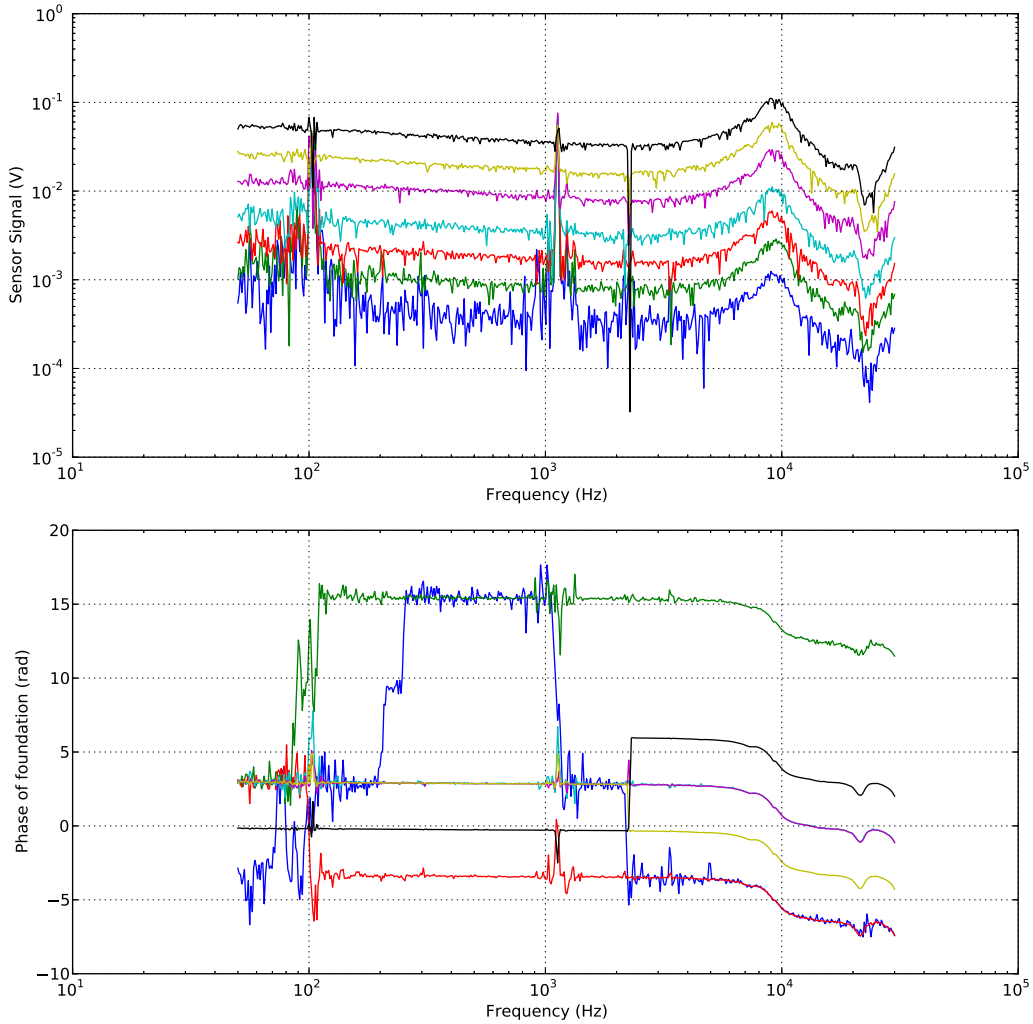

Figure 3.26: Measured transfer function of a piezo buzzer with stabilization, at different driving voltages (Blue - 0.02 V, Green - 0.05 V, Red - 0.1 V, Cyan - 0.2 V, Purple - 0.5 V, Yellow - 1 V, Black - 2 V)

Die approbierte gedruckte Originalversion dieser Diplomarbeit ist an der TU Wien Bibliothek verfügbar.
The approved original version of this thesis is available in print at TU Wien Bibliothek.

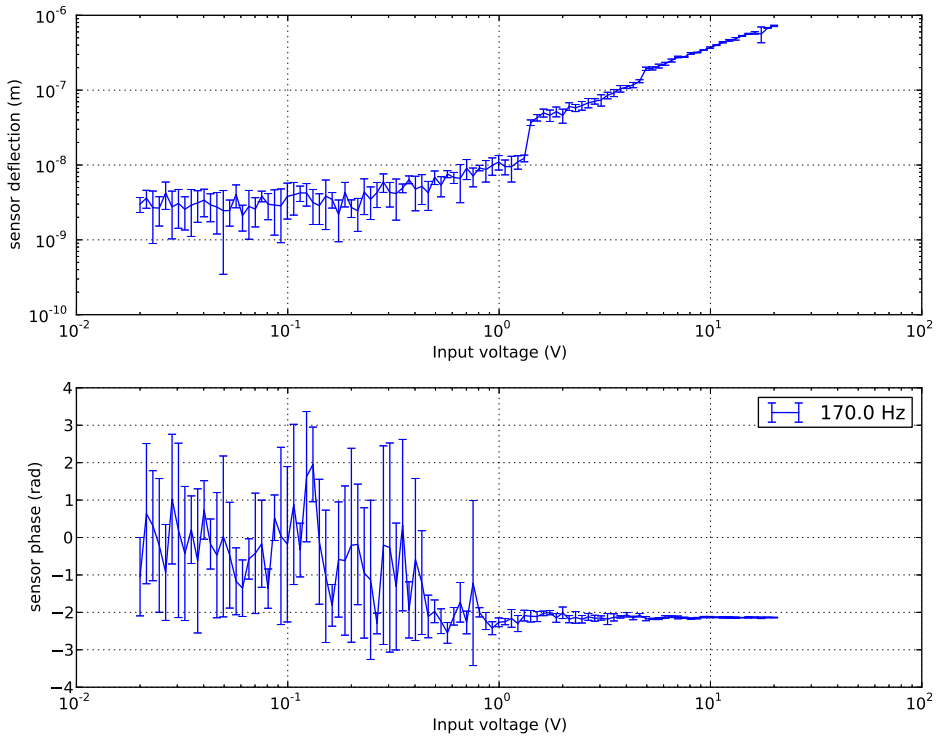

Figure 3.27: Amplitude sweep of the transducer at the resonant frequency

Die approbierte gedruckte Originalversion dieser Diplomarbeit ist an der TU Wien Bibliothek verfügbar.
The approved original version of this thesis is available in print at TU Wien Bibliothek.

Die approbierte gedruckte Originalversion dieser Diplomarbeit ist an der TU Wien Bibliothek verfügbar.
The approved original version of this thesis is available in print at TU Wien Bibliothek.

Conclusion and Outlook

3.5 Outlook, generation of a FM signal

The interferometer stabilization allows to maintain a constant working point, but the trade off is that it brings with it complications in form of stability issues. Due to the sensitivity of the Michelson interferometer a recalibration needs to be done before measurements or when the transducer is changed. If it is not done there could be stability issues in the measurement. A measurement without stabilization requires a signal that is independent of the working point. A possible solution is to introduce a carrier into the interference equation which yields

$$\frac{I}{2I_0} = 1 + \cos\left(\omega t + \psi + \psi_\mathrm{d} \sin(\Omega t)\right), \tag{3.25}$$

where ω is the carrier frequency. The interference function now is a FM signal with the carrier frequency ω that is modulated with a signal $\psi_\mathrm{d} \sin(\Omega t)$. The phase function caused by ωt is plotted in the first plot of Fig. 3.28. In the second plot the wrapped phase function is shown. This leads to the conclusion that by inducing the right sawtooth phase-shift into the system we can get an FM signal that is independent of the working point ψ. A change in ψ introduces a change in the phase of the carrier wave and not in the baseband signal.

Options for implementation are to do it mechanically by driving the piezoelectric reference mirror with a sawtooth voltage or to do it optically by driving the sawtooth voltage into a pockels cell. Because the speed of the pockels cell is far more superior the use of the second method is recommended. Fig. 3.29 shows a block diagram of the setup (similar to [15]). By applying an electric field to the pockels cell its refractive index changes, which results in a change of speed of the light propagating it, and therefore, its phase at the detector.

The detection of this signal can be performed by various FM detectors [8]. The detector used here consists of two parts: a differentiator and an envelope detector Fig. 3.30.

To verify the concept a LabView simulation is performed. The LabView code is represented in Fig. 3.31. Results of the simulation are shown in Fig. 3.32. The first is the FM modulated

Die approbierte gedruckte Originalversion dieser Diplomarbeit ist an der TU Wien Bibliothek verfügbar.
The approved original version of this thesis is available in print at TU Wien Bibliothek.
TU WIEN Bibliothek Your knowledge hub

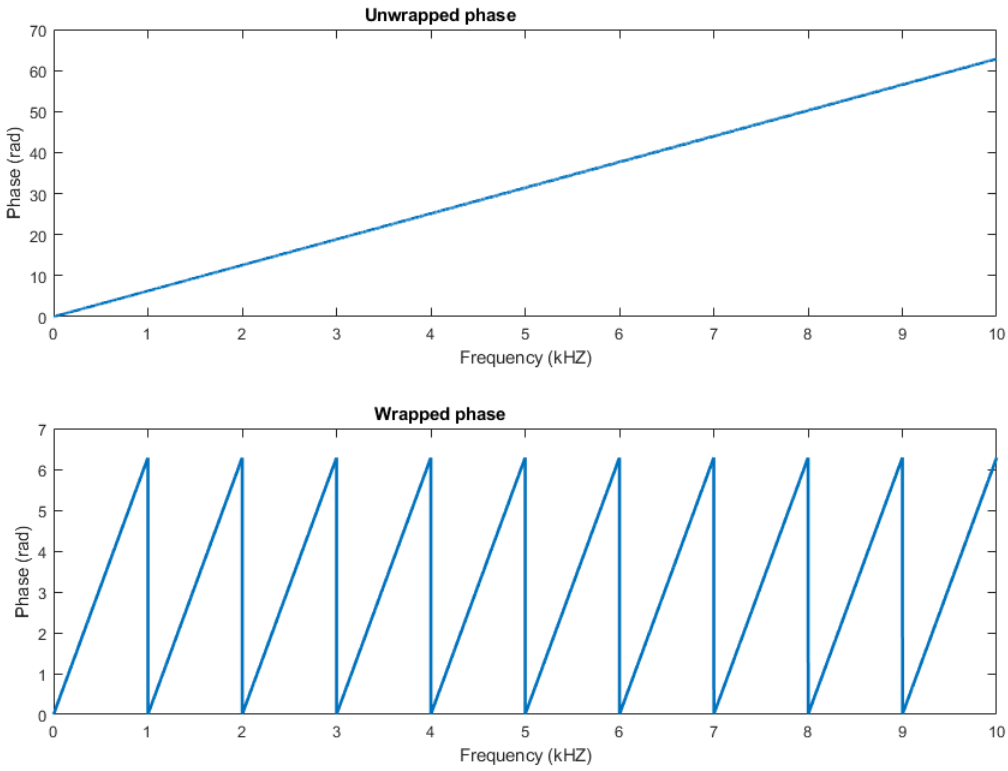

Figure 3.28: Unwraped and wrapped phase induced by the function ωt

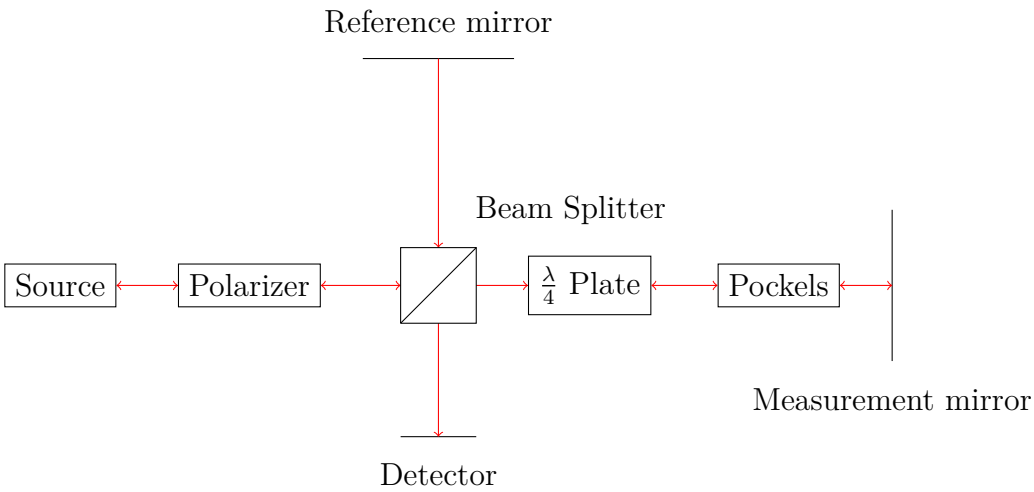

Figure 3.29: Schematic representation of the modified Michelson interferometer

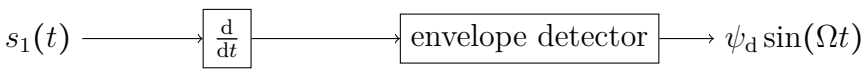

Figure 3.30: Block diagram of the FM demodulator

Die approbierte gedruckte Originalversion dieser Diplomarbeit ist an der TU Wien Bibliothek verfügbar.
The approved original version of this thesis is available in print at TU Wien Bibliothek.

signal. The second is the signal after the differentiation process. We already can see the modulation signal $\psi_\mathrm{d} \sin(\Omega t)$ in the envelope. By changing the phase ψ the carrier signal is phase-shifted, but the enveloping signal stays constant. In the third picture the signal after it leaves the envelope detector is shown. It is the signal that carries the information about the position of the measurement mirror.

Die approbierte gedruckte Originalversion dieser Diplomarbeit ist an der TU Wien Bibliothek verfügbar.
The approved original version of this thesis is available in print at TU Wien Bibliothek.
TU WIEN Bibliothek Your knowledge hub

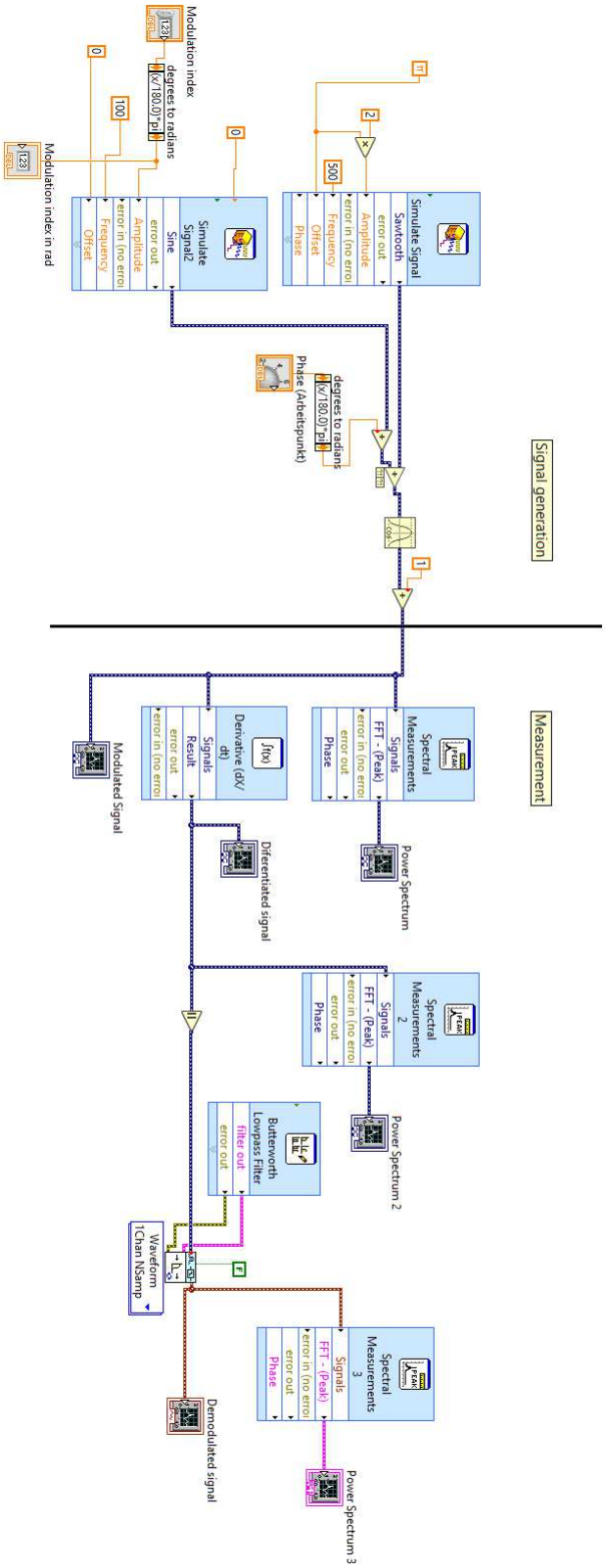

Figure 3.31: Simulation of the system in LabView. On the left side Eq. 3.25 is simulated. On the right side is the FM detector

Die approbierte gedruckte Originalversion dieser Diplomarbeit ist an der TU Wien Bibliothek verfügbar.
The approved original version of this thesis is available in print at TU Wien Bibliothek.
TU Bibliothek Your knowledge hub WIEN

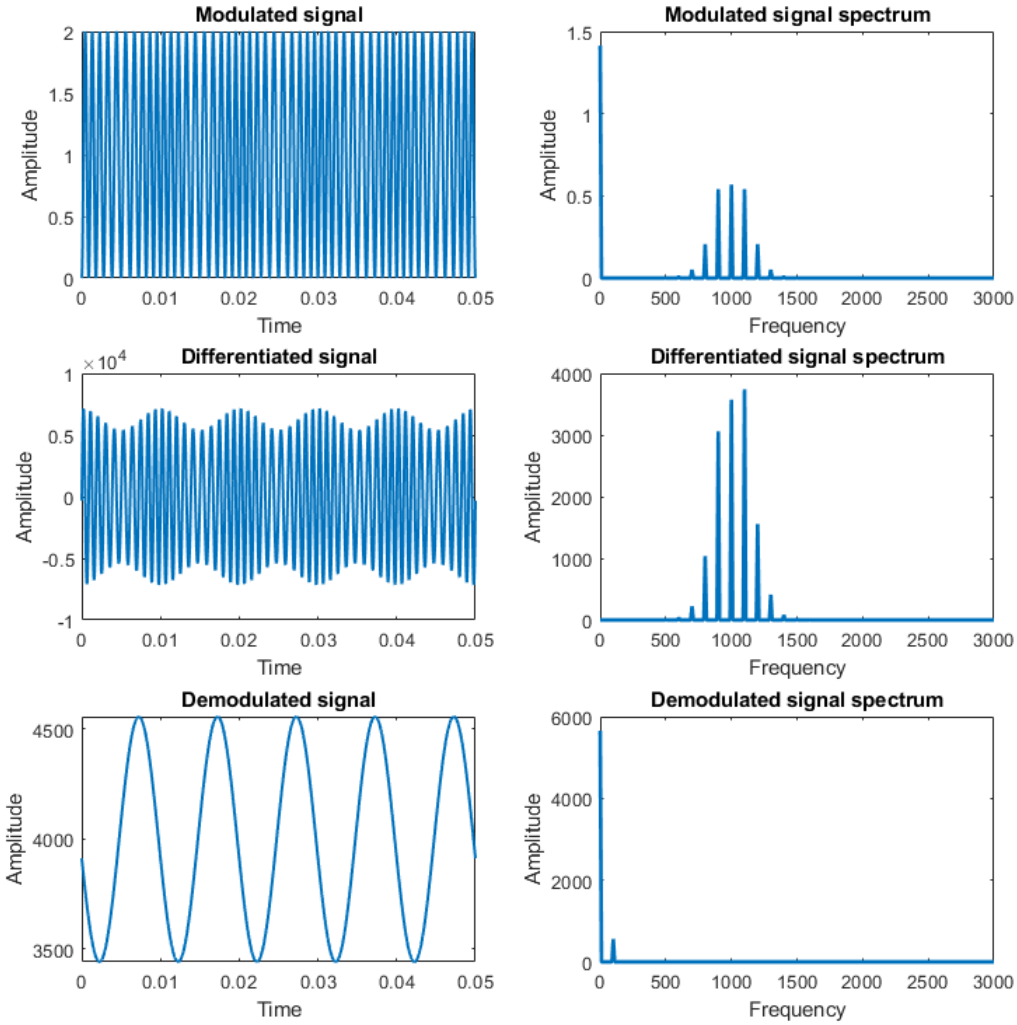

Figure 3.32: Signals with their respective spectrum at three different demodulation stages

Die approbierte gedruckte Originalversion dieser Diplomarbeit ist an der TU Wien Bibliothek verfügbar.
The approved original version of this thesis is available in print at TU Wien Bibliothek.

3.6 Conclusion

Measurements taken with the Michelson interferometer without stabilization revealed insufficient results. It was mainly by the noise induced drift of the mirrors that resulted in a change of the path lengths of the two interferometer arms and therefore a drift in the working point of the interferometer. Since the working point was not known changes of the signal of interest could not be revealed. With the introduction of the stabilization mechanism good results could be obtained. Two methods have been applied: hybrid and double quadrature demodulation methods. Both methods use a similar concept. They both need a piezoelectric mirror to be driven at a certain frequency that gave the information about the instantaneous working point of the system. They showed similar performance when the feedback is connected directly to the interferometer. If there is circuitry connected between the feedback and the interferometer, the double quadrature method is better due to its phase-lock mechanism. We also implemented the double quadrature demodulation method and the signal generator on a micro-controller, which made things more practical so there was no need for additional instruments. The results were very good and the working point showed to be very stable. The transducer exhibits a low resonant frequency that is in the domain of the relevant noise. An improvement could be achieved by using a transducer with a higher resonant frequency. The method presented in the outlook looks like a promising alternative that is superior to the current measurement method with stabilization, because it does not need a stabilization and it does not require a fixed working point. The simulation showed promising results, but the problems of a real-world implementation also needs to be solved.

Die approbierte gedruckte Originalversion dieser Diplomarbeit ist an der TU Wien Bibliothek verfügbar.
The approved original version of this thesis is available in print at TU Wien Bibliothek.
TU Bibliothek WIEN Your knowledge hub

Bibliography

[1] M. Kaltenbacher, H. Ecker, S. Gombots, J. Nowak. MESS- UND SCHWINGUNGSTECHNIK *TU Wien(Skriptum zur Vorlesung)*, 2019.

[2] Stephen H. Hall, Howard L. Heck. ADVANCED SGNAL INTEGRITY FOR HIGH-SPEED DIGITAL DESIGNS. *A John Wiley and Sons, Inc., Publication*, 2009.

[3] Georg A. Reider. PHOTONIK Eine Einführung in die Grundlagen 3. Auflage. *Springer-VerlagWien*, 2012.

[4] Alois M.J. Goiser. TELEKOMUNIKATION Robuste und Verlässliche Kommunikationssysteme *TU Wien, Institute of Telecommunications (Skriptum zur Vorlesung)*, 11. March 2019.

[5] Andreas Kugi AUTOMATISIERUNG *TU Wien, Automation and Control Institute (Skriptum zur Vorlesung)*, 2014/2015.

[6] A. Prechtl SIGNALE UND SYSTEME 1 *TU Wien, Institute of Elektrodynamics, Microwave and Circuit Engineering (Skriptum zur Vorlesung)*, 2010.

[7] E. Hering, K. Bressler, J. Gutekunst ELEKTRONIK FÜR INGENIEURE UND NATURWISSENSCHAFTLER *Springer-Verlag Berlin Heidelberg*, 2014.

[8] B.P. Lathi MODERN DIGITAL AND ANALOG COMMUNICATION SYSTEMS, Third edition *Oxford University Press*, 1998.

[9] Kenneth G. Libbrecht, Eric D. Black A BASIC MICHELSON LASER INTERFEROMETER FOR THE UNDERGRADUATE TEACHING LABORATORY DEMONSTRATING PICOMETER SENSITIVITY *264-33 Caltech, Pasadena, California 91125*, 2014.

[10] A. A. Freschi, J. Frejlich ADJUSTABLE PHASE CONTROL IN STABILIZED INTERFEROMETRY *Optics letters, 20(6):635-637*, 1995.

[11] B. Carter MOREGN ON A BUDGET *Texas Instruments, SLOA096*, 2001

[12] R. Mancini OP AMPS FOR EVERYONE *Texas Instruments, SLOD006*, 2002

[13] G. Doblinger ZEITDISKRETE SIGNALE UND SYSTEME Eine Einführung in die grundlegenden Methoden der digitalen Signalverarbeitung *TU Wien, Institut führ Nachrichtentechnik*, 2010

Die approbierte gedruckte Originalversion dieser Diplomarbeit ist an der TU Wien Bibliothek verfügbar.
The approved original version of this thesis is available in print at TU Wien Bibliothek.
TU Bibliothek Your knowledge hub WIEN

[14] Aircraft Armaments, inc. FM MODULATION OF A CW LASER BEAM *National aeronautics and space administration*, 1967.

[15] Aircraft Armaments, inc. FM MODULATION OF A CW LASER BEAM *National aeronautics and space administration*, 1967.

[16] M. Gschirtz OPTICAL READOUT FOR MICROMECHANICAL ELECTRIC FIELD SENSORS *TU Wien, Institute of Sensor and Actuator Systems (Master Thesis)*, 2020.

[17] A. Kainz, H. Steiner, J. Schalko, A. Jachimowicz, F. Kohl, M. Stiftler, R. Beigelbeck, F. Keplinger, W. Hortschitz DISTORTION-FREE MEASUREMENT OF ELECTRIC FIELD STRENGTH WITH A MEMS SENSOR *TU Wien, Institute of Sensor and Actuator Systems (Master Thesis)*, 2020.

[18] M. Abramowitz, I. A. Stegun HANDBOOK OF MATHEMATICAL FUNCTIONS: with Formulas, Graphs, and Mathematical Tables *Dover publications, inc., New York*, 1972.

[19] https://ccrma.stanford.edu/software/snd/snd/fm.html , 2020.

Die approbierte gedruckte Originalversion dieser Diplomarbeit ist an der TU Wien Bibliothek verfügbar.
The approved original version of this thesis is available in print at TU Wien Bibliothek.
TU Bibliothek WIEN Your knowledge hub